Improvement of existing design rules for cold-formed stainless steel square hollow sections under compression forces using numerical modelling and Monte Carlo simulations

by

Raphaël Démolis

Table of Contents

Improvement of existing design rules for cold-formed stainless steel hollow sections under compression forces
using numerical modelling and Monte Carlo simulations

List of Figures

List of Tables

Improvement of existing design rules for cold-formed stainless steel hollow sections under compression forces using numerical modelling and Monte Carlo simulations

University presentation

The University of Sheffield (UoS), often ranked in the world top-100 universities, educates its students in more than 50 different departments, shared among 6 faculties. The lectures and professors diversity, combined with strong links with industries and research, form skilful graduates and postgraduates in numerous domains. Additionally, it is a university with an international outlook, as more than 7000 out of the 26309 students of 2014/2015 come from non-European countries[1]. After getting their undergraduate degree, students can directly enter the labour market or continue their studies in Master's (postgraduate) and possibly complete their studies with a doctorate.

Sheffield, the fifth largest United Kingdom city by population, is located in South Yorkshire in England. The city was famous worldwide during the 19th century for metallurgy and steel production and next to a decline period during the 1970s and 1980s, Sheffield is now experiencing a strong revival in its economy. Strong links between the University and the nearby various industries contribute to the employment and innovation of the University of Sheffield students.

In the framework of my ARPE (Année Recherche Prédoctorale à l'Étranger), I am realising my research internship at the University of Sheffield, in the Civil and Structural Engineering Department, part of the Faculty of Engineering. I am affiliated to the Steel Structures group in the overarching Structures research area. My research group is particularly interested in three main topics, covering all issues that industries and engineers can face using either carbon steel or stainless steel:

(i) Stability of steel structures.

(ii) Steel connections.

(iii) Steel behaviour in fire.

As it will be detailed in section 1 of the Introduction chapter, this project concerns the stability issue, and more precisely the buckling of stainless steel columns. Thus, I am jointly supervised by Prof. Buick Davison and Dr. Jurgen Becque whose research themes interest in steel stability.

As expected, the laboratory of the Department offer all ranges of facilities require to lead experimental studies linked with civil engineering. However, I am not carrying out any experimental work here but only numerical modelling. Thus, I am using the Finite Element (FE) analysis package Abaqus [6], installed on the HPC (High Performance Computing) facility of the University of Sheffield, called 'Iceberg'. Iceberg provides a total of 3440 CPUs cores and 16 GPUs units, allowing the users to run computational expensive models.

---

[1]UoS 2014 figures - `https://www.shef.ac.uk/departmentProfiles/instprofile/student-population/2014`

Introduction

The first industrial manufacture of stainless steel started in 1912-1913 by Maurer and Strauss in Germany and Brearley in the United Kingdom. In its infancy, stainless steel was mainly used for household applications, like for cutlery for instance. In the 1920s, this new material expands its range of application to automotive industry (bumpers, radiators and trim), medicine (scalpels), chemical tanks and construction (facades and roofing). The installation of a stainless steel reinforcing chain to stabilize the dome of St. Paul's Cathedral in London in 1925 was one of its earliest uses in a structural project. In 1930-1931, the simultaneous constructions of Empire State Building and Chrysler Building in New-York really launched the use of this new material for architectural project. The top 88 meters of the latter are clad in stainless steel (see Fig. 1) and continue to gleam brightly even though it has been cleaned only twice in its entire life.
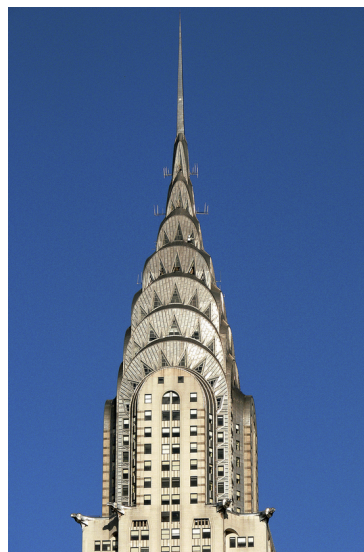
Figure 1: One of the early applications of stainless steel - Top of the Chrysler Building, New-York, 1931 - William van Alen Architect.

Since this early use, stainless steel has diversified its scope of usage with actual applications in aviation, aerospace, naval construction and of course civil engineering. Indeed, thanks to its numerous advantages, listed hereinbelow, stainless steel is an attractive answer to various structural projects. Those attractive properties obviously depend on the microstructure of the stainless steel and can vary from one grade to another. From a sustainable point of view, stainless steel is also indefinitely recyclable and has a low environmental impact (see Rossi publication [7]).

(i)   Excellent corrosion resistance.

(ii) High mechanical strength (from 250 to 1400 MPa).

(iii) Good fire behaviour (see Fig. 2 and recent experimental/design works [8, 9, 10, 11, 12, 13]).

(iv) Good explosion resistance, due to high ductility (a specific guide for blast-resistant structures made in stainless steel has been published by FABIG [14]).
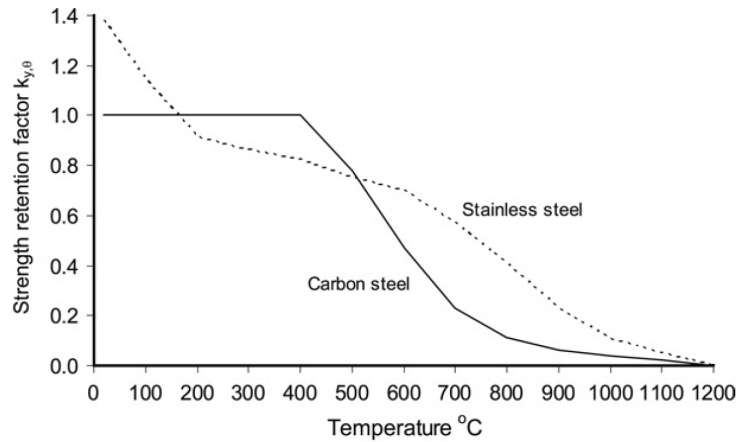
Figure 2: Comparison of strength retention factor $k_{y,\theta}$ for carbon steel and stainless steel.

However, stainless steel is seldom use in structural project face to normal steel. Indeed, in 2013, solely 5% of the 18.9 Mt stainless steel manufactured worldwide were used in construction [15, 16] to more than 50% of the 1607 Mt world steel production [17]. The initial cost (about four times that of carbon steel), the different stress-strain behaviour from carbon steel (Fig. 3) and the lack of design rules are some of the factors which restrained the stainless steel development in construction before the 1980s-90s.
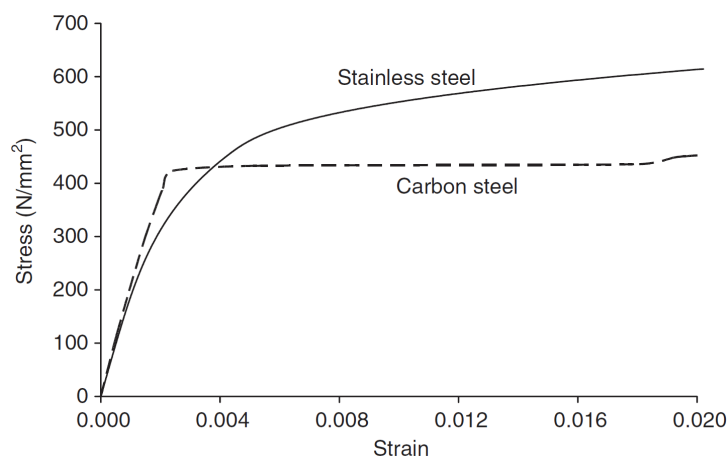
Figure 3: Comparison of stress-strain ($\sigma - \varepsilon$) relation for carbon steel and stainless steel.

Nevertheless, as explained by Gardner [18], the initial cost for a material cost comparison is not enough relevant. A whole-life costing study conducted by The Steel Construction Institute (SCI) [19] on offshore structures made of normal steel, aluminium and stainless steel concluded that aluminium and stainless steel enable interesting life-cycle cost savings. Initial material cost, corrosion protection, fire resistance, maintenance cost and other potential cost savings were considered. On the other hand, the accelerated current development of the duplex grades (with a low nickel percentage, material that suffers from highly speculative price) as a joint effort of industries and academics reduce the cost of stainless steel.

Based on the general equation proposed by Ramberg and Osgood [20] and later modified by Hill [21] (see Eq. 1 and 2), several models have been proposed by researchers [22, 23] to account for the non-usual rounded stress-strain curve of stainless steel and are still discussed today [24, 25]. However, as stainless steel is an anisotropic material (which emphasised whith cold-forming process), with different properties depending on the stresses applied (see Fig. 4), care is needed in the choice of the design strength.

$$\varepsilon = \frac{\sigma}{E_0} + 0.002 \left(\frac{\sigma}{\sigma_{0.2}} \right)^n \tag{1}$$

$$n = \frac{ln(20)}{ln\left(\frac{\sigma_{0.2}}{\sigma_{0.01}} \right)} \tag{2}$$
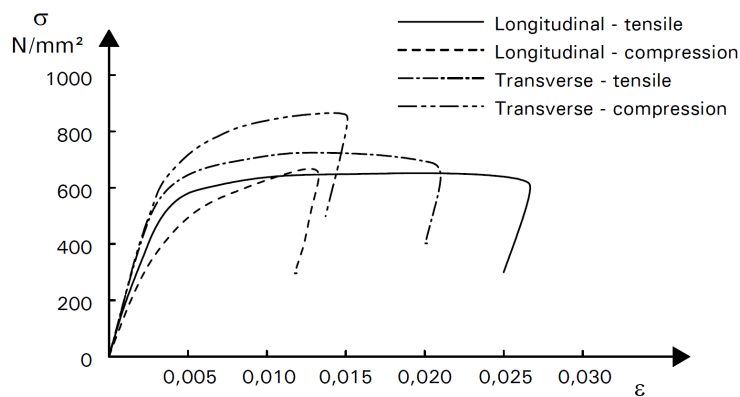
Figure 4: Anisotropic behaviour of stainless steel.

Finally, efforts have been made during the last decades to formulate relevant design rules. Thus, both North-America and Europe has published their own design guidance for the use of stainless steel in construction. However, as underlined in the next section, work is still needed in this field as all the existing design methods are currently too conservative.

1 Aim of the study

This project is interested in the buckling of cold-formed stainless steel columns, with the formulation of improved design rules as a final objective. Experimental studies often show disagreement between the design rules recommendations and experimental results. Quite often, the design standards appear to be too conservative leading to less than optimal usage of the full section to safeguard against buckling

and hence a cost increase in stainless steel construction, a problem which is exacerbated due to the price premium paid for stainless steel compared with conventional structural steels.

The buckling design rules will be formulated using numerical results obtained from simulations. These simulations will use Monte Carlo method to incorporate the notion of uncertainty into the numerical models, which has never been done before.

Indeed, researchers quite often conduct experimental buckling tests on a set of columns and then build a numerical model based on the experimental results. However, they tend to 'average' some of the input parameters of their numerical model using experimental measurements. For instance, the global imperfection factor of a column is often entered as $L/1500$ in numerical models, but this value usually varies between $L/500$ up to $L/2000$. $L/1500$ is only kept as studies have shown good agreement between experimental and numerical results for this value. However, the averaging of numerous inputs could lead to errors in the results and maybe to over-conservative results.

From this analysis, it has been decided to incorporate uncertainties in the numerical inputs in order to accurately model stainless steel columns. The notion of uncertainty is applied using Monte Carlo method to generate random sets of data. Thus, a numerical model has first to be build based on accurate experimental results. Then, a large amount of simulations can be carried out using the Monte Carlo generated inputs concurrently with the numerical model and finally, analysing statistically the results, design rules could be formulated. Furthermore, a literature work is beforehand needed in order to get familiar with specific properties and design rules of stainless steel. The initial given timeline for this project is shown Table 1.

It is important to note that it has been decided to work only on square hollow sections. Indeed, although stainless steel hollow sections are available in many shapes it is convenient to start with a symmetric geometry. Moreover, literature is more abundant for square hollow sections, which is important for the construction of the numerical model.

Month	Project step
October-November	Literature review and familiarisation with the FE software.
December-January	Building an FE model and verification against existing experimental data.
February	Scripting and setting up the parametric studies.
February-May	Simulations.
June	Reliability analysis and design rules.
July	Final report writing.

Table 1: Initial timeline of the project.

This report presents the whole work that have been realised on this project. The context and background of the study is given in Chapter 1. Thus, stainless steel grades, cold-forming effect and columns uses and characteristics are first described. Then, design rules and methods of the European and North-American standards applied to cold-formed stainless steel members in compression (columns) are explained. Finally, explanations on the Monte Carlo method and how it is applied to this project are given. Chapter 2 tackles the numerical part of this project, with first a presentation of the built and validated numerical model. Pyhton scripts and Monte Carlo data generation are explained. Finally, the Chapter 3 presents the obtained results next to the numerical simulation and the proposed design equation for the buckling of stainless steel square hollow sections.

Chapter 1

Context and background

This first chapter presents the frame of study of this project. Thus, the first section details the cold-formed stainless steel grades, characteristics and uses. The existing design rules of the European and North-American standards applied to cold-formed stainless steel columns in compression are explained in the second section. Finally, the last section of this chapter present the issues of the Monte Carlo method applied to this project.

Contents

1   Cold-formed stainless steel columns

1.1   Stainless steels grades

Stainless steel is an alloy of iron (Fe), carbon (C) and a minimum of 10.5% chromium (Cr) required for the corrosion resistance, which form a passive self-protecting layer thanks to the reaction of chromium with oxygen. Various alloying elements are added as nickel (Ni), manganese (Mn), molybdenum (Mo), copper (Cu), silicon (Si), sulphur (S), phosphorus (P) and nitrogen (N). Facing the alloying elements diversity, it exist currently more than 120 stainless steel grades, classified by the EN 10088 norm [26] in Europe (with a series of figures such as 1.4000) and by the American Iron and Steel Institute (AISI) norm [27] in the United States (with a series of three figures). However, stainless steel are usually classified into four main families, as listed hereinafter, corresponding to precise metallurgical structures and so to different chemical, corrosion and strength properties. The chemical composition of each nuances are based on ArcelorMittal data [28] with few precisions provided by Rossi [7] and Davis [29].

  (i)   Martensitic: 0.1 to 1.2% carbon (C), 11 to 18% chromium (Cr) and small amounts of nickel (Ni) and manganese (Mn).

 (ii)   Austenitic: 0.015 to 0.10% carbon (C), 16 to 18% chromium (Cr), 8 to 13% nickel (Ni) and 0 to 4% molybdenum (Mo).

(iii)   Ferritic: 0.02 to 0.06% carbon (C), 10.5 to 29% chromium (Cr) and 0 to 4% molybdenum (Mo).

(iv)   Duplex or austenoferritic: less than 0.1% carbon (C), 21 to 26% chromium (Cr), 3.5 to 8% nickel (Ni) and 0 to 4% other alloying element.

The most common grades of stainless steel in construction are austenitic, duplex and, though to a lesser extent, ferritic. Due to the addition of carbon, martensitic grades can be hardened and strengthened by heat treatment and are mainly used where strength is needed, as for surgical and dental instruments for instance but are not suitable for structural projects.

Austenitic is the more customary grade of stainless steel, accounting for 70% of the world stainless steel production. It success is historical as it was one of the first existing stainless steel grade and has been favoured by its versatility to welding and forming. The top cladding of the Chrysler Building (Fig. 1) is, unsurprisingly, made of austenitic stainless steel. Ferritics, as they do not contain nickel, are cheaper than austenitics and relatively price-stable. As underlined by Cashell and Baddoo [30], though they offer good durability and strength, ferritics are currently under-used in structural projects due to a lack of existing information in literature and in design manuals. However, it has been used in a few ambitious structural project such as the roofing of the Media Dome in Kitakyushu in 1998, shown Fig. 1.1 and should for sure be more valued in the next decades. Finally, duplex or austenoferritic stainless steel is, as expected, a combination between austenitic and ferritic grades. With a lower nickel ratio than austenitics, they are cheaper and offer even better properties without any concessions. Thus, they are more resistant to stress corrosion cracking (SCC) and their 0.2% proof stress is higher than the austenitic one. This high strength enable the construction of light and aesthetics structures, as the *Sölvesborgsbron* (Sölvesborg Bridge) in Sölvesborg, Sweden (Fig. 1.2). This pedestrian and cycle bridge, the longest in Europe, was completed in 2012, using 150 tons of Outokumpu duplex stainless steel [31].

A comparison of the stress-strain curve for those three stainless steel grades is shown Fig. 1.3.

Figure 1.1: Ferritic stainless steel application - Media Dome, Kitakyushu, 1998 - Kiyonori Kikutake Architects.

1.2   Cold-forming processes

Cold-forming process, in opposition to hot-forming process, is the way to form and shape cross-sections at ambient room temperature starting from coiled material sheets. This method, originally used for carbon steel, is suitable to all the grades of stainless steel presented hereinbefore. As explained by Cruise and Gardner [32], there are two main productions routes. The elementary one is press braking, whereby sheets are bend between a punch and a die (Fig. 1.4(a)). This is a manually controlled process befitting small quantities of members, suitable for angle sections. Cold rolling is a process in which sheets are uncoiled in a series of forming rollers that gradually deform it into the desired section shape (Fig. 1.4(b)). Larger production is possible as this is a more automated process, efficient for various columns shapes like open or hollow sections as a result of progress in rolling techniques. Thus, square hollow sections (SHS) and rectangular hollow sections (RHS) are produced by rolling circular hollow sections (CHS), as visible in Fig. 1.5(a), themselves obtained from the cold-rolling of steel sheets welded close. They can also be crushed from a CHS into the desire box shape as shown Fig. 1.5(b).

1.3   Cold-forming effects

Strength enhancements   Regardless of the production route, cold-forming induce strength enhancements of stainless steel sections (up to 25% on the yield and ultimate strengths according to Baddoo [33]), reduction of the ductility and even more rounded stress-strain behaviour. These strength enhancements, concerning all the stainless steel grades, occurs mainly in the corner region but can extend to the faces of box sections as shown by Cruise and Gardner [32] (up to $4t$ of distance of the corner for boxes, where t is the member thickness). In order to develop not too-conservative relations, these effects deserve particular interest for the formulation of design guides. Furthermore, this phenomenon is much more pronounced for stainless steel than carbon steel.

In 1990, Coetsee *et al.* [34] were the first to investigate the strength enhancements of cold-formed stainless steel members. From this first work, many researchers interested in this field [32, 35, 36] and

Figure 1.2: Duplex stainless steel application - Sölvesborg Bridge, Sölvesborg, 2012 - Ljusarkitektur Architects.

provided equations to account this latter point based on experimental data. The work carried out by Cruise and Gardner [32] enable for instance the prediction of the 0.2% proof test $\sigma_{0.2}$ in both the corner and faces members sections. However, only the prediction of the 0.2% proof test is possible and none of the models are able to predict the full stress-strain behaviour as well as the ductility reduction. Recent works [37, 38] are trying to fill this void with more efficient models accounting for all the different effects of cold-forming, in order to improve the exactness of FE models (which require the full stress-strain cold-formed region behaviour).

Residual stresses   Cold-working induce residual stress patterns in the cold-formed cross-sections. They can be categorised as (i) bending residual stresses, (ii) membrane residual stresses and (iii) layering residual stresses. The first one occurs as a result of plastic deformation during forming and the second are induced during the seam-welding operation. Layering residual stresses are introduced during the coiling, uncoiling and leveling of the material sheets. These residual stresses can cause premature yielding associated with loss of stiffness and a reduction in the load-carrying capacity. At first glance, they should therefore be considered in the design of cold-formed members, but studies [39, 40, 41] have found that the influence of residual stresses on the general design is generally small.

1.4   Cold-formed columns uses and characteristics

Stainless steel, due to its useful aforementioned properties, is drawing more and more attention for civil engineering projects. It can be used for simple solutions as presented by Rossi [7], like cladding anchors, glass facade spiders, tie rods, fasteners or even rebar in concrete structure but it can also extend it range of application to more ambitious project such as power plant or arches in bridges (see Fig. 1.2), as exposed by Baddoo [33]. Naturally, they are used in aggressive environments, for example near salt water or in very heavily polluted areas.

Facing the difficulty to cover all the range of applications, this report focus only on cold-formed members subjected to compression forces since they are one of the major components in a structural
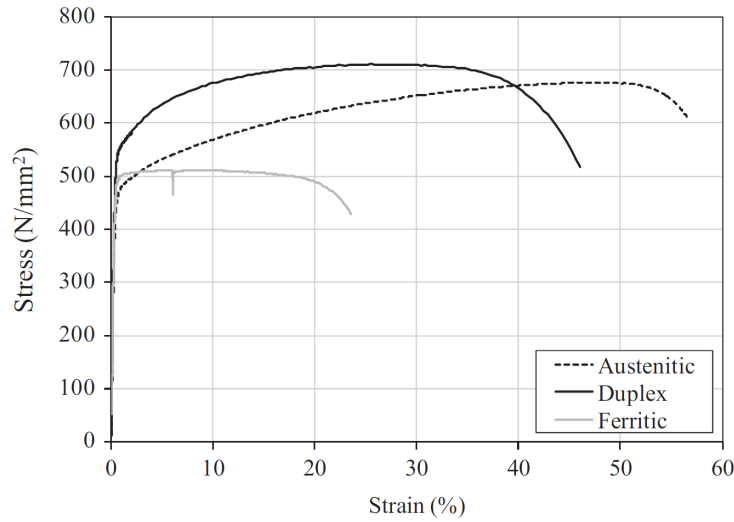
Figure 1.3: Comparison of stress-strain ($\sigma - \varepsilon$) relation for different stainless steel grades.

(a) Press braking.

(b) Cold rolling.
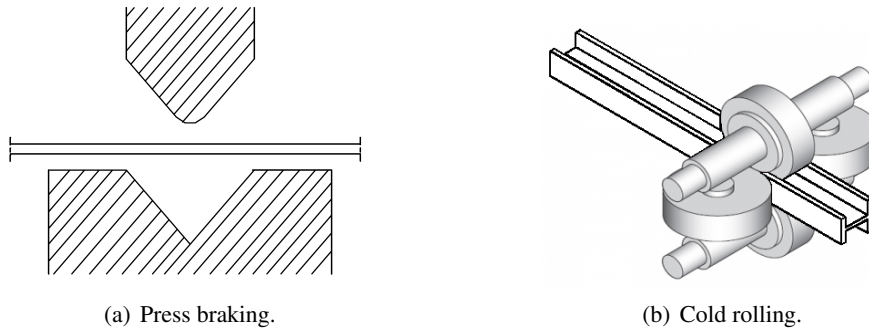
Figure 1.4: Cold-forming processes.

design. Their high efficiency turn it into an ideal solution for wall studs for instance. Cold-formed members can also be used as roof purlins, roof trusses or girders, but in those cases, bending forces are applied and go over our scope of study. The common column sizes, available to ArcelorMittal and listed in [28] are given hereinafter. Width-to-thickness ratio b/t from 1.5 to 600 are in this way theoretically available for SHS for example.

(i) 6m standard length and 0.5 to 8mm thickness.

(ii) 6 to 219.1mm diameter for CHS.

(iii) 12 to 300mm sides for SHS.

(iv) From 20×10 to 300×100mm for RHS.

Finally, several existing shapes for cold-formed stainless steel columns, developed to cover its extent range of applications, may be observed in Fig. 1.6.

(a) Cold rolling. (b) Press braking.
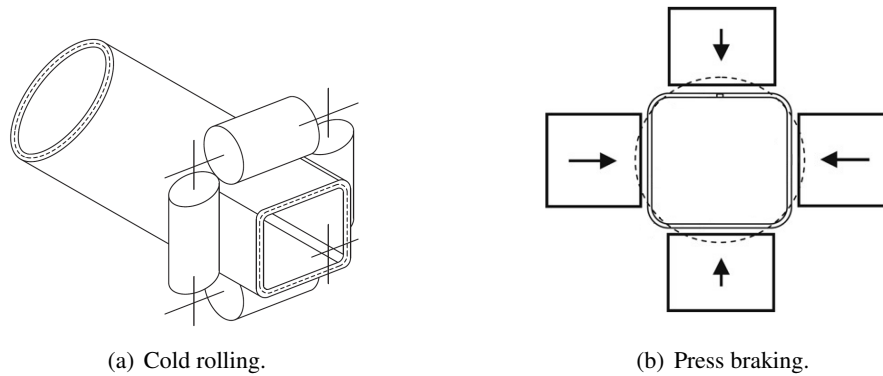
Figure 1.5: Cold-forming of a box section.
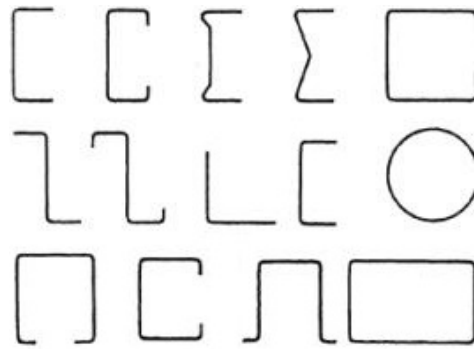
Figure 1.6: Typical cold-formed stainless steel members shapes.

2 Norms design rules and methods

This section present the different existing design rules for stainless steel columns in compression. Please note that a nomenclature is available at the end of this report.

2.1 Buckling

Columns, either carbon steel or stainless steel, are likely to buckle, due to their high slenderness. It can be flexural, local, torsional, global, distortional or a combination of those different buckling mode (see Fig. 1.7 for examples of typical members buckling). The local buckling (Fig. 1.7(a)) is for instance characterized by short and repeated buckling waves of the compressive portions of the element. The distortional buckling (Fig. 1.7(b)) occurs at an intermediate length of the buckling waves, resulting in the distortion and the rotation of the compression flange-lip.

The compression resistance of the section is also to verify, but is pretty often not the limiting factor in the designs. In order to account the buckling resistance, different methods have been proposed and progressively included in the norms standards. The compression resistance of the section is also to verify, but is pretty often not the limiting factor in the designs. In order to account the buckling resistance, different methods have been proposed and progressively included in the norms standards.

(a) Local.   (b) Distortional.   (c) Flexural-torsional.   (d) Flexural.
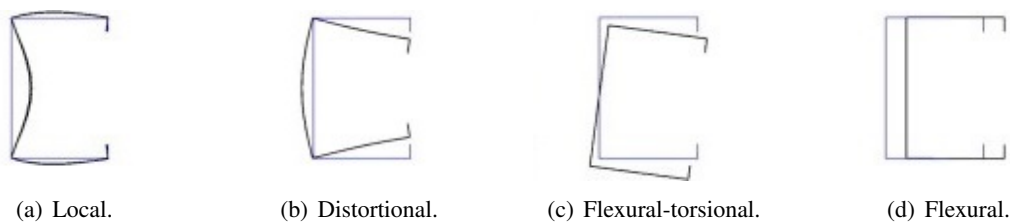
Figure 1.7: Lipped-channel column buckling modes examples.

2.2   Historical background

Despite earliest structural applications of stainless steel in the 1920-30s, the first dedicated design standard, the *Specification for the design of light gauge cold-formed stainless steel structural members*, was only published in 1968 by the American Iron and Steel Institute (AISI) [42], revised in 1974 [43]. However, the AISI standard has been challenged in North America by the American Society of Civil Engineers (ASCE) standard, first published in 1991 and revised in 2002 [2].This latter version superseded the AISI standard in North America. As others existing standards available worldwide, it is based on carbon steel design rules, modified to account for the different stress-strain behaviour of stainless steel (see Fig. 3).

The development of a design standard for stainless steel structures in Europe started in 1989 under the influence of the Steel Construction Institute (SCI) and a first version was published by Euro Inox in 1994 [44], revised in 2003 [45] and 2007 [46]. In 1996, on the basis of the guidance of the First Edition of the Euro Inox, the European Committee for Standardization (CEN) issued the 'pre-standard' Eurocode ENV 1993-1-4 *Design of steel structures, Supplementary rules for stainless steels* [47]. The current version of the European design standard applied to stainless steel, EN 1993-1-4 [1], was published in 2006, part of the Eurocode 3: Design of steel structures, and superseded the Euro Inox standard.

In the rest of the world, some countries decided to publish their own codes and some others to merely follow the recommendations of the North American standards or the ones from the ASTM International (previously the American Society for Testing and Materials, ASTM). Japan (1995), South Africa (1997), Australian/New Zealand (2001) or China (2002), with respectively [48], [49], [50] and [51] norm standards, are among the few countries which published their own codes. It can be noted that the Australian/New Zealand code is largely based on the American ones, but can occasionally lead to more reliable designs according to an experimental study carried out by Liu and Young [52].

Current desirable enhancements of the design rules are:

(i)   To be as reliable and precise as possible. Indeed, various experimental studies [4, 52, 53, 54, 55, 56] highlighted that norms standards are often too-conservative for the design of stainless steel cold-formed columns.

(ii)   To give more value to the cold-forming effect, also in case of fire.

(iii)   To appropriately recognised the non-linear material property and the geometric imperfection.

(iv)   To consider all the stainless steel grades.

(v)   To account for more intricate section geometries, with stiffeners for example.

With the aim of improving the designs standards, researchers have developed several different design methods. The methods advised by the European and North-American standards for the design of cold-formed stainless steel members in compression are presented hereinafter. Nevertheless, it is important to recognize that none of these design methods are theoretically correct and only turn a complicated non-linear problem into a simple working model for engineers, so each individual member does not have to be tested.

2.3 European design rules

The design of cold-formed stainless steel members in compression in the European standard is based on a section classification, for calculation of the compression and buckling resistances, itself using the Effective Width Method (EWM). This method, along with the way the cross-section classification use it, are here presented.

2.3.1 The Effective Width Method

The Effective Width Method has been developed to account the plate buckling effects in long slender plate elements ($L \gg b$ with length L and width b). It is a semi-empirical formulation attributed to von Kármán *et al.* in 1932 [57] and subsequently modified by Winter in 1947 [58]. The main idea of the method, as illustrated Fig. 1.8, is to account the strength reduction of local buckled elements by reducing its width b to an effective width b_{eff}. The effective width is then considered stressed with the yielding stress f_y and carrying the full compressive load whereas the non-effective portion is considered fully unstressed, which simplify the actual non-linear stress distribution that develops due to local buckling. The efficiency of the method lead it to be quickly adapted for steel columns, and thus to cold-formed stainless steel columns. The compressive strength of intricate cross-sections such as the ones exposed in Fig. 1.6 can be calculated by splitting it into single-plates taken as isolated elements. Each of the element is submitted to the EWM and the summation of all portions result in an effective section area of the member $A_{eff} \ll A$.
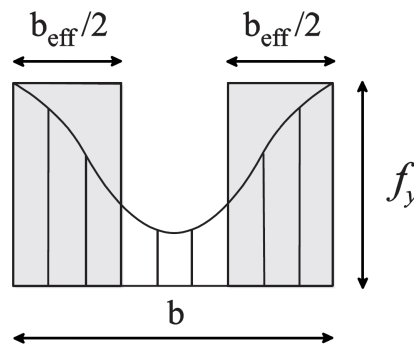
Figure 1.8: Effective Width Method concept.

This model utilise the critical plate buckling stress σ_{crl}, given by Eq. 1.1. It account for geometrical and material non-linearity imperfections and for boundary conditions and loading cases by mean of the plate buckling coefficient k, leading to more reliable calculations. Using Eq. 1.2, it is possible to calculate the plate slenderness ratio λ_p and in this way, to know the effective width b_{eff} with Eq. 1.3 or 1.4. These equations are the one adopted for stainless steel in the EN 1993-1-4 [1] for constantly stressed elements,

based on the equation proposed by Winter for carbon steel [58]. It should be noted that λ_p can also be calculated with Eq. 1.5 using the maximum design compressive stress at serviceability limit state $\sigma_{com,Ed,ser}$ instead of the yield stress f_y, as specified by Annex E of EN 1993-1-5 [59].

$$\sigma_{crl} = k \frac{\pi^2 E}{12(1-\nu^2)} \left(\frac{t}{b}\right)^2 \tag{1.1}$$

$$\lambda_p = \sqrt{\frac{f_y}{\sigma_{crl}}} \tag{1.2}$$

For cold-formed *internal* elements:

$$b_{eff} = \begin{cases} 1 & \text{for } \lambda_p \leq 0.673 \\ \left(0.772 - \frac{0.215}{\lambda_p}\right)\frac{b}{\lambda_p} & \text{for } \lambda_p > 0.673 \end{cases} \tag{1.3}$$

For cold-formed *outstand* elements:

$$b_{eff} = \begin{cases} 1 & \text{for } \lambda_p \leq 0.748 \\ \left(1 - \frac{0.231}{\lambda_p}\right)\frac{b}{\lambda_p} & \text{for } \lambda_p > 0.748 \end{cases} \tag{1.4}$$

$$\lambda_p = \sqrt{\frac{\sigma_{com,Ed,ser}}{\sigma_{crl}}} \tag{1.5}$$

In the Eurocodes EN 1993-1-1 for normal steel [3] and EN 1993-1-4 for stainless steel [1], the EWM is only applied to Class 4 cross-sections (see Section 2.3.2), through the calculation of an effective area A_{eff} with the reduction factor ρ as $A_{eff} = \rho A$. ρ is naturally calculated with the help of Eq. 1.3 or 1.4 and depend on geometric and material properties. Indications are given in section 5.2.3 of EN 1993-1-4 [1] for cold-formed stainless steel members. The ρ-λ curves of EN 1993-1-4 [1] are plotted Fig. 1.9 and compared with provisions of ASCE standard [2] (see Section 2.4.1). A discontinuity can be noticed for the Eurocode formulations, due to the adaptation of the formulas for stainless steel members.

Finally, the EWM is considered as one of the principal design method for columns and beams, included in the majority of design standards, mainly due to its simplicity of application. However, as denoted by Batista [60], the factor k of Eq. 1.1 is defined according to empirical studies, which result in large statistical deviations when theoretical and experimental results are compared. The incorporation of distortional buckling can also be awkward and determine the effective width of sections with intermediate-stiffeners added to the plates is cumbersome. The EWM is also often seen as a 'black box-type' model, so equations origins are not always obvious for users. As shown in the following, despite improvements added to the method at each new codes version, new structural design methods are developed and currently challenge the EWM.

2.3.2 The cross-section classification

The cross-section classification is a fundamental feature of modern carbon steel and stainless steel design codes. It is based on the influence of local buckling on their capacities, considering that lower are less prone to local buckling than highers one. The Eurocode EN 1993-1-1 [3] defined four classes for stainless steels, in the same way as for carbon steel, explained hereinafter using Baddoo and Burgan explanations [61]. The moment-rotation behaviour of each four classes defined in EN 1993-1-1 [3] may be observed Fig. 1.10.
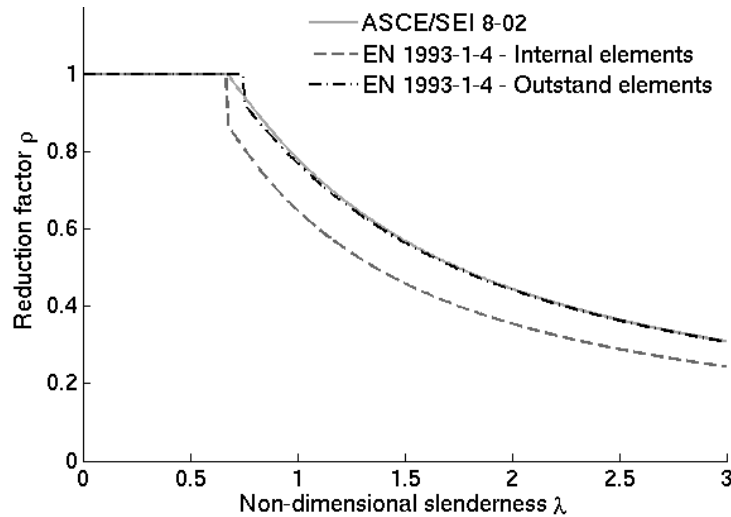
Figure 1.9: Buckling curves comparison of EN 1993-1-4 [1] and ASCE standard [2].
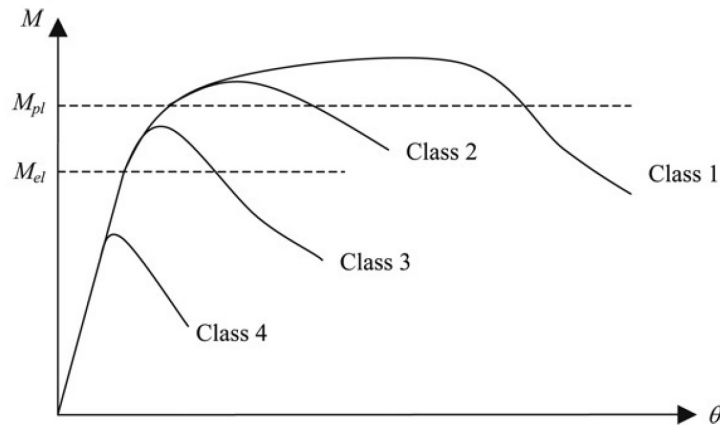
Figure 1.10: Cross-section classification of EN 1993-1-1 [3].

(i) Class 1 plastic: cross-sections that can develop their plastic moment capacity with the rotation capacity required for plastic analysis.

(ii) Class 2 compact: cross-sections that can develop their plastic moment capacity but with limited rotation capacity

(iii) Class 3 semi-compact: cross-sections that can reach the yield moment but local buckling prevents the development of the plastic moment capacity.

(iv) Class 4 slender: cross-sections in which local buckling is liable to prevent the development of the yield moment.

In the Eurocode EN 1993-1-4 [1], the classification is made comparing the width-to-thickness ratios (b/t) of the plate to a multiple of a factor ε (given in Eq. 1.6). The stress distribution along the section and the edge support conditions (i.e., internal or outstand) are also considered. For stainless steel sections,

the classification is given in Table 5.2 of EN 1993-1-4 [1]. The overall classification of intricate shapes, such as the ones of Fig. 1.6, require first the classification of each individual plate and then the final classification of the member is the one of the most slender constituent element. Hence, the beneficial interactions between flange and web are neglected.

Slenderness limits (on ε) in EN 1993-1-4 [1] are derived from few experimental results at the cross-section level. Based on more comprehensive experimental database, Gardner and Theofanous [62] shown that the current classification limits are overly conservative and may be relaxed.

$$\varepsilon = \sqrt{\frac{235}{f_y} \frac{E}{210000}} \tag{1.6}$$

In EN 1993-1-4 [1], once the cross-section classification has been made, the design of compression stainless steel members to buckling is very similar to these of carbon steel, using EN 1993-1-1 [3]. First, a cross-section design has to be made to yielding, local buckling and distortional buckling. The idea is to always satisfy Eq. 1.7, using Eq. 1.8 to calculate the design uniform compression strength $N_{c,Rd}$. It can be noticed that the Effective Width Method is thus applied only to class 4 elements, subject to local buckling.

$$\frac{N_{Ed}}{N_{c,Rd}} \leq 1,0 \tag{1.7}$$

$$N_{c,Rd} = \begin{cases} \frac{A f_y}{\gamma_{M0}} & \text{for classes 1,2 or 3} \\ \frac{A_{eff} f_y}{\gamma_{M0}} & \text{for class 4} \end{cases} \tag{1.8}$$

However, the cross-section resistance is pretty often not the design factor and a member design is necessary (except for members with a slenderness $\bar{\lambda} \leq 0.2$). The design to flexural, lateral-torsional, torsional and flexural-torsional buckling is therefore undertake, with the idea here to respect Eq. 1.9, using Eq. 1.10 to calculate the design buckling resistance of the compression member $N_{b,Rd}$, equals to the lowest value for all types of buckling. Eq. 1.10 use again the EWM for the class 4 elements prone to local buckling.

$$\frac{N_{Ed}}{N_{b,Rd}} \leq 1,0 \tag{1.9}$$

$$N_{b,Rd} = \begin{cases} \frac{\chi A f_y}{\gamma_{M1}} & \text{for classes 1,2 or 3} \\ \frac{\chi A_{eff} f_y}{\gamma_{M1}} & \text{for class 4} \end{cases} \tag{1.10}$$

Furthermore, the reduction factor χ need to be calculated according to Eq. 1.11 with special provision of the EN 1993-1-4 for the calculation of $\bar{\lambda}$ and ϕ. Indeed, $\bar{\lambda}$ is calculated according to Eq. 1.12 (with anew use of the EWM) and ϕ (Eq. 1.13) is a value depending on an imperfection factor α, a limiting slenderness $\bar{\lambda}_0$ and the already known slenderness $\bar{\lambda}$. For cold-formed stainless steel members, EN 1993-1-4 [1] recommend the values $\alpha = 0,49$ and $\bar{\lambda}_0 = 0,40$ for flexural buckling and $\alpha = 0,34$ and $\bar{\lambda}_0 = 0,20$ for torsional and torsional-flexural buckling. Those values are the same as the one adopted in the Second edition of the Euro Inox Design Manual [45] and account for the non-linear stress-strain curve of stainless steel. The experimental studies used to set α and $\bar{\lambda}_0$ are referenced in the commentary of this manual [63].

$$\chi = \frac{1}{\phi + \left[\phi^2 - \overline{\lambda}^2\right]^{0.5}} \leq 1 \tag{1.11}$$

$$\overline{\lambda} = \begin{cases} \sqrt{\dfrac{Af_y}{N_{cr}}} & \text{for classes 1,2 or 3} \\[2ex] \sqrt{\dfrac{A_{eff}f_y}{N_{cr}}} & \text{for class 4} \end{cases} \tag{1.12}$$

$$\phi = 0,5(1 + \alpha(\overline{\lambda} - \overline{\lambda}_0) + \overline{\lambda}^2) \tag{1.13}$$

The design procedure is similar to all the buckling modes (with design of the nature of Eq. 1.9) and the lowest value is considered as the critical buckling strength of the member. Thus, the buckling design can be undertake for cold-formed stainless steel members, using the cross-section classification and the EWM of the Eurocode.

2.4   North-American design rules

2.4.1   Flexural buckling design in compression

For the design of cold-formed stainless steel members in compression, the ASCE standard [2] does not class the cross-section but require the use of the Effective Width Method to consider local buckling. A different approach has the one of EN 1993-1-4 [1] is nevertheless used in the North-America specification, leading to different values for the reduction factor ρ. Indeed, F_n, the least of the flexural and torsional-flexural buckling stress, known with Eq. 1.14 or 1.15 respectively, is calculated first. Then, the effective area A_{eff} can be computed through Eq. 1.19 (which is the Winter equation for carbon steel, unchanged for stainless steel). This is a very similar equation to Eq. 1.3 or 1.4, but here, F_n is required to compute the slenderness λ in Eq. 1.18. Differences between the two standards are visible Fig. 1.9. Once F_n and A_{eff} are known, the design axial strength, $\phi_c P_n$ can be calculated with Eq. 1.20.

For *flexural* buckling:

$$F_n = \frac{\pi^2 E_t}{(KL/r)^2} \leq F_y \tag{1.14}$$

For *torsional-flexural* buckling:

$$F_n = \frac{1}{2\beta}\left(\sigma_{ex} + \sigma_t - \sqrt{(\sigma_{ex} + \sigma_t)^2 - 4\beta\sigma_{ex}\sigma_t}\right) \tag{1.15}$$

Where:

$$\sigma_{ex} = \frac{\pi^2 E_0}{(K_x L_x / r_x)^2}\left(\frac{E_t}{E_0}\right) \tag{1.16}$$

$$\sigma_t = \left(\frac{1}{Ar_0^2}\right)\left(G_0 J + \frac{\pi^2 E_0 C_w}{(K_t L_t)^2}\right)\left(\frac{E_t}{E_0}\right) \tag{1.17}$$

$$\lambda = \sqrt{\frac{F_n}{F_{cr}}} \tag{1.18}$$

$$b_{eff} = \begin{cases} 1 & \text{for } \lambda_p \leq 0.673 \\ \left(1 - \frac{0.22}{\lambda}\right) \frac{b}{\lambda} & \text{for } \lambda_p > 0.673 \end{cases} \tag{1.19}$$

$$\phi_c = 0.85$$
$$P_n = A_{eff} F_n \tag{1.20}$$

In the previous equations, E_t represent the tangent modulus in compression, accounting for the non-linear stress-strain curve of stainless steel, given in Eq. 1.21.

$$E_t = \frac{E_0 F_y}{F_y + 0.002 n E_0 (\sigma/F_y)^{n-1}} \tag{1.21}$$

A full and detailed example of application of ASCE provisions for stainless steel [2] has been published by Lin *et al.* [64]. It can be noticed that iterations are necessary, as the calculation of E_t require the knowledge of the normal stress σ. Indeed, to calculate the buckling strength resistance, the applied stress is not necessary known, so assumptions and comparisons with the calculated F_n value are needed. This is why, although this method is operational, some other methods are currently developed and studied in North-America. The promising Direct Strength Method, presented below, is one of them.

2.4.2 The Direct Strength Method

The Direct Strength Method (DSM) is an other design method, currently challenging the EWM because of its simplicity and efficiency in the design of intricate cross-sections. Its origins, much more recent than the EWM, come from the study of distortional buckling of industrial steel storage racks at the University of Sidney [65, 66]. Then, the firsts formulas proposed at that time were progressively extended to local, distortional, flexural and flexural-torsional buckling by Schafer and Peköz [67], leading it to become one of the major design method for members in compression. Thus, it has been adopted for the design of cold-formed steel members in the North-American Specification [68] and in the Australian/New Zealand code [69]. However, the DSM has not currently been adopted for the design of stainless steel members, even if Becque *et al.* proposed an accurate full set of equations in 2008 [70], subsequently modified by Rossi and Rasmussen in 2013 [71] to offer more accurate results in the low slenderness range. The DSM-equations for stainless steel should nonetheless be integrated in future code versions, which is the reason why this method is mentioned here.

The fundamental idea behind the DSM lie in the capacity of software to predict the accurate elastic buckling stress f_0. This can be done with the finite strip method (FS) or the general beam theory method (GBT), freely accessible with non-commercial computational programs, respectively CUFSM [72] and GBTUL [73]. Then, the column strength is predicted from the calculation of a slenderness λ (yield stress to elastic buckling stress ratio) in conjunction with a strength curve, the latter being specific to a type of buckling mode and selected statistically from test data. For example, the DSM distortional buckling formulas for stainless steel design published by Rossi and Rasmussen [71] are given in Eq. 1.22 to 1.26.

$$\lambda_d = \sqrt{\frac{f_y}{f_{od}}} \tag{1.22}$$

For *austenitic* stainless steel, with $\lambda_d \leq 0.533$:

$$N_{cd} = \left[(1 - 1.88\lambda_d) \left(\frac{\sigma_u}{\sigma_{0.2}} - 1 \right) + 1 \right] N_y \qquad (1.23)$$

For *austenitic* stainless steel, with $\lambda_d > 0.533$:

$$N_{cd} = \left(\frac{0.8}{\lambda_d^{1.1}} - \frac{0.15}{\lambda_d^{2.2}} \right) N_y \qquad (1.24)$$

For *ferritic* stainless steel, with $\lambda_d \leq 0.533$:

$$N_{cd} = \left[(1 - 1.88\lambda_d) \left(\frac{\sigma_u}{\sigma_{0.2}} - 1 \right) + 1 \right] N_y \qquad (1.25)$$

For *ferritic* stainless steel, with $\lambda_d > 0.533$:

$$N_{cd} = \left(\frac{0.9}{\lambda_d^{1.1}} - \frac{0.20}{\lambda_d^{2.2}} \right) N_y \qquad (1.26)$$

The DSM establish a real improvement of the design, as it is a much more understandable process, using less complex strength equations and leading to more reliable results compare to the EWM, according to Schafer review [74]. Furthermore, it utilise the entire cross-section in the elastic buckling determination, accounting for web-flange interactions of the members. However, the cross-sectional shape is not included and in this way, the method is currently limited to 'pre-qualified sections, *i.e.* those respecting specific geometric parameters. The shift in the effective cross-section is not included either and a computational tool, for example those referred before ([72, 73]) is required, which could be sometimes penalizing. Those few drawbacks are the main reasons explaining why the DSM is not currently adopted in the Eurocodes, even if the DSM goal is to become a comprehensive procedure replacing the EWM.

3 Monte Carlo simulations

3.1 Monte Carlo method

The Monte Carlo method was invented by Stanislaw Ulam in the early days of electronic computing during the late 1940s. The name *Monte Carlo* refers to the famous casino in Monaco. Indeed, the important initial issue of the method was the generation of large series of random numbers. Interests in the method led it to extend quickly to a wide variety of tasks in the 1980s such as statistic or computational biology and now, Monte Carlo methods are used everywhere, from chemistry, economics and finance to physics and engineering.

As nowadays, generating random numbers is not a problem, the method is mainly used to generate sampling to study mathematical problems for which analytical solutions are unavailable. Monte Carlo method is thus used to study properties of system that behave in a random fashion, with random generations of variables describing the behaviour of the system. Different statistical distributions, such as normal or log-normal can be used in this process.

For this project Monte Carlo method will be used to generate 'random' sets of inputs for the numerical model, respecting measurements realised on stainless steel products. The inputs would next be used in a numerical model in order to simulate uncertainties and evaluate the impact on the response of the model.The data generation is detailed in Section 3.3 of Chapter 2.

3.2 Parameters subjected to uncertainties

The chosen parameters subjected to uncertainties for this project are given in Table 1.1. It can be noted that width b and depth h are considered with the same distribution, as this project focus on square hollow section.

Category	Parameters (unit)
Geometry	Width b and Depth h (mm)
	Thickness t (mm)
	Inner radius r_i (mm)
	Global imperfection factor e_0
	Local imperfection factor w_0
Material	Modulus of elasticity in the flat part E_f (N/mm^2)
	Yield stress in the flat part $\sigma_{0.2,f}$ (N/mm^2)
	Strain-hardening exponent in the flat part n_f
	Second strain-hardening exponent in the flat part $n'_{0.2,1.0,f}$
	Modulus of elasticity in the corner part E_c (N/mm^2)
	Yield stress in the corner part $\sigma_{0.2,c}$ (N/mm^2)
	Strain-hardening exponent in the corner part n_c
	Second strain-hardening exponent in the corner part $n'_{0.2,1.0,c}$

Table 1.1: Input parameters for the numerical model subjected to tolerances.

3.2.1 Geometric parameters

The geometric parameters of a column cover the classic outward dimensions, all represented Fig. 1.11 (except from the length L), as well as the global and local imperfections. It has been decided that, even if measurements have been done for the corner enhancement extend, this dimension would not be included in the Monte Carlo process, as the distribution of enhancement varies along the width of the column. Accurate proposed model would be used instead to include this parameter in the numerical model (see Section 1.1 of Chapter 2). Likewise, the eccentricity of the applied load is not included in the Monte Carlo process, as measurements of this value in laboratories and on construction sites are not available.

3.2.2 Material parameters

The key material parameters of this study are the modulus of elasticity E, the yield stress $\sigma_{0.2}$ and the two Ramberg-Osgood coefficient n and $n'_{0.2,1.0}$, both in the flat and corner parts. All those parameters are used in the adopted stress-strain model for the numerical simulations.
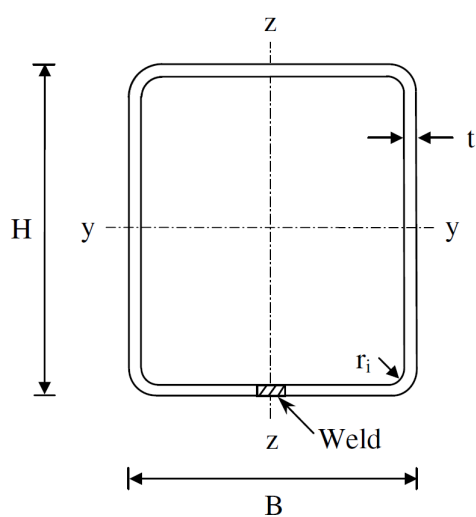
Figure 1.11: Section labelling convention (from Theofanous and Gardner [4]).

Chapter 2

Numerical modelling

This chapter is interested in the numerical work of this project. The first section presents the construction of the numerical model in Abaqus face to one experimental test. Choice of geometric imperfection factors and numerical parameters are discussed. The Python script used to submit almost one thousand numerical model is described in the second section. This script is next validate to 67 experimental tests available in literature. Finally, the generation of data, using Monte Carlo and statistical curve fitting methods is detailed in the last section of this chapter.

Contents

1   Numerical model

As the goal of this project is to run hundreds of numerical simulations, it is important to build a reliable numerical model. This model needs to be validated against previously conducted experimental tests. The tested column chosen for this step is the roll-formed duplex stainless steel (grade EN 1.4162) SHS $80 \times 80 \times 4$ - 2000 ($b \times h \times t - L$) described by of Theofanous and Gardner [4]. Nominal dimensions, measured dimensions and measured material properties are given in Table 2.1 to Table 2.3. In the first place the nominal dimensions of the column were used to build the FE model.

b_{nom} (mm)	h_{nom} (mm)	t_{nom} (mm)	L_{nom} (mm)
80	80	4	2000

Table 2.1: Nominal dimensions.

b_m (mm)	h_m (mm)	t_m (mm)	L_m (mm)	$r_{i,m}$	e_0	w_0
79.5	79.6	3.80	1999	3.40	0.41	-

Table 2.2: Measured dimensions.

E_f (MPa)	$\sigma_{0.2,f}$ (MPa)	n_f	$n'_{0.2,1.0,f}$	$\sigma_{u,f}$ (MPa)	E_c (MPa)	$\sigma_{0.2,c}$ (MPa)	n_c	$n'_{0.2,1.0,c}$
197200	657	4.7	2.6	773	210000	731	5.6	3.7

Table 2.3: Measured material properties.

As done in the test, the aim of the numerical simulation is to model a full non-linear buckling analysis. Basic modelling assumptions recommended by Gardner and Nethercot [39] and Ashraf *et al.* [5] were used to build the most accurate numerical model possible. Thus, the simulation is divided into two times, (i) elastic analysis firstly and (ii) a plastic analysis, which is necessary for the inclusion of geometric imperfections (see Section 1.3). The general purpose Finite Element software package Abaqus [6] is used in this project.

1.1   Material modelling

1.1.1   Theoretical material model

As previously mentioned, many models have been proposed in order to model the non-linear behaviour of stainless steel [22, 23], and this field of research is still active [24, 25]. The chosen material model is based on the one proposed by Gardner and Ashraf [23], given in Eq. 2.1. The only difference is that the equation is changed to pure elastic behaviour for $\sigma \leq \sigma_{0.2}/5$, as it is a requirement of Abaqus to have at least one point of pure elastic behaviour before the plastic one. The choice of $\sigma_{0.2}/5$ as an upper limit for the pure elastic part is a personal choice but corresponds to the fact that the first and second sub-equations of Eq. 2.1 lead to really close values for this range of stress.

Applying this model to a large set of data is convenient as the full stress-strain behaviour of a column can be determined from only two common parameters, $\sigma_{0.2}$ and E_0. Indeed, Eq. 2.2, 2.3 and 2.4 enables

the calculation of $E_{0.2}$, $\varepsilon_{t0.2}$ and $\varepsilon_{t1.0}$ respectively and specific values have been proposed for the strain-hardening exponents n and $n'_{0.2,1.0}$ by Afshan *et al.* [75] and for the $\sigma_{1.0}/\sigma_{0.2}$ ratio by Ashraf [76].

$$\varepsilon = \begin{cases} \frac{\sigma}{E_0} & \text{for } \sigma \le \sigma_{0.2}/5 \\ \frac{\sigma}{E_0} + 0.002 \left(\frac{\sigma}{\sigma_{0.2}}\right)^n & \text{for } \sigma_{0.2}/5 < \sigma \le \sigma_{0.2} \\ \frac{\sigma - \sigma_{0.2}}{E_{0.2}} + \left(\varepsilon_{t1.0} - \varepsilon_{t0.2} - \frac{\sigma_{1.0} - \sigma_{0.2}}{E_{0.2}}\right) \left(\frac{\sigma - \sigma_{0.2}}{\sigma_{1.0} - \sigma_{0.2}}\right)^{n'_{0.2,1.0}} + \varepsilon_{t0.2} & \text{for } \sigma > \sigma_{0.2} \end{cases} \quad (2.1)$$

$$E_{0.2} = \frac{\sigma_{0.2}E_0}{\sigma_{0.2} + 0.002nE_0} \quad (2.2)$$

$$\varepsilon_{t0.2} = 0.002 + \frac{\sigma_{0.2}}{E} \quad (2.3)$$

$$\varepsilon_{t1.0} = 0.01 + \frac{\sigma_{0.2}}{E} \quad (2.4)$$

1.1.2 Corner strength enhancement

As explained in Chapter 1, the cold-forming process induces strength enhancement in the corner region and therefore the corner stress-strain behaviour of the column differs from the flat part behaviour. Thus, key corner material parameters E_c and $\sigma_{0.2,c}$ need to be measured in the corner of the column before using them in Eq. 2.1. If proper measurements have not been conducted in the corner of the column, it is possible, as proposed by Ashraf [76], to use the same values as the one measured in the flat parts, except for $\sigma_{0.2,c}$ where Eq. 2.5, proposed by Cruise and Gardner [32], can be used. Nevertheless, this equation supposes that the ultimate stress of the flat material $\sigma_{u,f}$ has been measured, which is not always the case.

$$\sigma_{0.2,c} = 0.83\sigma_{u,f} \quad (2.5)$$

Once corner material parameters have been fixed, the corner enhancements are extended up to t for press-braked sections and $2t$ for roll-formed sections, as recommended by Ashraf *et al.* [5] and illustrated in Fig. 2.1. This reflects previously observed cold-forming mechanical property enhancements outside of the corner and this enables better numerical results to be achieved.

1.1.3 Abaqus material model

Using Eq. 2.1 for both flat and corner parts, the full stress-strain curve of the column was generated. Stress values were fixed from 0 up to 1200 MPa, with a fixed increment equal to 5 MPa, which means that the created curve is an approximation of the real curve made up of small segments. It should be noted that less points could have been entered.

Next, the point coordinates need to be entered as true stress σ_{true} and log plastic strain ε_{ln}^{pl} in Abaqus. Thus, Eq. 2.6 and 2.7 have been used before entering the points in the software.

$$\sigma_{true} = \sigma_{nom}(1 + \varepsilon_{nom}) \quad (2.6)$$

(a) Corner region plus *t*.   (b) Corner region plus 2*t*.
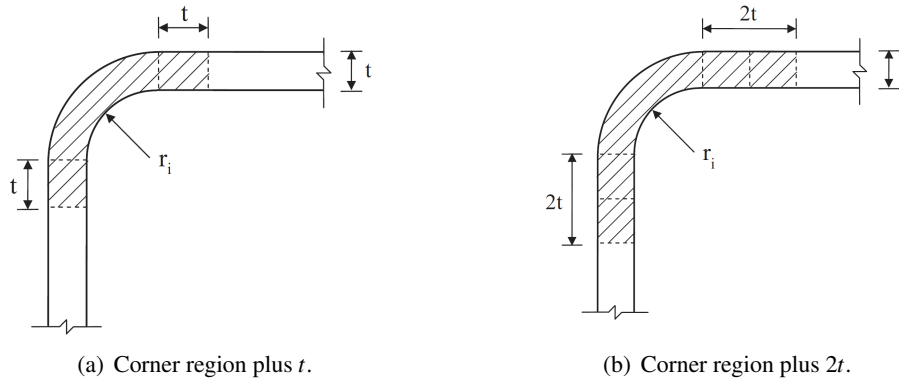
Figure 2.1: Different corner enhancement extent (from Ashraf *et al.* [5]).

$$\varepsilon_{ln}^{pl} = ln(1+\varepsilon_{nom}) - \frac{\sigma_{true}}{E} \qquad (2.7)$$

1.1.4 Residual stresses

As mentioned in Section 1.3 of Chapter 1, the cold-forming of the sections induces residual stresses, namely (i) bending residual stresses, (ii) membrane residual stresses and (iii) layering residual stresses. For numerical simulations, studies of Cruise and Gardner [77], Jandera and Machacek [78] and Key and Hancock [41] have come to the same conclusions, namely:

 (i) Bending residual stresses do not have to be explicitly introduced in a numerical model as they are inherently present in the measured material properties.

 (ii) Membrane residual stresses are relatively insignificant in stainless steel hollow sections and do not have to be modelled.

(iii) Layering residual stresses have very small influence on the ultimate load and do not have to be modelled as well.

   Consequently, residual stresses were not introduced in the numerical model but their influence on the stress-strain behaviour was present through the measured material values.

1.2 Boundary conditions and applied load

Usually, only one rotational degree of freedom is enabled at each end of the experimentally tested columns (using knife edges), as well as the vertical translation on top of it. As in Abaqus it is simple to apply any boundary conditions, both ends were pin ended in order to not favour any buckling direction. The vertical translation of the top end of the column is obviously still enabled.

   It has been decided to use a displacement controlled analysis which is more adapted for a non-linear buckling analysis. Thus, a displacement, incremented at each step of the analysis, is applied to a reference point located at the centre of the top of the column. This reference point is tied to the top edge to ensure

(i) an equal distribution of the displacement (and therefore the load) in the column and (ii) that the top end moves as a plan. To ensure the same motion of each point of the top end, these points were tied together. The tied condition was also applied at the bottom of the column.

1.3 Geometric imperfections

The incorporation of geometric imperfections is realised in two steps. An elastic buckling analysis is carried out first, in order to then use the elastic buckling shapes as initial geometric imperfections in the non-linear analysis. Thus, the first elastic global buckling shape multiplied by the global imperfection factor e_0 is used to simulate the global imperfection and in the same way, the first elastic local buckling shape times the local imperfection factor w_0 is used to simulate the local imperfection. In Abaqus, this is done using the keyword *IMPERFECTION.

In order to obtain accurate results from the numerical model, values employed for the global imperfection factor e_0 and the local imperfection factor w_0 in the latter are the ones measured during experiments. In the case of a lack of data, recommendations of Ashraf *et al.* [5] and of Gardner and Nethercot [39] can be used instead. Values of $L/1500$ can therefore be used for the global imperfection factor e_0 and Eq. 2.8 is used to compute the local imperfection factor w_0. These values have been shown to provide the best agreement between experimental and numerical results. However, using these values corresponds to the use of 'averages', which is not desirable keeping in mind the goal of this project. This is why it has been preferred to use measured data when they are available.

$$w_0 = 0.023 \left(\frac{\sigma_{0.2}}{\sigma_{cr}} \right) t \tag{2.8}$$

1.4 Numerical parameters

Element type   Owing to the thin-walled nature of tubular sections, shell elements were employed to discretise the model. As already used in previous studies, the four-noded doubly curved shell element with reduced integration S4R [6] were utilised in this study.

Mesh size   A uniform mesh size equal to the thickness t was used in the model. As the mesh size has an important impact on the results, a convergence study has been conducted to validate this choice. It has been decided to test six different mesh sizes. The mesh size in the flat part M_f was ranging from 2 ($t/2$) to 32mm ($8 \times t$) and the mesh size in the corner M_c was equal to 2 or 4mm (bigger size elements in the corner would lead to use of rectangular elements instead of square ones, as the corners are quite small.

The mesh inputs of this study are given in Table 2.4 and the corresponding results are given in Table 2.5 and plotted in Fig. A.1. The numerical elastic buckling load $F_{u,el,FE}$ was compared to the Euler elastic buckling load $F_{u,el}$ equals to 545.7 *kN* for the SHS 80 × 80 × 4 - 2000 studied experimentally by Theofanous and Gardner [4]. Simulation times (elastic and plastic simulations), $F_{u,FE}/F_{u,Test}$ ratio and $\Delta_{u,FE}/\Delta_{u,Test}$ ratio are also given.

According to Table 2.5 and Fig. A.1, the best $F_{u,FE}/F_{u,Test}$ ratio is obtained for the 1st model. Furthermore, this is also the model presenting the best $\Delta_{u,FE}/\Delta_{u,Test}$ ratio, as well as a ratio $F_{u,el,FE}/F_{u,el}$ very close to one. The simulation time associated to this model is quite high but is not penalising in relation to the quality of the obtained results. Thus, the 1st model is considered as the most accurate one and a mesh size equals to the thickness t of the model is kept.

Improvement of existing design rules for cold-formed stainless steel hollow sections under compression forces using numerical modelling and Monte Carlo simulations

Model	Mesh		
	N	M_f (mm)	M_c (mm)
1st	38000	4	4
2nd	148000	2	2
3rd	80000	4	2
4th	22000	8	4
5th	14000	16	4
6th	12000	32	4

Table 2.4: Convergence study models.

Model	Time (s)	$F_{u,el,FE}/F_{u,el}$	$F_{u,FE}/F_{u,Test}$	$\Delta_{u,FE}/\Delta_{u,Test}$
1st	1919	1.017	1.056	0.757
2nd	10966	1.020	1.133	0.602
3rd	5249	1.020	1.133	0.602
4th	1254	1.016	1.129	0.603
5th	729	1.008	1.176	0.279
6th	623	1.000	1.117	0.695

Table 2.5: Convergence study results.

1.5   Validation of the model

Using the measured dimensions (Table 2.2) instead of the nominal dimensions (Table 2.1), the final numerical results obtained for the SHS 80 × 80 × 4 - 2000 tested experimentally by Theofanous and Gardner [4] are given in Table 2.6. Applied to that specific column, $F_{u,el,FE}/F_{u,el} = 0.94$, being -5.5% of relative error to the theoretical elastic buckling load and $F_{u,FE}/F_{u,Test} = 1.06$, being 5.64% of relative error to the experimental buckling load. As the errors for this particular column are low, the numerical model built previously has been judged satisfactory to serve as a basis in the next step of this project, namely the application of the the Monte Carlo method.

Time (s)	$F_{u,el,FE}/F_{u,el}$	$F_{u,FE}/F_{u,Test}$	$\Delta_{u,FE}/\Delta_{u,Test}$
1807	0.94	1.06	0.67

Table 2.6: Final model construction results.

2   Python scripting

2.1   Python script

As the goal of this project is to run hundreds of numerical models, it is convenient to use a script to run them all in one loop instead of modifying manually each model. For that purpose, a script has been written in Python [79]. Python is a powerful object-oriented programming language easily usable jointly with Abaqus, as in the background, Abaqus is scripted in Python. An overview of the loop that the Python script realises is displayed Fig. 2.2. The Python script goal is mainly to automate the steps that have been realised manually in the construction of the numerical model developed in section 1. It enable

the user to easily submit and post-analyse jobs without any efforts. Details of the code steps are given in the sections hereinafter.
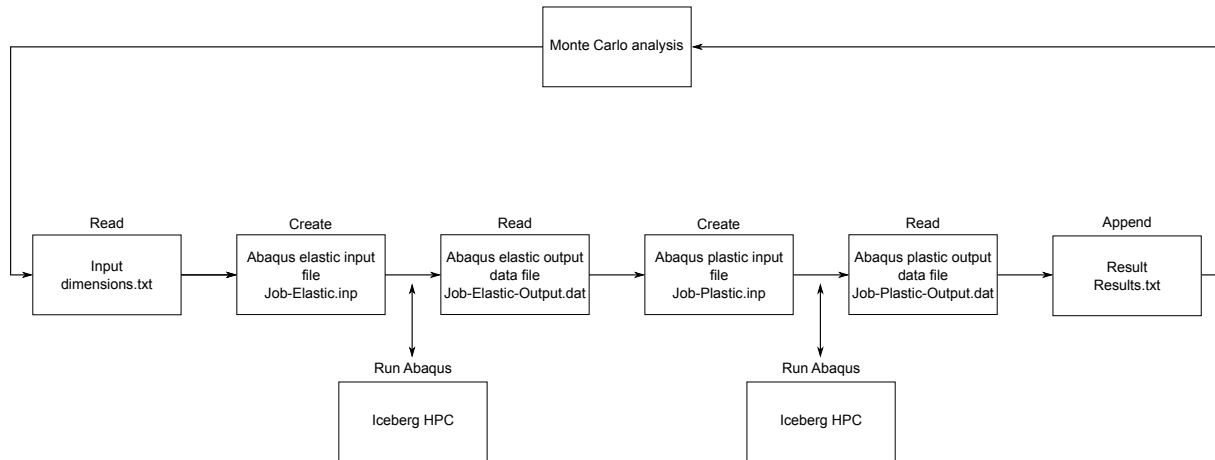
Figure 2.2: Overview of the Python script loop.

2.1.1 Dimensions reading

Before submitting a column or several columns, the script stores all the geometrical and material values associated to each column in one list and one dictionary: *all_columns_names* and *all_columns_dictionary* respectively. The list *all_columns_names* obviously contain all the names of the column and the dictionary *all_columns_dictionary* contains the list with all the important parameters associated to a column as a value, associated with a key having the name of the column. For instance, column name and column parameters can be called in Python shell with:

```
>>> all_columns_names[0]
'theofanous2009_a_0'
>>> all_columns_dictionary[all_columns_names[0]]
['79.50000', '79.60000', '3.80000', '1999.00000', '3.40000',
'1.33267', '0.12037', '197200.00000', '657.00000', '755.55000',
 '4.70000', '2.60000', '51603.70896', '0.00533', '0.01333',
'210000.00000', '731.00000', '840.65000', '5.60000', '3.70000',
 '49792.40999', '0.00548', '0.01348', '0.30000']
>>>
```

When the code is started, the first initial step is therefore the reading of the file **dimensions.txt**, generated from an Excel sheet containing all the important data, obviously written in a specific order. The name of the column is written first, then the geometrical parameters, the material properties in the flat part next, the material properties in the corner part next and finally the Poisson's ratio.

The name of the column are chosen to be quickly understandable: the first author of the experimental paper is written, with the year of paper publication next and a column index for that author at the end. The additional 0 means that it corresponds to the original column, as close from the one tested as possible.

For instance, the SHS 80 × 80 × 4 - 2000 tested by Theofanous and Gardner [4] and mentioned in section 1 is given the name *theofanous2009_a_0*.

2.1.2   Elastic analysis

After reading the column parameters, the Python script inject them into a 'virgin' elastic Python file. It means that the corresponding inputs (geometrical and material properties) are written at the correct place into a Python file which is next used to generate the Abaqus input file. That 'virgin' elastic Python file is written using a function of the main Python script. All the parameters (geometrical and material) of any column can be injected in that function, which generate a Python file which can afterwards generate an Abaqus input file.

That 'virgin' elastic Python file has been included in the main Python script in analysing the **abaqus.rpy** generated automatically by Abaqus when the user builds a model. It is a very specific file which is only valid for the particular topic of this project, the non-linear analysis of cold-rolled stainless steel square hollow section. Press-braked sections are indeed very seldom for SHS stainless steel and thus, the corner enhancement is always fixed to 2*t* (see Fig. 2.1(b)). Otherwise, the 'virgin' elastic Python file respects all the modelling assumptions described in section 1. The generated elastic Python file is understandably named, such as **theofanous2009_a_0_elastic.py**.

The elastic Python file is then send to Iceberg (the HPC of the University of Sheffield) in a folder named as the column name and executing a remote command on the server through the main Python script, an Abaqus input file **Job-Elastic.inp** is generated on the server. Executing a new remote command, the Python main script submit the **Job-Elastic.inp** to the Iceberg Abaqus calculator. The elastic submission is usually quite fast and the main Python script waits for 5 minutes in order to make sure that the submission is over. When the submission is completed, a series of **Job-Elastic-Output** files is created. The most important one at this step is the file **Job-Elastic-Output.dat**, containing the buckling values associated with each buckling mode.

2.1.3   Plastic analysis

First local buckling mode detection   Once the elastic analysis is completed, it is time to start the plastic one. However, results from the elastic analysis are required in order to include the geometric imperfections (see Section 1.3 of current chapter). In this way, it is necessary to detect the first local buckling mode of the column.

In order to do this, the main Python script downloads the file **Job-Elastic-Output.dat** from the server. As the length of the file may vary from one analysis to another, it has been decided to browse the file backwards, as the end of the file is always the same. An example of **Job-Elastic-Output.dat** file end is written hereinafter. Browsing the buckle table frontward, the idea was to use the symmetric properties of the column, so that any global buckling mode would repeat once (on both X and Y axes) and so the mode associated with the first unique value to be meet correspond to the first local buckling mode. Browsing the file backward uses the same idea, and when two equal values are encountered, the function returns the first local buckling mode as the one located two positions before.

However, is has been noted that as the columns are finally non-symmetric, the first local buckling mode is not correctly detected, as no buckling loads does repeat, although very close . By chance, the

code returns (in a way due to an error) that the first local buckling mode is the number 3, which is true in a majority of the buckling analysis. Indeed, the first and second modes always correspond to the first order global buckling along the X and Y axes and so the third mode is the first local one, as quite often, the second order global buckling does not develop in the column.

```
MODE NO       EIGENVALUE



     1        2.48844E+05
     2        2.49805E+05
     3        5.55599E+05
     4        5.55692E+05
     5        5.59998E+05
     6        5.60297E+05
     7        5.67527E+05



        THE ANALYSIS HAS BEEN COMPLETED




                        ANALYSIS COMPLETE
                        WITH      565 WARNING MESSAGES ON THE DAT FILE
                        AND         1 WARNING MESSAGES ON THE MSG FILE




    JOB TIME SUMMARY
      USER TIME (SEC)      =    59.860
      SYSTEM TIME (SEC)    =    2.1700
      TOTAL CPU TIME (SEC) =    62.030
      WALLCLOCK TIME (SEC) =          64
```

Plastic stress-strain points generation   As the model runs a non-linear buckling analysis, plastic stress-strain curves need to be entered in Abaqus. The stress-strain points for both flat and corner parts are therefore generated from the main Python script using two functions, *create_plastic_points_flat* and *create_plastic_points_corner* respectively. Using stress points ranging from 0 up to 1200 MPa with an increment of 5 MPa, the corresponding strain points are created using Eq. 2.1 (in respect of flat or corner parameters). Then, they are converted for Abaqus with Eq. 2.6 and Eq. 2.7. All negative strain points are then removed, corresponding points of the stress list are also removed and the first strain point is fixed to zero. Finally, the stress-strain curve is written on a string, in a format of a tabular (one line for each point).

Plastic analysis   When the first local buckling mode has been detected and the plastic points created, the main Python script is ready to create, in the same fashion as the previously conducted elastic analysis, a plastic Python file from a 'virgin' plastic python file. That file is remarkably similar to the 'virgin'

Improvement of existing design rules for cold-formed stainless steel hollow sections under compression forces
using numerical modelling and Monte Carlo simulations

elastic Python file used formerly, with just a few nuances. For instance this time, the analysis is changed from an elastic buckling one to a non-linear plastic one, the plastic parameters are added along with the elastic ones and it is asked to use the buckling shapes of the elastic analysis as initial imperfections. However, the idea is the same, and hence, the main script generate a plastic python file, such as **theofanous2009_a_0_plastic.py**.

That file is sent to the server and this time, executing a remote command on the server, an Abaqus input file **Job-Plastic.inp** is generated. This file is then submitted to the Iceberg Abaqus calculator and after 30 minutes of waiting time, the plastic submission is supposed to be completed. A series of **Job-Plastic-Output** files is created.

2.1.4 Results reading and saving

The outputs in which this study is interested are mainly the numerical elastic buckling load $F_{u,el,FE}$ and the numerical buckling load $F_{u,FE}$. It can also be interesting to request the numerical end-shortening at buckling load $\delta_{u,FE}$ as well as the numerical buckling displacement at mid-length $\Delta_{u,FE}$. These values are probably written down somewhere in the **Job-Plastic-Output.dat** file but it has been judged simpler to request them using an external and new python file.

Node detection   To obtain the displacement at mid-length of the column, is it necessary to know the closest node number on the face of interest. As from the code point of view, no visual analysis is possible, it is also important to know which face had buckled. Indeed, the column can buckle around the Y-axis and that has been named a X node number as the displacement of the column occurs along the X-axis, as represented in Fig. 2.3(a). Or, on the contrary, the column buckle around the X-axis, resulting in a displacement along the Y-axis as visible in Fig. 2.3(b), named therefore a Y node number . In the case of a buckling occurring in the two directions, the code will only return the displacement of the point located in the middle of the most buckled face. The final numerical buckling displacement at mid-length $\Delta_{u,FE}$ is judged to be the maximum of the X and Y axis displacement.

(a) X-axis displacement.   (b) Y-axis displacement.
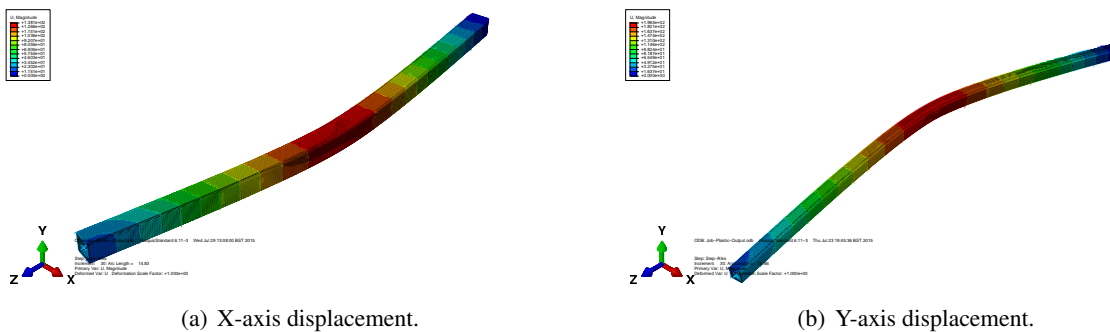
Figure 2.3: X and Y axes buckling directions.

Using two functions, two Python scripts, executable by Abaqus on the server, are generated locally. The function asks Abaqus to use one of its inherent module called 'findNearestNode'. Using the mid-length real point coordinates of the column, Abaqus returns the nearest node number. So theses scripts

are again sent to Abaqus, submitted from the main Python script and the values obtained from these two runs are stored with the names *node_number_X* and *node_number_Y*.

Results extraction   Finally, knowing the node number the closest of each center faces, a last Python file named for instance **theofanous2009_a_0_extract.py** is generated. This last Python file request that the buckling value, the end-shortening and the displacements at mid-length of each face are written down in different rpt files named for instance **LD_theofanous2009_a_0.rpt**, **LLD_X_theofanous2009_a_0.rpt** and **LLD_Y_theofanous2009_a_0.rpt** respectively. These .rpt files contain the evolution of each of the outputs in the course of the plastic simulation steps. Graphs representing respectively the end-shortening, the displacement at mid-length of the 'X-face' and the displacement at mid-length of the 'Y-face' each time versus the load are also generated and saved as .png files.

The whole of the folder containing all the files used and generated during the full submission of the column is ultimately retrieved on the computer and with a final function, the main Python script browse the .rpt files quoted hereinbefore and find the final outputs. There are written down in the following order in the **Results.txt** file:

(i) Name of the column.

(ii) Numerical elastic buckling load $F_{u,el,FE}$ in kN.

(iii) Numerical buckling load $F_{u,FE}$ in kN.

(iv) Numerical end-shortening at buckling load $\delta_{u,FE}$ in mm.

(v) Numerical buckling displacement at mid-length along the X-axis $\Delta_{u,X,FE}$.

(vi) Numerical buckling displacement at mid-length along the Y-axis $\Delta_{u,Y,FE}$.

2.1.5   Submission threads

As the full submission of a column takes on average around 70 minutes, it has been decided to submit several column in the same time using threads in Python. It has been decided to limit the maximum number of simultaneous submission to 10 to counterbalance the interpenetration problems that can occur with several submission at a time. In the Python main script, a loop was implemented to submit 10 new files each 4000 seconds (approximately the average time used by one simulation). A top loop enable to submit as many files as desired, respecting the 10 maximum submission at a time with the 4000 seconds waiting time.

2.2   Script validation

2.2.1   Experimental results data collection

In order to validate the Python script and the numerical model built, the script was firstly used to simulate a total of 67 previously conducted flexural buckling tests. A summary of the origin of the collected data is given in Table 2.7. For each test, using the measured geometrical and material properties, the elastic buckling load $F_{u,el}$ was computed, and the experimental buckling load $F_{u,Test}$ was collected. Although rarely available, the displacement at mid-length of the column at the buckling load was also collected.

Reference	Number of tests	Material grade
Theofanous and Gardner [4]	6	EN 1.4162 (Duplex)
Afshan and Gardner [54]	7	EN 1.4003 and EN 1.4309 (Ferritic)
Huang and Young [55]	8	EN 1.4162 (Duplex)
Liu and Young [52]	8	EN 1.4301 (Austenitic)
Rasmussen and Hancock [80]	3	EN 1.4307 (Austenitic)
Gardner and Nethercot [81, 82]	8	EN 1.4301 (Austenitic)
Young and Lui [83]	10	EN 1.4162 (Duplex)[1]
Gardner *et al.* [84]	6	EN 1.4318 (Austenitic)
Ala-Outinen and Oksanen [85]	2	EN 1.4301 (Austenitic)
Talja and Salmi [86]	3	EN 1.4301 (Austenitic)
Talja [87]	6	EN 1.4318 (Austenitic)

[1] Supposed grade as only the nuance is specified.

Table 2.7: Summary of available flexural buckling tests conducted on roll-formed stainless steel square hollow sections.

2.2.2   Comparison with experimental results

Once the data collection has been done, the Python script was used to submit all these 67 different columns. Table 2.8 presents the obtained result ratios. The ultimate load is generally well-predicted, with an average equals to 0.98 and a small coefficient of variation (COV) of 0.12, which indicates that the results are not too spread around the average. The elastic buckling load is however less well predicted, with an average of 0.84 with a COV equals to 0.24. Thus, the elastic buckling load is quite often underestimated and even sometimes far from the computed Euler buckling load (see sub-model young2006_f_0 tested by Young and Lui [83] for instance). Furthermore, the COV is too important and indicate that the model is not clearly reliable in this prediction. Finally, compared to the small amounts of available data, the displacement at mid-length of the columns is badly predicted. Indeed, even if the ratio average is equal to 1.01, the corresponding COV of 1.04 is far too large and so the ratio can not be deemed correct. It should be noted that the simulations gardner2006_e_0 and talja2002_e_0 have failed, despite several attempts to run it.

In view of the results, the Python script has been judged accurate in the prediction of the ultimate buckling load, average for the computation of the elastic buckling load and not relevant in the estimation of the displacement at mid-length. The inaccuracy in the prediction of the displacement at mid-length can nevertheless be explained by the idea that it is hard to detect the buckling moment. Indeed, idealised buckling would suppose that the column is progressively loaded with no displacement at mid-length, and suddenly, it buckles, with the corresponding displacement. However, both in experimental and numerical tests, the displacement is progressive and after the peak load (ultimate buckling load), the displacement continue to increase. As the load is applied through steps, it is quite hard to obtain a correct value for this displacement at mid-length.

Reference	Name in Python script	Name in paper	$F_{u,el,FE}/F_{u,el}$	$F_{u,FE}/F_{u,Test}$	$\Delta_{u,FE}/\Delta_{u,Test}$
Theofanous and Gardner [4]	theofanous2009_a_0	$80 \times 80 \times 4$ 2000	0.94	1.06	0.67
	theofanous2009_b_0	$80 \times 80 \times 4$-1200	0.93	0.88	1.45
	theofanous2009_c_0	$60 \times 60 \times 3$-2000	0.94	1.02	1.04
	theofanous2009_d_0	$60 \times 60 \times 3$-1600	0.94	1.02	0.72
	theofanous2009_e_0	$60 \times 60 \times 3$-1200	0.94	1.02	0.72
	theofanous2009_f_0	$60 \times 60 \times 3$-800	0.92	1.02	0.73
Afshan and Gardner [54]	afshan2013_a_0	SHS $80 \times 80 \times 3$-1577	0.94	0.99	0.98
	afshan2013_b_0	SHS $80 \times 80 \times 3$-2077	0.94	0.77	4.38
	afshan2013_c_0	SHS $80 \times 80 \times 3$-2577	0.95	1.11	0.60
	afshan2013_d_0	SHS $60 \times 60 \times 3$-1177	0.93	1.06	0.43
	afshan2013_e_0	SHS $60 \times 60 \times 3$-1577	0.93	1.11	0.38
	afshan2013_f_0	SHS $60 \times 60 \times 3$-2077	0.94	1.17	0.45
	afshan2013_g_0	SHS $60 \times 60 \times 3$-2577	0.94	1.20	0.65
Huang and Young [55]	huang2013_a_0	C2L550	0.36	0.96	-[1]
	huang2013_b_0	C2L900	0.86	1.09	-[1]
	huang2013_c_0	C2L1200	0.96	1.01	-[1]
	huang2013_d_0	C2L1550	0.97	1.04	-[1]
	huang2013_e_0	C3L550	0.92	0.93	-[1]
	huang2013_f_0	C3L900	0.95	0.84	-[1]
	huang2013_g_0	C3L1200	0.95	1.07	-[1]
	huang2013_h_0	C3L1550	0.96	1.05	-[1]
Liu and Young [52]	liu2003_a_0	S1L1200	0.13	0.73	-[1]
	liu2003_b_0	S1L2000	0.38	0.73	-[1]
	liu2003_c_0	S1L2800	0.72	0.81	-[1]
	liu2003_d_0	S1L3600	0.96	0.94	-[1]
	liu2003_e_0	S2L1200	0.85	0.93	-[1]
	liu2003_f_0	S2L2000	0.90	0.98	-[1]
	liu2003_g_0	S2L2800	0.91	0.97	-[1]
	liu2003_h_0	S2L3600	0.91	1.11	-[1]
Rasmussen and Hancock [80]	rasmussen1993_a_0	S1L1000C	0.95	0.82	-[1]
	rasmussen1993_b_0	S1L2000C	0.96	1.05	-[1]

Table 2.8 – *Continued from previous page*

Reference	Name in Python script	Name in paper	$F_{u,el,FE}/F_{u,el}$	$F_{u,FE}/F_{u,Test}$	$\Delta_{u,FE}/\Delta_{u,Test}$
	rasmussen1993_c_0	S1L3000C	0.97	1.30	-[1]
Gardner and Nethercot [81, 82]	gardner2004_a_0	SHS 80 × 80 × 4-LC-1.9 m	0.95	1.07	-[1]
	gardner2004_b_0	SHS 80 × 80 × 4-LC-2 m	0.93	0.88	-[1]
	gardner2004_c_0	SHS 100 × 100 × 2-LC-2 m	0.35	0.96	-[1]
	gardner2004_d_0	SHS 100 × 100 × 3-LC-2 m	0.82	0.85	-[1]
	gardner2004_e_0	SHS 100 × 100 × 4-LC-2 m	0.94	0.96	-[1]
	gardner2004_f_0	SHS 100 × 100 × 6-LC-2 m	0.92	0.84	-[1]
	gardner2004_g_0	SHS 100 × 100 × 8-LC-2 m	0.89	0.83	-[1]
	gardner2004_h_0	SHS 150 × 150 × 4-LC-2 m	0.28	0.82	-[1]
Young and Lui [83]	young2006_a_0	SHS1L1000	0.90	1.02	-[1]
	young2006_b_0	SHS1L1500	0.92	1.10	-[1]
	young2006_c_0	SHS1L2000	0.93	1.01	-[1]
	young2006_d_0	SHS1L2500	0.93	1.08	-[1]
	young2006_e_0	SHS1L3000	0.93	1.09	-[1]
	young2006_f_0	SHS2L1000	0.23	0.82	-[1]
	young2006_g_0	SHS2L1500	0.51	0.89	-[1]
	young2006_h_0	SHS2L2000	0.90	1.10	-[1]
	young2006_i_0	SHS2L2500	0.95	1.06	-[1]
	young2006_j_0	SHS2L3000	0.96	1.11	-[1]
Gardner *et al.* [84]	gardner2006_a_0	80 × 80 × 3 − C850 (1.15m)	0.81	1.03	-[1]
	gardner2006_b_0	80 × 80 × 3 − C850 (1.85m)	0.94	0.93	-[1]
	gardner2006_c_0	80 × 80 × 3 − C850 (2.85m)	0.94	1.02	-[1]
	gardner2006_d_0	100 × 100 × 3 − C850 (1.45m)	0.50	0.86	-[1]
	gardner2006_e_0	100 × 100 × 3 − C850 (2.25m)	-[2]	-[2]	-[1]
	gardner2006_f_0	100 × 100 × 3 − C850 (3.55m)	0.96	0.97	-[1]
Ala-Outinen and Oksanen [85]	ala_outinen1997_a_0	N1	0.85	0.97	-[1]
	ala_outinen1997_b_0	N2	0.85	0.97	-[1]
Talja and Salmi [86]	talja1995_a_0	RHS-1a - CC-2	0.90	0.90	-[1]
	talja1995_b_0	RHS-1a - CC-3	0.91	0.89	-[1]
	talja1995_c_0	RHS-1a - CC-4	0.91	0.97	-[1]

Table 2.8 – *Continued from previous page*

Reference	Name in Python script	Name in paper	$F_{u,el,FE}/F_{u,el}$	$F_{u,FE}/F_{u,Test}$	$\Delta_{u,FE}/\Delta_{u,Test}$
	talja2002_a_0	R1C2B1	0.51	0.86	-[1]
	talja2002_b_0	R1C2B2	0.95	0.89	-[1]
Talja [87]	talja2002_c_0	R1C2B3	0.95	0.95	-[1]
	talja2002_d_0	R4C2B1	0.82	1.06	-[1]
	talja2002_e_0	R4C2B2	-[2]	-[2]	-[1]
	talja2002_f_0	R4C2B3	0.96	1.02	-[1]
Mean			0.84	0.98	1.01
COV			0.24	0.12	1.04

[1] Not measured during the real experiments.

[2] Error in the numerical model.

Table 2.8: Comparison of Python script and experimental results.

3   Monte Carlo data generation

3.1   Data collection

In order to generate the Monte Carlo input points used afterwards into the Python script, this project is interested in the statistical distribution of the different inputs used in the script. To evaluate the statistical distribution of these parameters, a data collection was first necessary. The maximum data found in literature concerning stainless steel square hollow sections, regardless of the experimental test applied (buckling, bending, stub column etc.) were therefore collected. References of the accumulated data are given in Table 2.9. The number of measures for the geometrical parameters, deemed to be not dependent to the stainless steel grade are given in Table 2.10. The height h of the column is not indicated as the statistical distribution used for this parameter will be the same as for the width b.

The material properties were collected only from tensile and compressive coupon tests and not from stub column tests, which average the values for flat and corner parts. To have enough data for the material properties from experimental measurements, the used grades in the Monte Carlo process are the following:

  (i)   EN 1.4301, EN 1.4318, EN 1.4307 and EN 1.4571 for the austenitic nuance.

 (ii)   EN 1.4003 and EN 1.4509 for the ferritic nuance.

(iii)   EN 1.4162 for the duplex nuance.

In regard of this choice, the actual number of existing measures for each material parameters are given in Table 2.11.

Reference	Number of measures		Material grade
	Geometric	Material	
Theofanous and Gardner [4]	12	3	EN 1.4162
Afshan and Gardner [54]	15	8	EN 1.4003 and EN 1.4309
Huang and Young [55]	12	2	EN 1.4162
Liu and Young [52]	12	2	EN 1.4301
Rasmussen and Hancock [80, 88]	9	3	EN 1.4307
Gardner and Nethercot [81, 82]	30	8	EN 1.4301
Young and Lui [83]	16	2	EN 1.4162[1]
Gardner *et al.* [84]	6	4	EN 1.4318
Ala-Outinen and Oksanen [85]	10	1	EN 1.4301
Talja and Salmi [86]	13	10	EN 1.4301
Talja [87]	8	6	EN 1.4318
Afshan *et al.* [75]	10	30	Multiple[2]
Bock *et al.* [89]	4	2	EN 1.4003
Theofanous and Gardner [90]	6	12	EN 1.4162
Zhao *et al.* [91]	18	3	Multiple[3]
Real [92]	-[4]	1	EN 1.4301
Zhou and Young [93]	8	8	Multiple[5]
Zhou and Young [94]	34	4	EN 1.4162 and EN 1.4318
Zhou and Young [95]	33	8	Multiple[6]
Zhou and Young [96]	6	-[4]	EN 1.4162 and EN 1.4318
Jandera *et al.* [97]	14	6	EN 1.4301
Mirambell and Real [98]	1	1	EN 1.4301
Zhou and Young [99]	16	4	EN 1.4301
Talja and Hradil [100]	4[7]	4	EN 1.4509

[1] Supposed grade as only the nuance is specified.

[2] Grades EN 1.4301, EN 1.4571, EN 1.4404, EN 1.4509, EN 1.4003 and EN 1.4162.

[3] Grades EN 1.4301, EN 1.4571 and EN 1.4162.

[4] No data available.

[5] Grades EN 1.4301, EN 1.4162[1] and EN 1.4318[1].

[6] Grades EN 1.4301, EN 1.4162 and EN 1.4318[1].

[7] More data were available as some measurements were repeated.

Table 2.9: Summary of available geometrical and material properties measured on roll-formed stainless steel square hollow sections.

b	t	r_i	e_0	w_0
297	305	288	38	41

Table 2.10: Number of experimental measurements conducted for each geometric parameter.

Parameter	Austenitic				Ferritic		Duplex	Total
	EN 1.4301	EN 1.4318	EN 1.4307	EN 1.4571	EN 1.4003	EN 1.4509	EN 1.4162	
E_f	40	14	5	7	10	16	29	121
$\sigma_{0.2,f}$	44	14	5	7	10	16	29	125
n_f	26	4	3	6	8	13	23	83
$n'_{0.2,1.0,f}$	17	0	3	6	6	9	19	60
E_c	12	2	3	5	6	0	11	39
$\sigma_{0.2,c}$	12	4	3	5	6	0	11	41
$\sigma_{u,f}$	-[1]	14	3[2]	-[1]	-[1]	15	-[1]	32
n_c	12	2	2	2	4	0	11	33
$n'_{0.2,1.0,c}$	12	0	2	2	1	0	9	26

[1] Not necessary as enough data were available for $\sigma_{0.2,c}$ to fit a statistical distribution.

[2] Not enough data to fit a statistical distribution.

Table 2.11: Number of experimental measurements conducted for each material parameters, classified per grade.

3.2 Statistical distribution analysis

Statistical distribution fitting The distribution fitting study for each parameter was realised using the package *fitdistrplus* of the statistical software R [101]. This powerful package, combined with the statistical tools offered in R makes it easy and fast to fit the best distribution to a set of data. The procedure adopted is described hereinbelow, and has been automated in an R script:

(i) The set of data to analyse is read from a text file containing the values.

(ii) Using the function *fitdist* of the package *fitdistrplus*, the script try to fit different statistical distributions to the set of data. The tested distributions are the normal (NO), log-normal (LN), logistic (LO), Weibull (WE), gamma (GA), beta (BE) and exponential (EX) distributions. They are the most common and versatile distribution to fit to a set of data. For each tested theoretical distribution, the script returns a log-likelihood coefficient. The uniform distribution was not tested as no log-likelihood is associated given with that distribution.

(iii) Then, the adopted distribution corresponds to the highest log-likelihood coefficient. A visual control is displayed, the p-value is calculated and the best distribution have been fitted

It is quite often admitted in statistics that a test (here Shapiro or Kolmogorov-Smirnov statistical tests) is valid for a p-value superior to 5%. However, from a civil engineering point of view, the curve fitting has much more importance. Indeed, suppose that a normal distribution is fitted to set of data with a quite good curve fitting but with a wrong p-value. From a statistician point of view, the data generated then are wrong, as they does not have the same mathematical properties, such as density etc. However, from a civil engineering point of view, it is not really important if this is about a yield stress for instance. Indeed, as long as the general look of the fitted distribution is correct, then the generated data will be in a range observed experimentally, which therefore need to be considered in this project. Furthermore, the p-value was quite often mis-computed, as ties were present in the initial set of data, which is not appropriate for a distribution fitting. Finally, as the goal of this project is to generate 'random' points, best fitted distribution to a set of experimental data is the best way to guarantee a randomization of the Monte Carlo process. This idea is crucial in this project and explain why it has been chosen to use statistical distributions.

Geometrical parameters Using the described approach, distributions were fitted to the different geometrical inputs used in the Pyhton script. The results of this distribution fitting are summarised in Table 2.12 and distribution parameters values are detailed in Table B.1. As outlined in Table 1.1, five geometrical parameters are subjected to uncertainties. Therefore, as it has been decided to study the ratios measure/nominal, the ratios studied were b_{MC}/b_{nom}, h_{MC}/h_{nom} and t_{MC}/t_{nom}, where *MC* subscript refer to Monte Carlo, so an imperfect value (as a measure), in opposition to the *nom* subscript which refers to the nominal dimensions. As no nominal values exists for the inner radius r_i, the ratio $r_{i,MC}/t_{MC}$ was studied as the inner radius is strongly linked to the thickness. The global imperfection factor $e_{0,MC}$ was studied through the ratio $L_{MC}/e_{0,MC}$, as it has a tendency to increase with the length. Finally, the local imperfection factor $w_{0,MC}$ was also studied.

Material parameters In a similar fashion, each material parameters used in the numerical model has been studied, as well as the ultimate stress of the flat material $\sigma_{u,f}$ which can be used to compute $\sigma_{0.2,c}$ with Eq. 2.5. All the fitted distributions are listed in Table 2.13 and details are given in Table B.2. When

not enough data were available, values recommended by Afshan *et al.* [75] were used in priority. As some stainless steel grades are not present in Afshan *et al.* [75], the mean value of collected data was used instead. For yield stress in the corner $\sigma_{0.2,c}$, if data are also not available for $\sigma_{u,f}$, it has been decide to use:

$$\sigma_{0.2,c} = 1.15 \times \sigma_{0.2,f} \tag{2.9}$$

b_{MC}/b_{nom}	h_{MC}/h_{nom}	t_{MC}/t_{nom}	$r_{i,MC}/t_{MC}$	$L_{MC}/e_{0,MC}$	$w_{0,MC}$
LO	LO[1]	LN	GA	LN	LN
LO: Logistic, LN: Log-normal, GA: Gamma.					

[1] Same statistical distribution with same parameters as for *b*.

Table 2.12: Fitted statistical distribution for each geometrical parameters.

Parameter	Austenitic				Ferritic		Duplex
	EN 1.4301	EN 1.4318	EN 1.4307	EN 1.4571	EN 1.4003	EN 1.4509	EN 1.4162
E_f	LO	LN	WE	GA	WE	LN	LN
$\sigma_{0.2,f}$	GA	GA	LN	WE	LN	LN	NO
n_f	GA	4.73[1]	5.83[1]	LN	LN	LN	LN
$n'_{0.2,1.0,f}$	LN	3.6[2]	2.93[1]	LN	WE	LN	LO
E_c	LN	LN[3]	WE[3]	WE	WE	LN[3]	WE
$\sigma_{0.2,c}$	LN	(1)	$1.15 \times \sigma_{0.2,f}$	NO	LN	(1)	NO
$\sigma_{u,f}$	-[4]	WE	-[4]	-[4]	-[4]	LN	-[4]
n_c	WE	3.65[1]	3.4[1]	6.9[5]	6.1[5]	6.3[5]	LN
$n'_{0.2,1.0,c}$	LN	3.6[2]	5.35[1]	2.6[5]	3[5]	3.1[5]	LN
LO: Logistic, NO: Normal, LN: Log-normal, WE: Weibull, GA: Gamma.							

(1) Equals to $0.83 \times \sigma_{u,f}$ if then $\sigma_{0.2,c} > \sigma_{0.2,f}$. Else, equals $1.15 \times \sigma_{0.2,f}$.

[1] Mean value of collected data.

[2] According to chemical composition, judged to be closer to EN 1.4404 and hence, chose according to Afshan *et al.* [75].

[3] Same statistical distribution with same parameters as for E_f.

[4] Not necessary as enough data were available for $\sigma_{0.2,c}$ to fit a statistical distribution.

[5] Chose according to Afshan *et al.* [75].

Table 2.13: Fitted statistical distribution for each material parameters or value adopted in case not enough data were available, classified per grade.
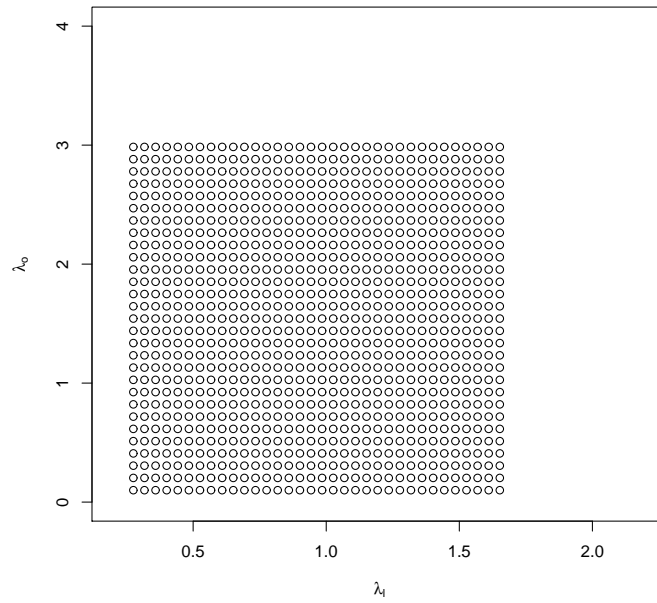
3.3   Data generation

Knowing the distributions of each geometric and material parameters, the Monte Carlo data generation is really fast. The goal of the Monte Carlo data generation is now to cover a broad range of column slenderness ranging from 0.1 to 3 for the overall slenderness λ_0 and having b/t ratio (directly related to the plate local slenderness $\lambda_l = \lambda_p$ see Eq. 1.2) included between 10 and 60. This has been done using anew a R script. The steps of the script are detailed hereinbelow:

(i) Firstly, a nominal width b_{nom} (and therefore a nominal height h_{nom}) is picked among some usual stainless steel square hollow section dimensions ranging from 30 to 200mm for each generated point. From this, nominal other dimensions (t_{nom} and L_{nom}) respecting the fixed conditions on the slenderness values are generated. 986 points were computed at this step and the nominal slenderness grid generated is displayed Fig. 2.4(a). In order to calculate these slenderness, as no material parameters have been fixed yet, average values (based on average measured values) are used for the yield stress and the Young modulus.

(ii) Monte Carlo process is applied to the nominal points with the help of the fitted distributions and then, a grid named the geometric grid is generated, displayed Fig. 2.4(b). The material parameters are not fixed and still based on average measured values. It can be seen that the Monte Carlo processing of the dimension values does not have a strong impact on the slendernesses.

(iii) Finally, based on the occurrence of each stainless steel grade in literature, a random choice of stainless steel grade is done. In a way, this does not reflect the reality, but data giving the occurrence of usage of different stainless steel square hollow sections grades in civil engineering has not been found. The pick probability associated to first the nuance of stainless steel and then the grade within a fixed nuance are detailed in Table 2.14. Once the nuance has been chosen, material parameters respecting the previously fitted distribution are computed and the final grid is displayed Fig. 2.5 is generated.

Austenitic [50%]	Ferritic [25%]	Duplex [25%]
EN 1.4301 [50%]	EN 1.4003 [50%]	
EN 1.4318 [25%]		EN 1.4162 [100%]
EN 1.4307 [12.5%]	EN 1.4509 [25%]	
EN 1.4571 [12.5%]		

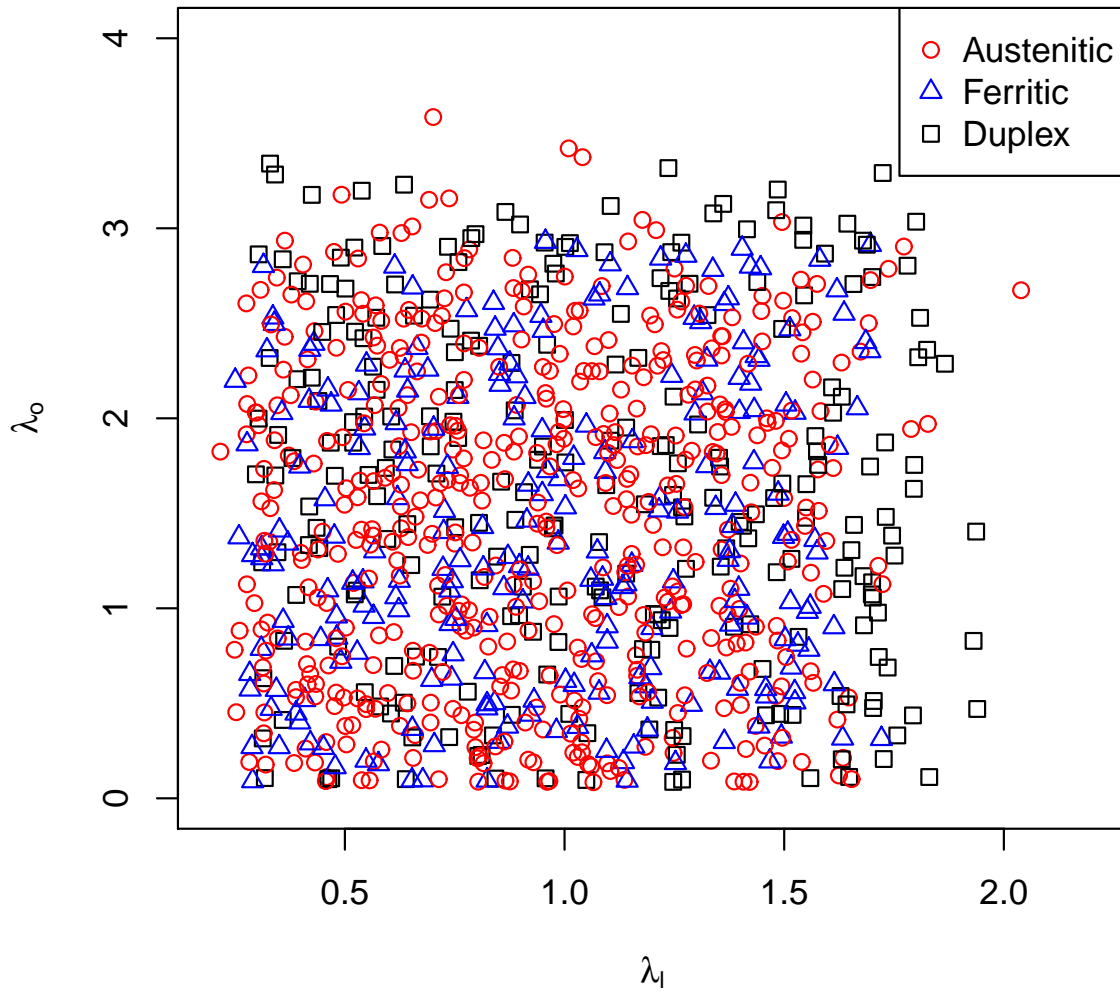**Table 2.14:** Stainless steel grade selection chosen probability.

(a) Nominal grid.
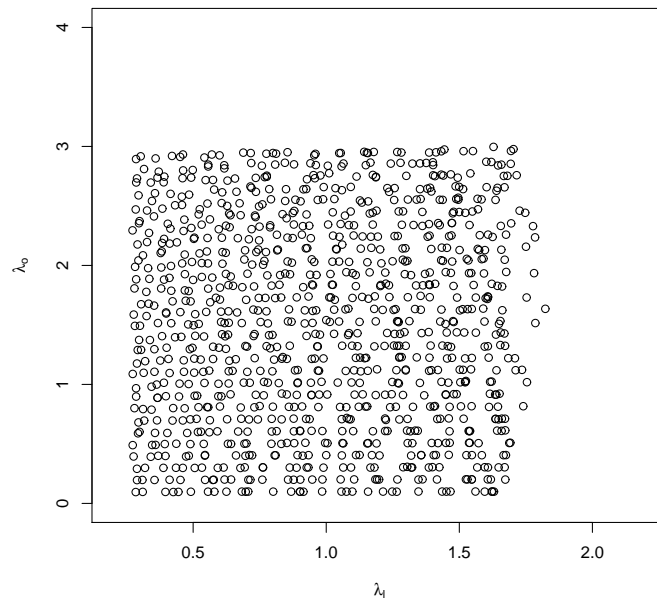
(b) Geometrical grid.

Figure 2.4: Grid generation during the Monte Carlo data generation.

Figure 2.5: Final Monte Carlo grid.

Chapter 3

Simulation results

In this third chapter, the obtained results from numerical simulations are presented. An equation, formulated in a Direct Strength Method fashion is given for design according to the obtained results.

Contents

1   Numerical results

Next to the Monte Carlo data generation, all the generated points were submitted to Iceberg using the Python script described in Section 2.1 of Chapter 2. The whole submission took three days and due to errors with the Iceberg server or with the Python script, only 507 over the 986 points submitted actually worked. The results are displayed in Fig. 3.1 with λ_l and A calculated using the nominal dimensions of each column. The material properties (E and f_y) were chosen from indications of BS EN 10088-4 [102].

It can be seen that the points are very spread, with the ratio $F_{u,FE}/Af_y$ ranging from 0.06 to 3.77. The mean of this ratio is equal to 0.97 with a COV equals to 0.67. It can also be noted that the maximum slendernesses ($\lambda_l > 1.35$) are obtained only for duplex nuances. This is explained by the high yield stress value recommended for this nuance by the BS EN 10088-4 [102], equals to 530 MPa, which is two times higher than for the other nuances.

2   Recommendation for design guidance

As it is a very convenient method to use (see Section 2.4.2 of Chapter 1), the proposed design equation is in a Direct Strength Method fashion, given Eq. 3.1. $N_{cl,d}$ is the design local and flexural buckling resistance of the column and the local slenderness λ_l is computed using Eq. 1.2 ($\lambda_l = \lambda_p$).

$$N_{cl,d} = \begin{cases} 1 & \text{for } \lambda_l \leq 0.781 \\ \frac{1}{\lambda_l^{0.9}}\left(1.05 - \frac{0.2}{\lambda_l^{0.9}}\right) & \text{for } \lambda_l > 0.781 \end{cases} \tag{3.1}$$

Using this equation, the mean of $F_{u,FE}/N_{cl,d}$ is equal to 0.94 with a COV equals to 0.59 for the 507 result points obtained. With the help of recommendations of Blum [103], a reliability analysis has been conducted. The resistance factor Φ is equal to 0.36, which is low (taget values are often superior to 0.9). Choosing other values for the coefficients in Eq. 3.1 could have improved the resistance factor but also increased the COV, which is not desirable. Indeed, the COV obtained for the current equation is high, corresponding to the wide spread of the data.
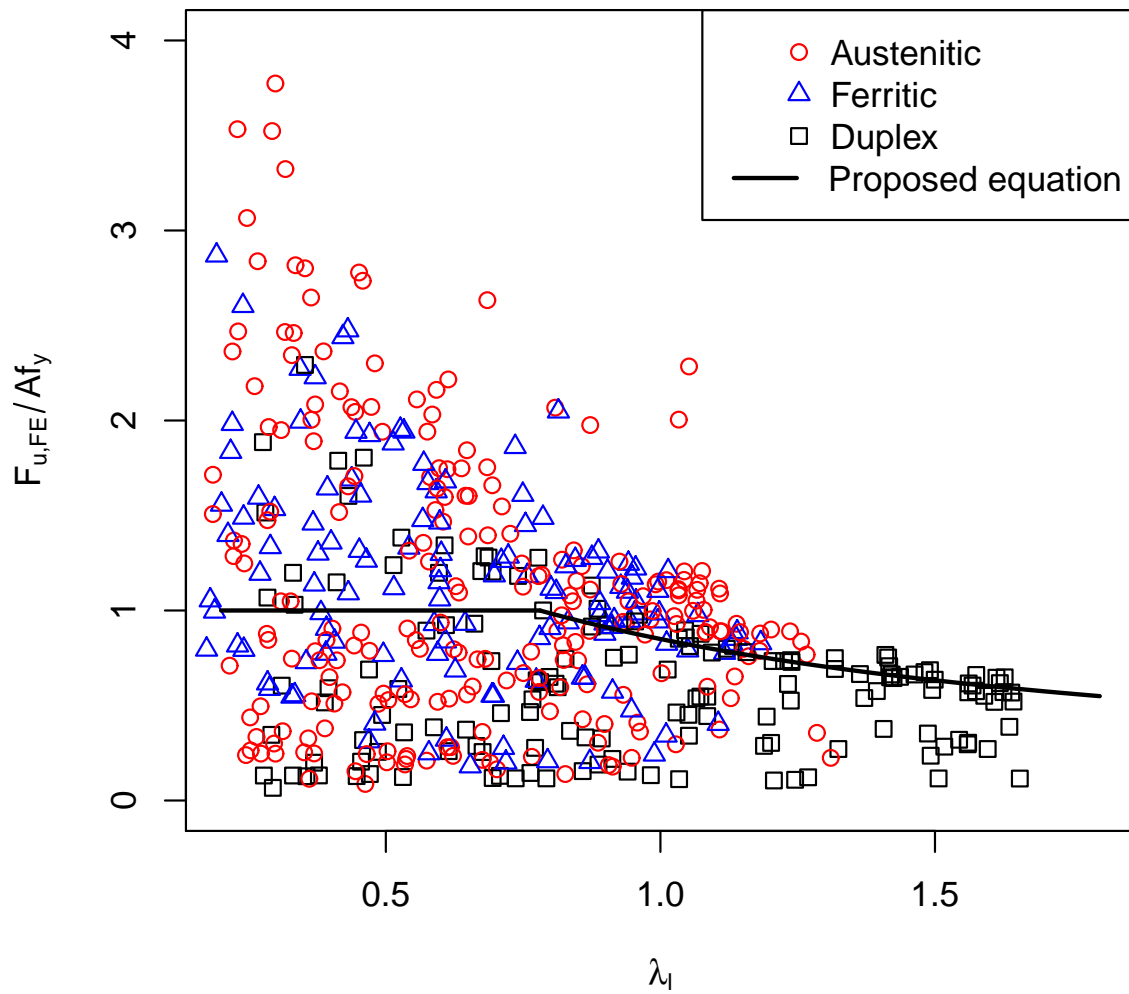
Figure 3.1: Results of submission.

Conclusion and outlooks

Stainless steel is a reliable material, combining better mechanical properties and corrosion resistance than carbon steel. The chemical compositions of the four main grades of stainless steel were detailed, along with the uses and properties of cold-formed stainless steel columns. As the aim of this project is to develop improved design rules for the buckling of these columns, the existing design rules of the European and North-American standards were presented. Therefore, explanations about the Effective Width Method (EWM), the Direct Strength Method (DSM) and others designing methods are given, along with the advantages and drawbacks of each methods. Finally, the Monte Carlo method, and its link with the data generation of this project was introduced.

A validated numerical model of the problem has been built on Abaqus. Material modelling, geometric imperfections and numerical parameters have been chosen with care and are discussed in this report. A Python script (built with the Abaqus model), automating the submission of a column has been built and validated to 67 previously conducted tests. Using a Monte Carlo method combined concurrently with a statistical analysis of experimental measurements, a set of 986 inputs was generated, covering realistic slendernesses from 0.2 to 2.0 for local slenderness λ_l and from 0.1 to 3.0 for overall slenderness λ_o. These inputs were submitted to Iceberg with the Python script and, due to erors, 507 results were obtained. From these result values, a design equation, respecting the Direct Strength Method fashion was proposed. Leading a reliability analysis, the resistance factor Φ is equal to 0.36, which is not high enough to guarantee safety using this equation. Other equations could have been proposed, but leading to a larger spread of the results. Therefore, this equation has been considered to be the best agreement between safety and spread of the results.

With a view of the different number of existing nuances and grades of stainless steel, it could be in the future desirable to propose different equations for each nuance of stainless steel. Indeed, as the results are very spread here, it is ambitious to gather them all together with one equation.

Among the other points to improve, the residual stresses resulting from seam-welding operation could be added. Currently, no proper models have been proposed for stainless steel, but it is possible to use some existing ones for carbon steel. In the Python script, some changes could be applied so no interpenetration occurs, leading to more results at the end. And in order to improve the accuracy of the results, more experimental data should be available. A new campaign of experimental measures, with the idea of a statistical fitting afterward could be done.

In a personal capacity, this internship has enabled me to acquire an important autonomy on a research project, very important for a future Ph.D., as I mainly conducted the project by myself. The later was very interesting to me as it combined an important literature work, therefore very instructive, a numerical modelling and a completely new approach to design rules formulation. The topic, namely the buckling

of cold-formed stainless steel square hollow sections was moreover very pertinent, as the use of stainless steel is relatively low compared to carbon steel in construction, partly due to too conservative design rules combined with higher initial material costs. The meetings with my supervisors finally helped to focus our ideas for the next steps of the project. A final timeline of the project is given in Table 3.1.

Month	Project step
October-November	Literature review and familiarisation with the FE software.
December - January	Building an FE model and verification against existing experimental data.
February - May	Python scripting adn verification against existing experimental data.
May - June	Monte Carlo data generation.
July	Simulations and design rules.
July-August	Final report writing.

Table 3.1: Updated timeline of the project.

Nomenclature

α	imperfection factor (EN)	$\sigma_{0.2}$	yield stress (corresponding to a 0.2% plastic strain)
β	coefficient (ASCE)		
χ	reduction factor for relevant buckling mode (EN)	$\sigma_{1.0}$	1.0% stress (corresponding to a 1.0% plastic strain)
$\Delta_{u,FE}$	numerical buckling displacement at mid-length	$\sigma_{com,Ed,ser}$	maximum design compressive stress at serviceability limit state (EN)
$\Delta_{u,Test}$	experimental buckling displacement at mid-length	σ_{crl}	critical plate buckling stress (EN)
$\Delta_{u,X,FE}$	numerical buckling displacement at mid-length along the X-axis	σ_{cr}	elastic critical buckling stress
		σ_{ex}	buckling stress about x-axis (ASCE)
$\Delta_{u,Y,FE}$	numerical buckling displacement at mid-length along the Y-axis	σ_{nom}	engineering stress
		σ_{true}	true stress
γ_{M0}	partial factor for resistance of cross-sections (EN)	σ_t	torsional buckling stress (ASCE)
		$\sigma_{u,f}$	ultimate stress of the flat material
γ_{M1}	partial factor for resistance of members to instability (EN)	θ	rotation
		ε	strain
λ	slenderness factor (ASCE)	ε_{ln}^{pl}	log plastic strain
λ_b	conversion slenderness (Shu *et al.* method)	ε_{nom}	engineering strain
		$\varepsilon_{t0.2}$	total strains at $\sigma_{0.2}$
λ_d	distortional slenderness (DSM)	$\varepsilon_{t1.0}$	total strains at $\sigma_{1.0}$
λ_l	local slenderness	A	gross section area
λ_o	overall slenderness	A_{eff}	effective area
λ_p	plate slenderness ratio (EWM)	b	plate element width or column width
ν	coefficient of Poisson	b_{eff}	plate element effective width (EWM)
$\overline{\lambda}$	non-dimensional slenderness (EN)	b_{MC}	Measured width for Monte Carlo simulation
$\overline{\lambda}_0$	limiting slenderness (EN)		
ϕ	value to determine the reduction factor χ (EN)	b_{nom}	Nominal width
		C_w	torsional warping constant of cross-section (ASCE)
ϕ_c	resistance factor for concentrically loaded compression member (ASCE)	d	corner enhancement extend
		E	modulus of elasticity
ρ	reduction factor (EN)	E_0	initial modulus of elasticity
σ	normal stress	e_0	global imperfection factor
$\sigma_{0.01}$	proof stress corresponding to a 0.01% plastic strain	E_t	tangent modulus of elasticity in compression (ASCE)
$\sigma_{0.2,c}$	yield stress in the corner	$e_{0,MC}$	Measured global imperfection factor

Improvement of existing design rules for cold-formed stainless steel hollow sections under compression forces using numerical modelling and Monte Carlo simulations

	for Monte Carlo simulation	M_{pl}	plastic moment (EN)
$E_{0.2}$	tangent stiffness at $\sigma_{0.2}$	N	number of element
f_0	elastic buckling strength (DSM)	n	strain-hardening exponent
F_n	nominal buckling stress (ASCE)	$n'_{0.2,1.0,c}$	second strain-hardening exponent in the corner part
f_y	yield stress (F_y in ASCE)		
F_{cr}	plate elastic buckling stress (ASCE)	$n'_{0.2,1.0,f}$	second strain-hardening exponent in the flat part
f_{od}	elastic distortional buckling strength (DSM)		
		$n'_{0.2,1.0}$	second strain-hardening exponent
$F_{u,el,FE}$	numerical elastic buckling load	N_u	ultimate capacity
$F_{u,el}$	Euler elastic buckling load	N_y	yield strength
$F_{u,FE}$	numerical buckling load	$N_{b,Rd}$	design buckling resistance of the compression member (EN)
$F_{u,Test}$	experimental buckling load		
G_0	initial shear modulus (ASCE)	$N_{c,Rd}$	design uniform compression strength (EN)
h	depth of the column		
h_{MC}	Measured height for Monte Carlo simulation	N_{cd}	distortional buckling strength (DSM)
		$N_{cl,d}$	design local and flexural buckling resistance of the column
h_{nom}	Nominal height		
J	St. Venant torsion constant (ASCE)	N_{Ed}	design compression force (EN)
K	effective length factor (ASCE)	P_n	nominal axial strength of member (ASCE)
k	plate buckling coefficient (EWM)		
K_t	effective length factor for torsion (ASCE)	r	radius of gyration of full, unreduced cross-section (ASCE)
K_x	effective length factor for bending about x-axis (ASCE)	r_0	polar radius of gyration of cross-section about shear centre (ASCE)
L	unbraced length of member	r_i	inner radius
L_t	unbraced length of compression member for torsion (ASCE)	r_x	radius of gyration of cross-section about x-axis (ASCE)
L_x	unbraced length of compression member for bending about x-axis (ASCE)	t	thickness of the plate element or of the column
L_{MC}	Measured length for Monte Carlo simulation	t_{MC}	Measured thickness for Monte Carlo simulation
M	moment	t_{nom}	Nominal thickness
M_c	size of the element in the corner part	w_0	local imperfection factor
M_f	size of the element in the flat part	$w_{0,MC}$	Measured local imperfection factor for Monte Carlo simulation
M_{el}	elastic moment (EN)		

Note that EWM (Effective Width Method), EN (Eurocode), ASCE (American Society of Civil Engineers) and DSM (Direct Strength method) respectively refer to notations use in Section 2.3.1, 2.3.2, 2.4.1and 2.4.2.

References

[1] EN 1993-1-4, "Eurocode 3 – Design of steel structures – Part 1-4: General rules – Supplementary rules for stainless steels," 2006.

[2] ASCE, "Specification for the Design of Cold-Formed Stainless Steel Structural Members - Standards ASCE/SEI 8-02," American Society of Civil Engineers, 2002.

[3] EN 1993-1-1, "Eurocode 3 – Design of steel structures – Part 1-1: General rules and rules for buildings," 2005.

[4] M. Theofanous and L. Gardner, "Testing and numerical modelling of lean duplex stainless steel hollow section columns," *Engineering Structures*, vol. 31, no. 12, pp. 3047–3058, 2009.

[5] M. Ashraf, L. Gardner, and D. A. Nethercot, "Finite element modelling of structural stainless steel cross-sections," *Thin-Walled Structures*, vol. 44, no. 10, pp. 1048 – 1062, 2006.

[6] Abaqus 6.11 Documentation - www.sharcnet.ca/Software/Abaqus/6.11.2/index.html.

[7] B. Rossi, "Discussion on the use of stainless steel in constructions in view of sustainability," *Thin-Walled Structures*, vol. 83, no. 0, pp. 182–189, 2014.

[8] L. Gardner and N. R. Baddoo, "Fire testing and design of stainless steel structures," *Journal of Constructional Steel Research*, vol. 62, no. 6, pp. 532 – 543, 2006.

[9] L. Gardner and K. T. Ng, "Temperature development in structural stainless steel sections exposed to fire," *Fire Safety Journal*, vol. 41, no. 3, pp. 185 – 203, 2006.

[10] K. T. Ng and L. Gardner, "Buckling of stainless steel columns and beams in fire," *Engineering Structures*, vol. 29, no. 5, pp. 717 – 730, 2007.

[11] L. Gardner, A. Insausti, K. T. Ng, and M. Ashraf, "Elevated temperature material properties of stainless steel alloys," *Journal of Constructional Steel Research*, vol. 66, no. 5, pp. 634 – 647, 2010.

[12] N. Tondini, B. Rossi, and J.-M. Franssen, "Experimental investigation on ferritic stainless steel columns in fire," *Fire Safety Journal*, vol. 62, Part C, no. 0, pp. 238 – 248, 2013.

[13] N. Lopes and P. M. M. V. Real, "Class 4 stainless steel i beams subjected to fire," *Thin-Walled Structures*, vol. 83, no. 0, pp. 137 – 146, 2014.

[14] FABIG, ed., *Design guide for stainless steel blast walls*. The Steel Construction Institute, 1999.

[15] "Handbook of stainless steel," 2013. Outokumpu.

[16] www.worldstainless.org (website of the International Stainless Steel Forum, accessed on 28 October 2014).

[17] www.worldsteel.org (website of the World Steel Association, accessed on 28 October 2014).

[18] L. Gardner, "The use of stainless steel in structures," *Progress in Structural Engineering and Materials*, vol. 7, pp. 45–55, 2005.

[19] E. P. Shuttleworth, "Structural applications for stainless steel offshore - Report to The Nickel Development Institute," tech. rep., The Steel Construction Institute, 1989.

[20] W. Ramberg and W. R. Osgood, "Description of stress-strain curves by three parameters," tech. rep., National Advisory Committee for Aeronautics, Technical note No. 902, 1943.

[21] N. H. Hill, "Determination of stress-strain relations from "offset" yield strength values," tech. rep., National Advisory Committee for Aeronautics, Technical note No. 927, 1944.

[22] K. J. R. Rasmussen, "Full-range stress-strain curves for stainless steel alloys," *Journal of Constructional Steel Research*, vol. 59, no. 1, pp. 47–61, 2003.

[23] L. Gardner and M. Ashraf, "Structural design for non-linear metallic materials," *Engineering Structures*, vol. 28, no. 6, pp. 926–934, 2006.

[24] P. Hradil, A. Talja, E. Real, E. Mirambell, and B. Rossi, "Generalized multistage mechanical model for nonlinear metallic materials," *Journal of Constructional Steel Research*, vol. 63, no. 0, pp. 63–69, 2013.

[25] E. Real, I. Arrayago, E. Mirambell, and R. Westeel, "Comparative study of analytical expressions for the modelling of stainless steel behaviour," *Thin-Walled Structures*, vol. 83, no. 0, pp. 2–11, 2014.

[26] "BS EN 10088-1. Stainless steels - Part 1: List of stainless steels.," 2005.

[27] American Iron and Steel Institute.

[28] E. Jouannais, "Stainless Steel in construction," tech. rep., ArcelorMittal.

[29] J. R. Davis, *Handbook of Materials for Medical Devices.* ASM International, 2003.

[30] K. A. Cashell and N. R. Baddoo, "Ferritic stainless steels in structural applications," *Thin-Walled Structures*, vol. 83, no. 0, pp. 169–181, 2014.

[31] www.outokumpu.com (Outokumpu website, accessed on 24 October 2014.

[32] R. B. Cruise and L. Gardner, "Strength enhancements induced during cold forming of stainless steel sections," *Journal of Constructional Steel Research*, vol. 64, no. 11, pp. 1310–1316, 2008.

[33] N. R. Baddoo, "Stainless steel in construction: A review of research, applications, challenges and opportunities," *Journal of Constructional Steel Research*, vol. 64, no. 11, pp. 119–1206, 2008.

[34] J. S. Coetsee, G. J. van den Berg, and P. van der Merwe, "The effect of workhardening and residual stresses due to cold work of forming on the strength of cold-formed stainless steel lipped channel section," in *Tenth International Specialty Conference on Cold-formed Steel Structures*, October 1990.

[35] M. Ashraf, L. Gardner, and D. A. Nethercot, "Strength enhancement of the corner regions of stainless steel cross-sections," *Journal of Constructional Steel Research*, vol. 61, no. 0, pp. 37–52, 2005.

[36] B. Rossi, H. Degée, and F. Pascon, "Enhanced mechanical properties after cold process of fabrication of non-linear metallic profiles," *Thin-Walled Structures*, vol. 47, no. 12, pp. 1575–1589, 2009.

[37] J. Marik and M. Jandera, "Cold-forming effect on material properties of stainless steel," in *Eurosteel 2014*, September 2014.

[38] W. M. Quach and P. Qiu, "Strength and ductility of corner materials in cold-formed stainless steel sections," *Thin-Walled Structures*, vol. 83, no. 0, pp. 28–42, 2014.

[39] L. Gardner and D. A. Nethercot, "Numerical Modeling of Stainless Steel Structural Components–A Consistent Approach," *Journal of Structural Engineering*, vol. 130, no. 10, pp. 1586–1601, 2004.

[40] E. Ellobody and B. Young, "Structural performance of cold-formed high strength stainless steel columns," *Journal of Constructional Steel Research*, vol. 61, no. 12, pp. 1631–1649, 2005.

[41] P. W. Key and G. J. Hancock, "A theoretical investigation of the column behaviour of cold-formed square hollow sections," *Thin-Walled Structures*, vol. 16, no. 4, pp. 31 – 64, 1993. Special Issue on Cold-Formed Steel Structures.

[42] AISI, "Specification for the Design of Light Gauge Cold-Formed Stainless Steel Structural Members," American Iron and Steel Institute, 1968.

[43] AISI, "Stainless Steel Cold-Formed Structural Design Manual," American Iron and Steel Institute, 1974.

[44] Euro Inox, "Design Manual for Structural Stainless Steel," 1994.

[45] Euro Inox, "Design Manual for Structural Stainless Steel (Second Edition)," 2003.

[46] Euro Inox, "Design Manual for Structural Stainless Steel (Third Edition)," 2007.

[47] ENV 1993-1-4, "Eurocode 3 – Design of steel structures – Part 1-4: General rules – Supplementary rules for stainless steels," 1996.

[48] SSBA, "Design and Construction Standards of Stainless Steel Buildings," Stainless Steel Building Association of Japan, 1995. (In Japanese).

[49] SABS, "SANS 10162-4 - Structural Use Of Steel - Part 4: The Design Of Cold-formed Stainless Steel Structural Members," South African Bureau of Standards, 1997.

[50] AS/NZS 4673, "Cold-formed stainless steel structures," 2001.

[51] GB/T 14975–2002, "Stainless steel seamless tubes for structures," 2002. (In Chinese).

[52] Y. Liu and B. Young, "Buckling of stainless steel square hollow section compression members," *Journal of Constructional Steel Research*, vol. 59, no. 2, pp. 165–177, 2003.

[53] B. A. Burgan, N. R. Baddoo, and K. A. Gilsenan, "Structural design of stainless steel members – comparison between eurocode 3, part 1.4 and test results," *Journal of Constructional Steel Research*, vol. 54, no. 1, pp. 51–73, 2000.

[54] S. Afshan and L. Gardner, "Experimental Study of Cold-Formed Ferritic Stainless Steel Hollow Sections," *Journal of Structural Engineering*, vol. 139, pp. 717–728, 2013.

[55] Y. Huang and B. Young, "Tests of pin-ended cold-formed lean duplex stainless steel columns," *Journal of Constructional Steel Research*, vol. 82, no. 0, pp. 203–215, 2013.

[56] Y. Huang and B. Young, "Experimental investigation of cold-formed lean duplex stainless steel beam-columns," *Thin-Walled Structures*, vol. 76, no. 0, pp. 105–117, 2014.

[57] T. von Kármán, E. E. Sechler, and L. H. Donnell, "The Strength of Thin Plates in Compression," *Transactions of the American Society of Mechanical Engineers*, vol. 139, pp. 53–57, 1932.

[58] G. Winter, *Strength of Thin Steel Compression Flanges*. Cornell University, 1947.

[59] EN 1993-1-5, "Eurocode 3 – Design of steel structures – Part 1-5: General rules – Plated structural elements," 2006.

[60] E. de Miranda Batista, "Effective section method: A general direct method for the design of steel cold-formed members under local-global buckling interaction," *Thin-Walled Structures*, vol. 48, no. 5, pp. 345–356, 2010.

[61] N. R. Baddoo and B. A. Burgan, *Structural Design of Stainless Steel*. The Steel Construction Institute, 2002.

[62] L. Gardner and M. Theofanous, "Discrete and continuous treatment of local buckling in stainless steel elements," *Journal of Constructional Steel Research*, vol. 64, no. 11, pp. 1207 – 1216, 2008. International Stainless Steel Experts Seminar.

[63] Euro Inox, "Design Manual for Structural Stainless Steel - Commentary (Second Edition)," 2003.

[64] S.-H. Lin, W.-W. Yu, T. V. Galambos, and E. Wang, "Revised ASCE specification for the design of cold-formed stainless steel structural members," *Engineering Structures*, vol. 27, no. 9, pp. 1365 – 1372, 2005.

[65] S. Lau and G. Hancock, "Distortional Buckling Formulas for Channel Columns," *Journal of Structural Engineering*, vol. 113, no. 5, pp. 1063–1078, 1987.

[66] Y. Kwon and G. Hancock, "Tests of Cold-formed Channels with Local and Distortional Buckling," *Journal of Structural Engineering*, vol. 118, no. 7, pp. 1786–1803, 1992.

[67] B. W. Schafer and T. Peköz, "Direct strength prediction of cold-formed steel members using numerical elastic buckling solutions," in *Fourteenth International Specialty Conference on Cold-Formed Steel Structures*, October 1998.

[68] NAS, "Supplement 2004 to the north american specification for the design of cold-formed steel structural members (2001 Edition)," *American Iron and Steel Institute*, 2004.

[69] AS/NZS 4600, "Cold-formed steel structures," 2005.

[70] J. Becque, M. Lecce, and K. J. R. Rasmussen, "The direct strength method for stainless steel compression members," *Journal of Constructional Steel Research*, vol. 64, no. 11, pp. 1231 – 1238, 2008. International Stainless Steel Experts Seminar.

[71] B. Rossi and K. J. R. Rasmussen, "Carrying Capacity of Stainless Steel Columns in the Low Slenderness Range," *Journal of Structural Engineering*, vol. 139, pp. 1088–1092, 2013.

[72] B. W. Schafer and S. Ádány, "Buckling analysis of cold-formed steel members using CUFSM: conventional and constrained finite strip methods," in *Eighteenth International Specialty Conference on Cold-Formed Steel Structures*, October 2006.

[73] R. Bebiano, P. Pina, N. Silvestre, and D. Camotim, "Gbtul–buckling and vibration analysis of thin-walled members," *DECivil/IST, Technical University of Lisbon (www.civil.ist.utl.pt/gbt)*, 2008.

[74] B. W. Schafer, "Review: The direct strength method of cold-formed steel member design," *Journal of Constructional Steel Research*, vol. 64, no. 7-8, pp. 766–778, 2008. International Colloquium on Stability and Ductility of Steel Structures 2006.

[75] S. Afshan, B. Rossi, and L. Gardner, "Strength enhancements in cold-formed structural sections – part I: Material testing," *Journal of Constructional Steel Research*, vol. 83, pp. 177 – 188, 2013.

[76] M. Ashraf, *Structural stainless steel design: Resistance based on deformation capacity.* PhD thesis, Imperial College London, UK, 2006.

[77] R. Cruise and L. Gardner, "Residual stress analysis of structural stainless steel sections," *Journal of Constructional Steel Research*, vol. 64, no. 3, pp. 352 – 366, 2008.

[78] M. Jandera and J. Machacek, "Residual stress influence on material properties and column behaviour of stainless steel SHS," *Thin-Walled Structures*, vol. 83, no. 0, pp. 12 – 18, 2014.

[79] Python 2.7.9 Documentation - https://docs.python.org/2.7/.

[80] K. J. R. Rasmussen and G. J. Hancock, "Design of Cold-Formed Stainless Steel Tubular Members. I: Columns," *Journal of Structural Engineering*, vol. 119, no. 8, pp. 2349–2367, 1993.

[81] L. Gardner and D. Nethercot, "Experiments on stainless steel hollow sections–Part 1: Material and cross-sectional behaviour," *Journal of Constructional Steel Research*, vol. 60, no. 9, pp. 1291 – 1318, 2004.

[82] L. Gardner and D. Nethercot, "Experiments on stainless steel hollow sections–Part 2: Member behaviour of columns and beams," *Journal of Constructional Steel Research*, vol. 60, no. 9, pp. 1319 – 1332, 2004.

[83] B. Young and W.-M. Lui, "Tests of cold-formed high strength stainless steel compression members," *Thin-Walled Structures*, vol. 44, no. 2, pp. 224 – 234, 2006.

[84] L. Gardner, A. Talja, and N. Baddoo, "Structural design of high-strength austenitic stainless steel," *Thin-Walled Structures*, vol. 44, no. 5, pp. 517 – 528, 2006.

[85] T. Ala-Outinen and T. Oksanen, "Stainless steel compression members exposed to fire," tech. rep., VTT Building Technology, Finland, Research note 1864, 1997.

[86] A. Talja and P. Salmi, "Design of stainless steel RHS beams, columns and beam-columns," tech. rep., VTT Building Technology, Finland, Research note 1619, 1995.

[87] A. Talja, "Test results of RHS, tophat and sheeting profiles," tech. rep., VTT Building Technology, Finland, Research note 1864, 2002. Name of Project: Structural design of cold-worked austenitic stainless steel.

[88] K. J. R. Rasmussen and G. J. Hancock, "Design of Cold-Formed Stainless Steel Tubular Members. II: Beams," *Journal of Structural Engineering*, vol. 119, no. 8, pp. 2368–2386, 1993.

[89] M. Bock, I. Arrayago, and E. Real, "Experiments on cold-formed ferritic stainless steel slender sections," *Journal of Constructional Steel Research*, vol. 109, pp. 13 – 23, 2015.

[90] M. Theofanous and L. Gardner, "Experimental and numerical studies of lean duplex stainless steel beams," *Journal of Constructional Steel Research*, vol. 66, no. 6, pp. 816 – 825, 2010.

[91] O. Zhao, B. Rossi, L. Gardner, and B. Young, "Behaviour of structural stainless steel cross-sections under combined loading – Part I: Experimental study," *Engineering Structures*, vol. 89, pp. 236 – 246, 2015.

[92] E. Real, *Aportaciones al estudio del comportamiento a flexión de estructuras de acero inoxidable*. PhD thesis, Universitat Politècnica de Catalunya. Departament d'Enginyeria de la Construcció, 2001. (In Spanish).

[93] F. Zhou and B. Young, "Tests of cold-formed stainless steel tubular flexural members," *Thin-Walled Structures*, vol. 43, no. 9, pp. 1325 – 1337, 2005.

[94] F. Zhou and B. Young, "Cold-Formed High-Strength Stainless Steel Tubular Sections Subjected to Web Crippling," *Journal of Structural Engineering*, vol. 133, no. 3, pp. 368–377, 2007.

[95] F. Zhou and B. Young, "Experimental and numerical investigations of cold-formed stainless steel tubular sections subjected to concentrated bearing load," *Journal of Constructional Steel Research*, vol. 63, no. 11, pp. 1452 – 1466, 2007.

[96] F. Zhou and B. Young, "Experimental Investigation of Cold-Formed High-Strength Stainless Steel Tubular Members Subjected to Combined Bending and Web Crippling," *Journal of Structural Engineering*, vol. 133, no. 7, pp. 1027–1034, 2007.

[97] M. Jandera, L. Gardner, and J. Machacek, "Residual stresses in cold-rolled stainless steel hollow sections," *Journal of Constructional Steel Research*, vol. 64, no. 11, pp. 1255 – 1263, 2008. International Stainless Steel Experts Seminar.

[98] E. Mirambell and E. Real, "On the calculation of deflections in structural stainless steel beams: an experimental and numerical investigation," *Journal of Constructional Steel Research*, vol. 54, no. 1, pp. 109 – 133, 2000.

[99] F.Zhou and B. Young, "Cold-Formed Stainless Steel Sections Subjected to Web Crippling," *Journal of Structural Engineering*, vol. 132, no. 1, pp. 134–144, 2006.

[100] A. Talja and P. Hradil, "Structural Applications of Ferritic Stainless Steels (SAFSS) WP2: Structural performances of steel members - Model calibration tests," tech. rep., VTT Building Technology, Finland, Research Report No. VTT-R-06130-12 2012.

[101] R Development Core Team, *R: A Language and Environment for Statistical Computing*. R Foundation for Statistical Computing, Vienna, Austria, 2008. ISBN 3-900051-07-0.

[102] "BS EN 10088-4. Stainless steels - Part 4: Technical delivery conditions for sheet/plate and strip of corrosion resisting steels for construction purposes.," 2009.

[103] H. Blum, "Reliability-Based Design of Truss Structures by Advanced Analysis," tech. rep., The University of Sidney - School of Civil Engineering, 2013.

Appendix A

Mesh convergence study
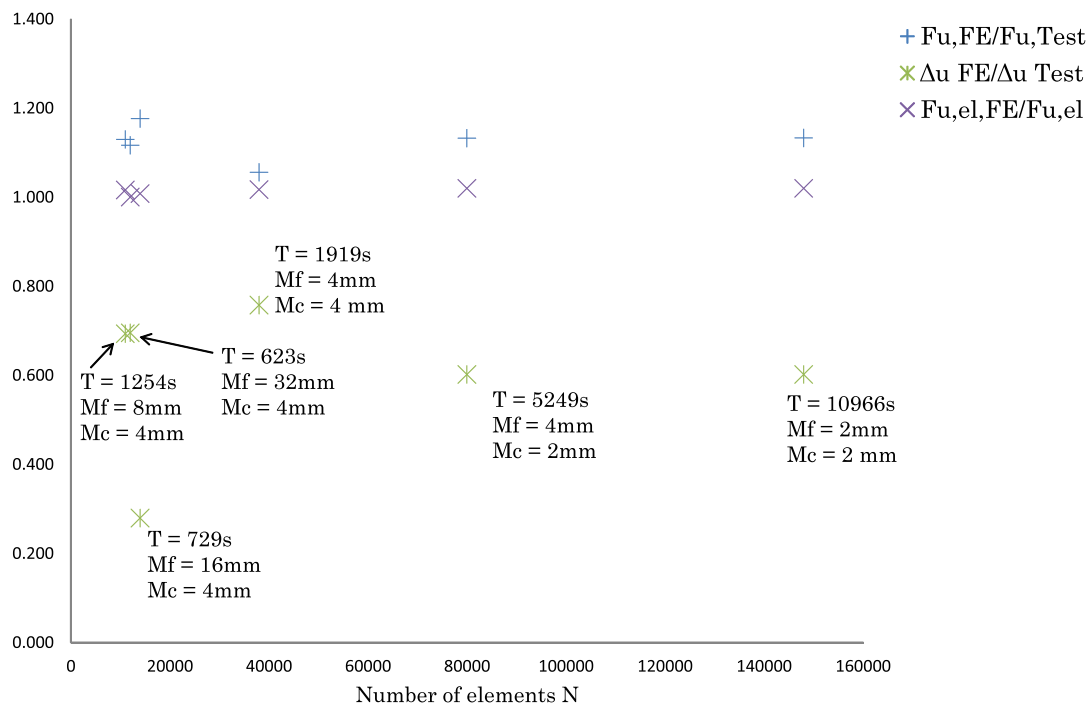
Figure A.1: Mesh convergence study.

Appendix B

Distribution fitting study

Parameter	Distribution	p-value	1st parameter	2nd parameter
b_{MC}/b_{nom}	LO	<2.2e-16[1]	location = 1.001329120	scale = 0.002248568
h_{MC}/h_{nom}	LO[2]	<2.2e-16[2]	location = 1.001329120[2]	scale = 0.002248568[2]
t_{MC}/t_{nom}	LN	<2.2e-16[1]	meanlog = -0.02770792	sdlog = 0.03490599
$r_{i,MC}/t_{MC}$	GA	6.05e-6	shape = 9.421589	rate = 8.501117
$L_{MC}/e_{0,MC}$	LN	<2.2e-16[1]	meanlog = 8.2283640	sdlog = 0.8140854
$w_{0,MC}$	LN	<2.2e-16[1]	meanlog = -2.4956198	sdlog = 0.7356126
LO: Logistic, LN: Log-normal, GA: Gamma.				

[1] Error in the calculation of the p-value by R.

[2] Same statistical distribution with same parameters as for *b*.

Table B.1: Details of fitted statistical distribution for each geometrical parameters.

Parameter	Grade	Distribution	p-value	1st parameter	2nd parameter
E_f	EN 1.4301	LO	<2.2e-16[1]	location = 194562.764	scale = 6052.423
E_f	EN 1.4318	LN	1.38e-12	meanlog = 12.1392427	sdlog = 0.0723124
E_f	EN 1.4307	WE	0.8835	shape = 128.0892	scale = 195681.2779
E_f	EN 1.4571	GA	0.7929	shape = 2841.346	rate = 0.01494719
E_f	EN 1.4003	WE	0.9543	shape = 13.18808	scale = 204722.93506
E_f	EN 1.4509	LN	2.53e-14	meanlog = 12.18696608	sdlog = 0.04732482
E_f	EN 1.4162	LN	<2.2e-16[1]	meanlog = 12.2177309	sdlog = 0.0411148
$\sigma_{0.2,f}$	EN 1.4301	GA	0.3342	shape = 47.6650100	rate = 0.1047185
$\sigma_{0.2,f}$	EN 1.4318	GA	0.7299	shape = 41.99725063	rate = 0.07213275
$\sigma_{0.2,f}$	EN 1.4307	LN	<2.2e-16[1]	meanlog = 5.9518348	sdlog = 0.2115851
$\sigma_{0.2,f}$	EN 1.4571	WE	0.8051	shape = 9.243393	scale = 418.041707
$\sigma_{0.2,f}$	EN 1.4003	LN	<2.2e-16[1]	meanlog = 6.0861248	sdlog = 0.1177779
$\sigma_{0.2,f}$	EN 1.4509	LN	<2.2e-16[1]	meanlog = 6.20958687	sdlog = 0.05266284
$\sigma_{0.2,f}$	EN 1.4162	NO	0.0463	mean = 634.10345	sd = 72.31032
n_f	EN 1.4301	GA	0.5718	shape = 21.07948	rate = 4.23849
n_f	EN 1.4571	LN	2.20e-7	meanlog = 1.8021933	sdlog = 0.2217027

Table B.2 – *Continued from previous page*

Parameter	Grade	Distribution	p-value	1st parameter	2nd parameter
n_f	EN 1.4003	LN	1.13e-6	meanlog = 2.0067343	sdlog = 0.3192104
n_f	EN 1.4509	LN	1.95e-10	meanlog = 2.0544909	sdlog = 0.3290943
n_f	EN 1.4162	LN	<2.2e-16[1]	meanlog = 1.6955987	sdlog = 0.2610013
$n'_{0.2,1.0,f}$	EN 1.4301	LN	1.61e-9	meanlog = 1.0830978	sdlog = 0.1635712
$n'_{0.2,1.0,f}$	EN 1.4571	LN	9.683e-4	meanlog = 0.90815009	sdlog = 0.05377268
$n'_{0.2,1.0,f}$	EN 1.4003	WE	0.9507	shape = 14.531172	scale = 2.564985
$n'_{0.2,1.0,f}$	EN 1.4509	LN	9.448e-4	meanlog = 0.9060007	sdlog = 0.5776728
$n'_{0.2,1.0,f}$	EN 1.4162	LO	1.59e-13	location = 2.6818030	scale = 0.2505802
E_c	EN 1.4301	LN	7.55e-11	meanlog = 12.21080064	sdlog = 0.04637593
E_c	EN 1.4318	LN[2]	1.38e-12[2]	meanlog = 12.1392427[2]	sdlog = 0.0723124[2]
E_c	EN 1.4307	WE[2]	0.8835[2]	shape = 128.0892[2]	scale = 195681.2779[2]
E_c	EN 1.4571	WE	0.4282	shape = 28.13099	scale = 189755.15603
E_c	EN 1.4003	WE	0.7512	shape = 11.26199	scale = 209939.35707
E_c	EN 1.4509	LN[2]	2.53e-14[2]	meanlog = 12.18696608[2]	sdlog = 0.04732482[2]
E_c	EN 1.4162	WE	0.8758	shape = 70.77724	scale = 209298.92817
$\sigma_{0.2,c}$	EN 1.4301	LN	3.33e-16	location = 608.45487	scale = 30.83762
$\sigma_{0.2,c}$	EN 1.4571	NO	0.8959	mean = 527.00000	sd = 21.30728
$\sigma_{0.2,c}$	EN 1.4003	LN	<2.2e-16[1]	meanlog = 6.29324598	sdlog = 0.03962735
$\sigma_{0.2,c}$	EN 1.4162	NO	0.3287	mean = 818.45455	sd = 59.21204
$\sigma_{u,f}$	EN 1.4318	WE	0.3625	shape = 7.9233	scale = 931.8442
$\sigma_{u,f}$	EN 1.4509	LN	1.87e-13	meanlog = 6.28320012	sdlog = 0.04022548
n_c	EN 1.4301	WE	0.7524	shape = 4.370980	scale = 5.726338
n_c	EN 1.4162	LN	5.58e-09	meanlog = 1.8636704	sdlog = 0.2296406
$n'_{0.2,1.0,c}$	EN 1.4301	LN	4.52e-08	meanlog = 1.6751029	sdlog = 0.7652542
$n'_{0.2,1.0,c}$	EN 1.4162	LN	8.01e-07	meanlog = 1.5099570	sdlog = 0.2274294
LO: Logistic, NO: Normal, LN: Log-normal, WE: Weibull, GA: Gamma.					

[1] Error in the calculation of the p-value by R.

[2] Same statistical distribution with same parameters as for E_f.

Table B.2: Details of fitted statistical distribution for each material parameters, classified per grade.

(a) Width b.

(b) Thickness t.

(c) Inner radius ratio r_i/t
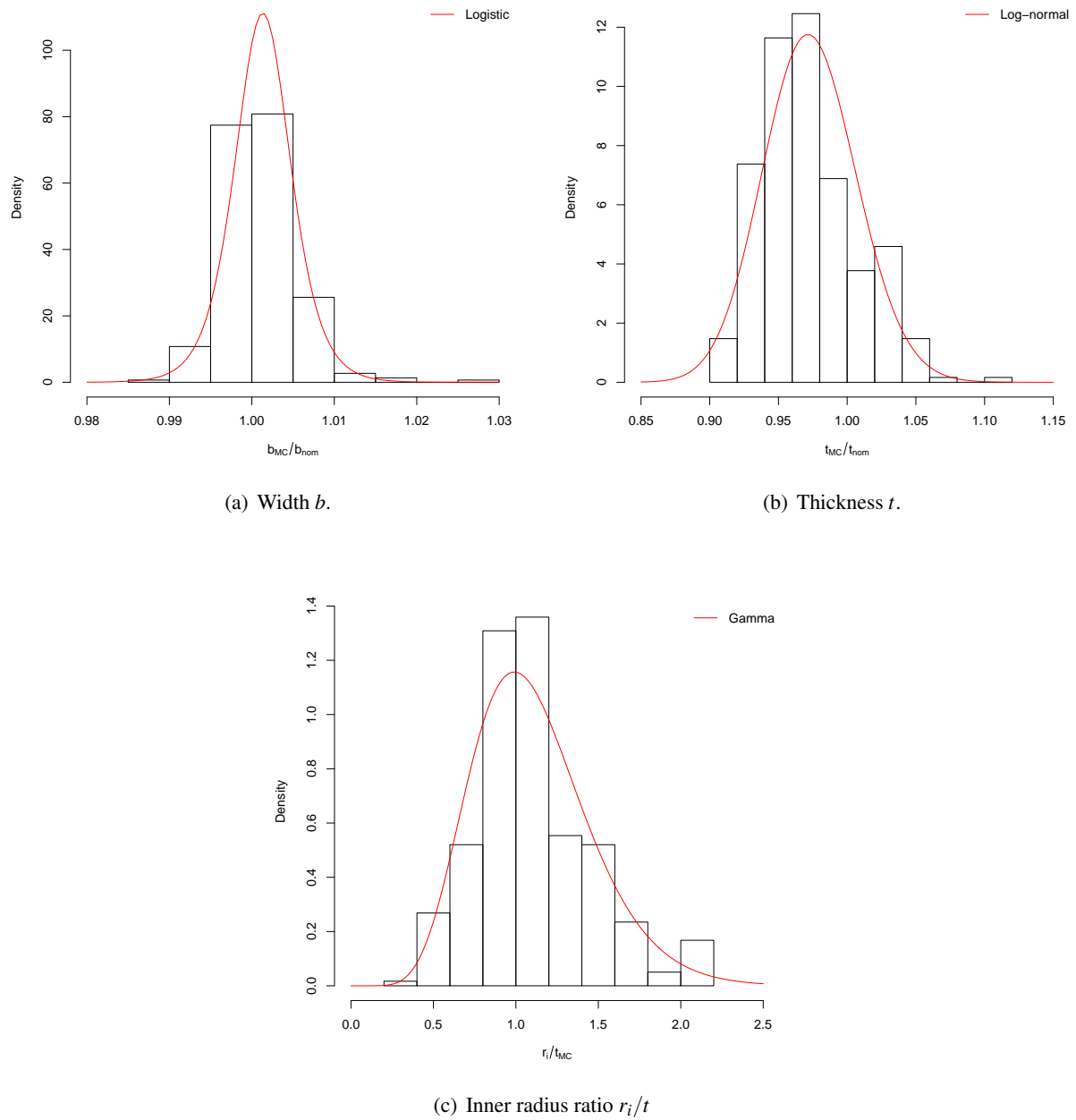
Figure B.1: Histograms and theoretical densities of geometric parameters.

(a) Global imperfection factor e_0 (ratio L/e_0).

(b) Global imperfection factor w_0.
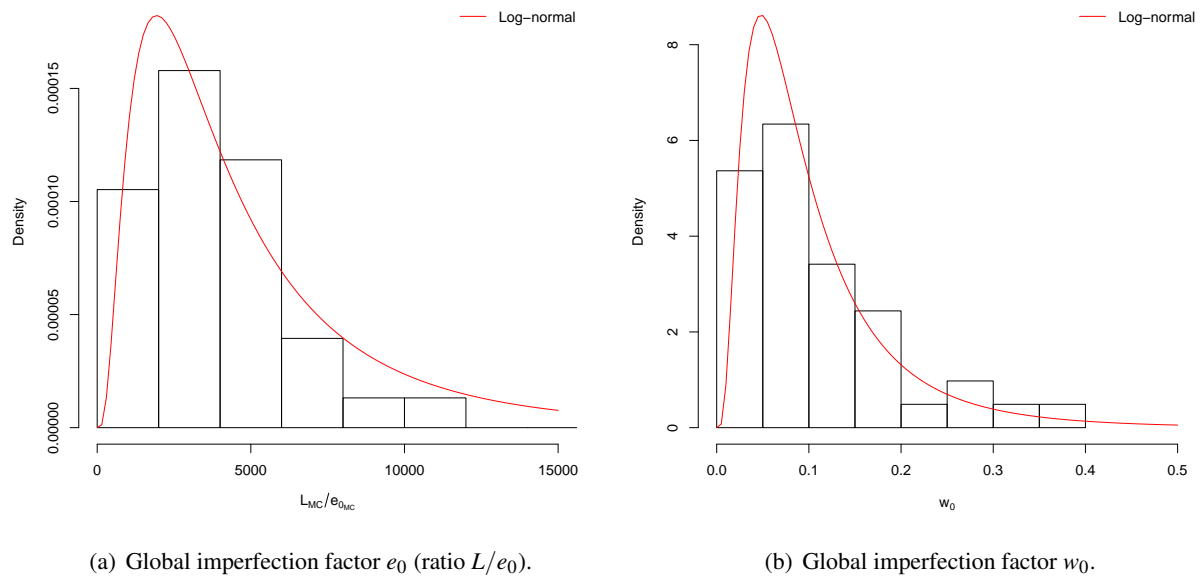
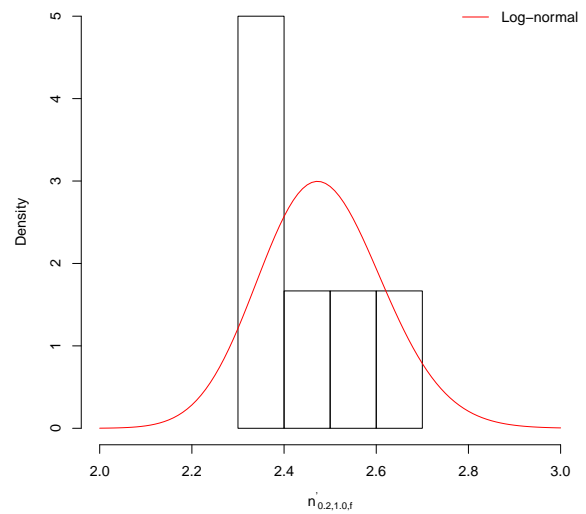**Figure B.2:** Histograms and theoretical densities of imperfection factors.
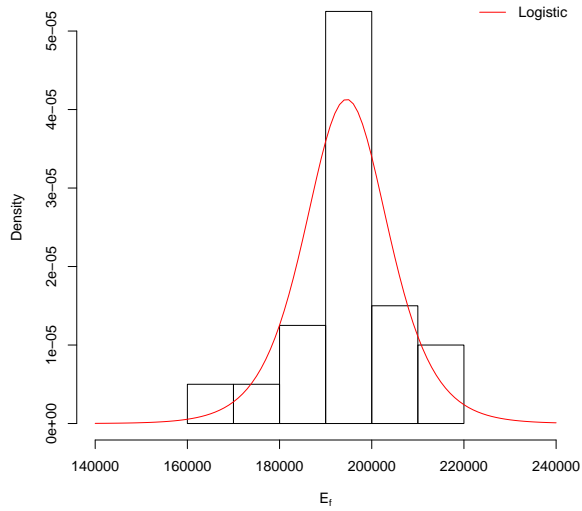
(a) EN 1.4301 (Austenitic).
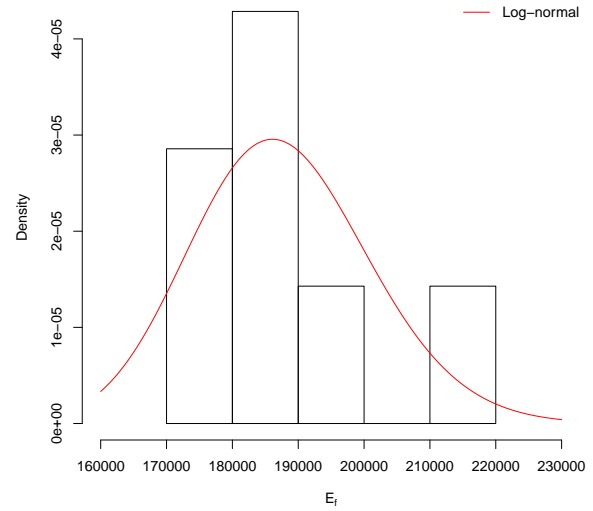
(b) EN 1.4318 (Austenitic).
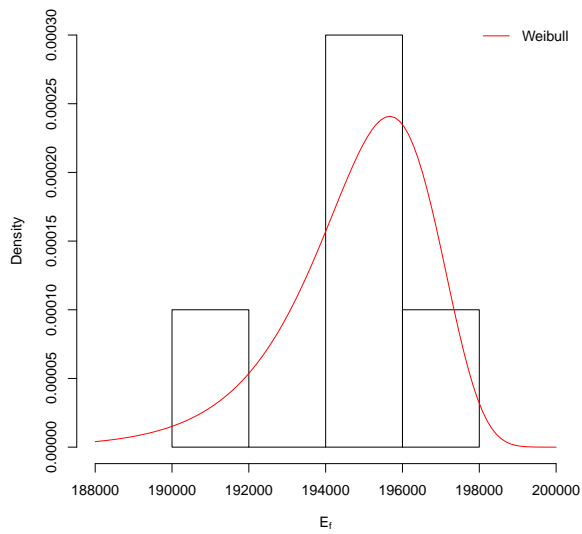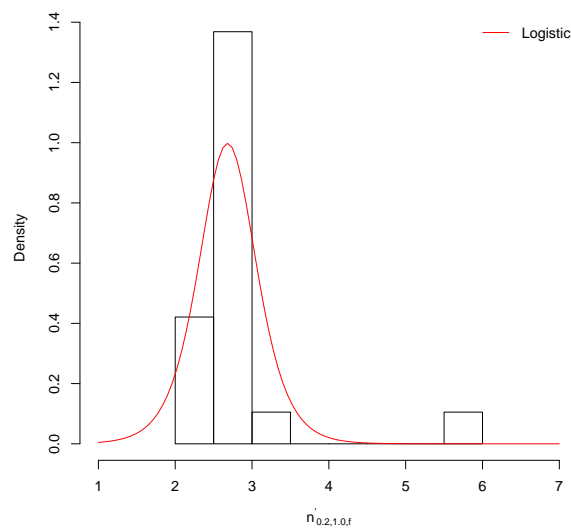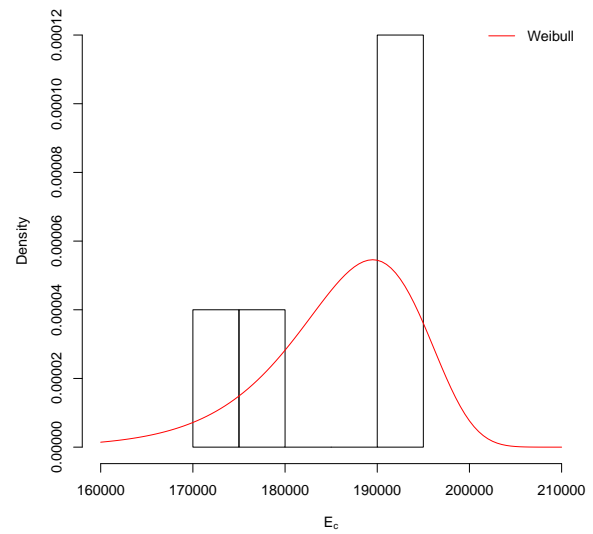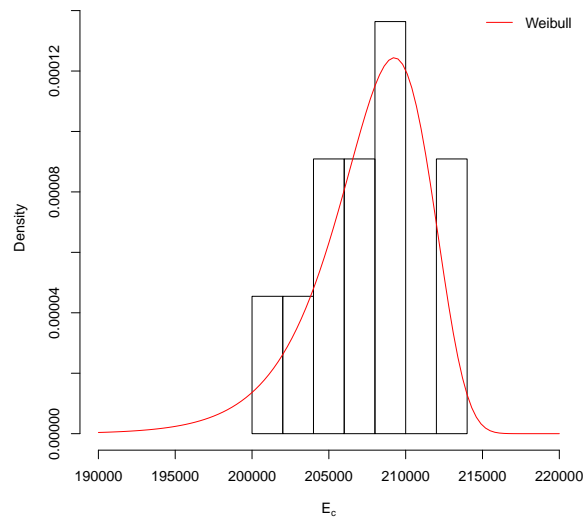
(c) EN 1.4307 (Austenitic).
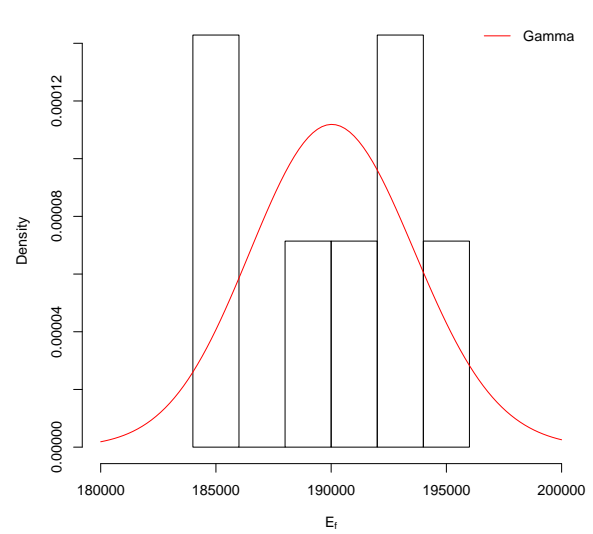
(d) EN 1.4571 (Austenitic).

Figure B.3: Histograms and theoretical densities of modulus of elasticity E_f in the flat parts for austenitic grades.
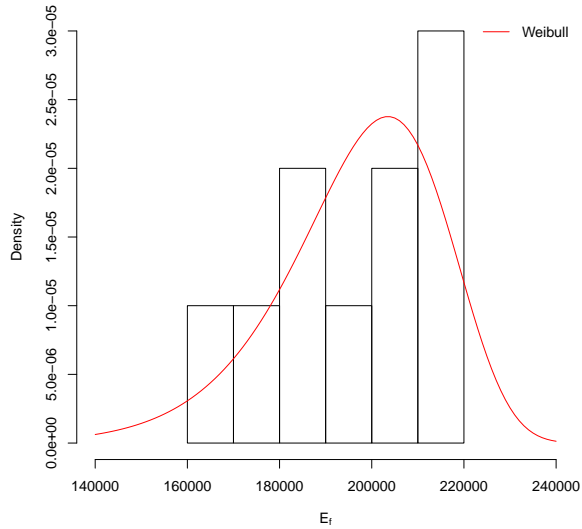
(a) EN 1.4003 (Ferritic).
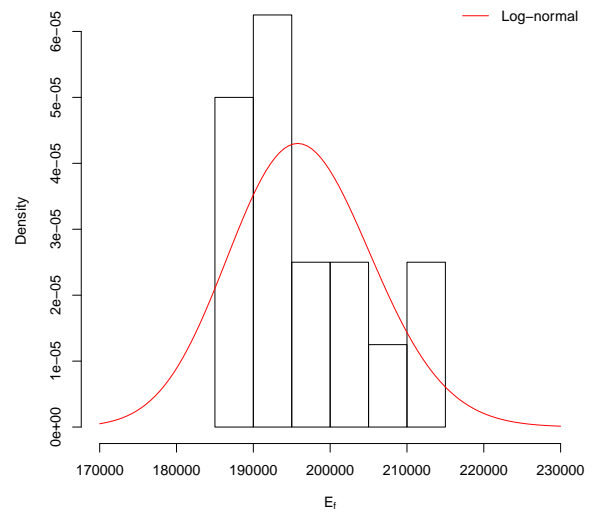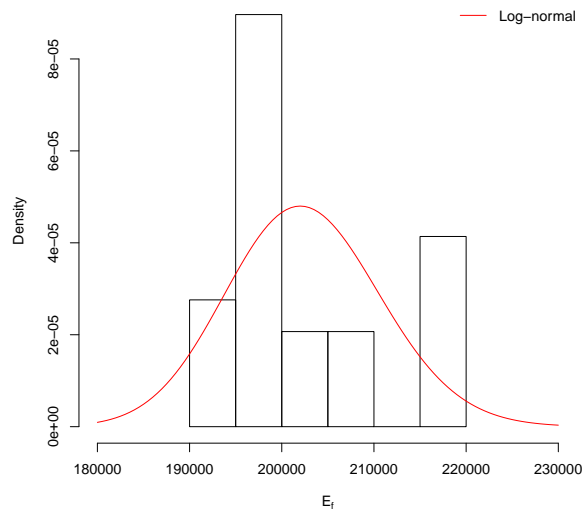
(b) EN 1.4509 (Ferritic).

(c) EN 1.4162 (Duplex).

Figure B.4: Histograms and theoretical densities of modulus of elasticity E_f in the flat parts for ferritic and duplex grades.
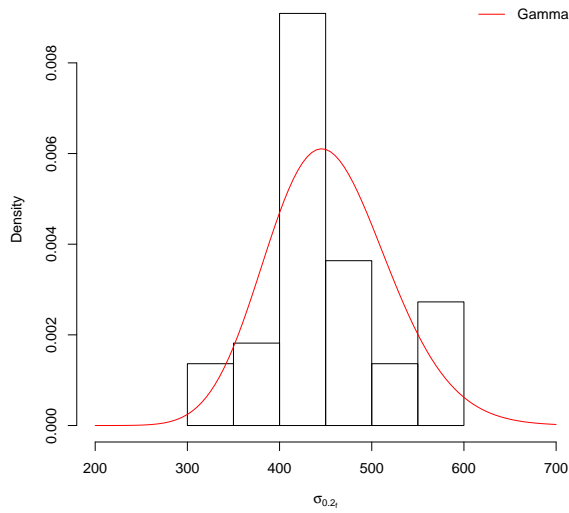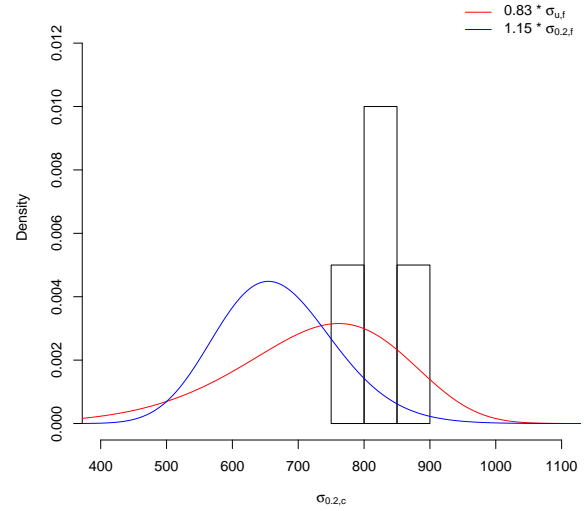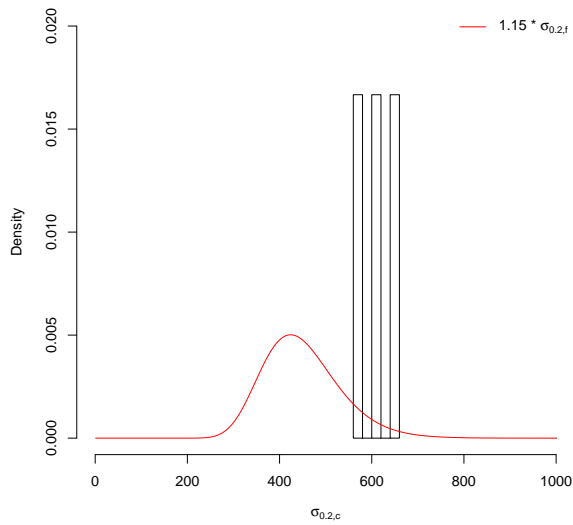
(a) EN 1.4301 (Austenitic).
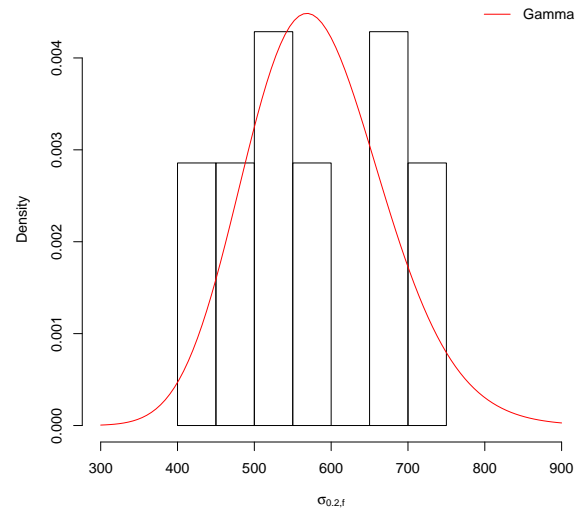
(b) EN 1.4318 (Austenitic).
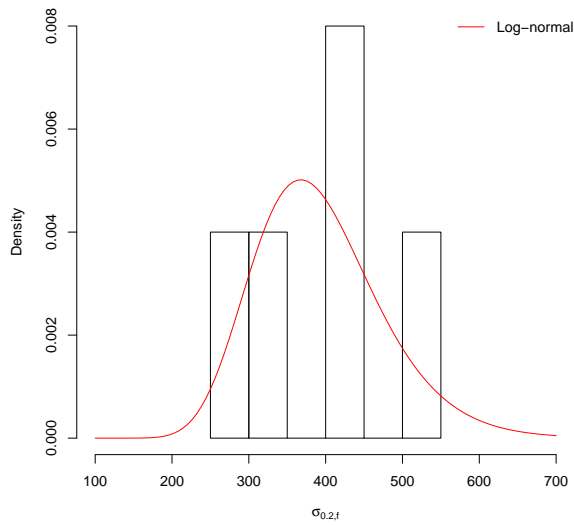
(c) EN 1.4307 (Austenitic).
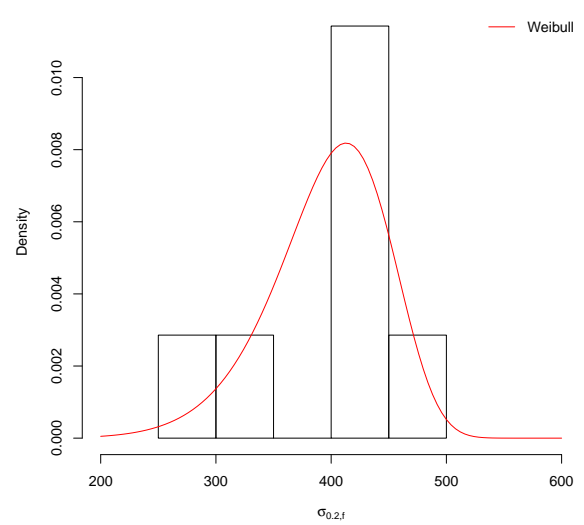
(d) EN 1.4571 (Austenitic).

Figure B.5: Histograms and theoretical densities of yield stress $\sigma_{0.2,f}$ in the flat parts for austenitic grades.
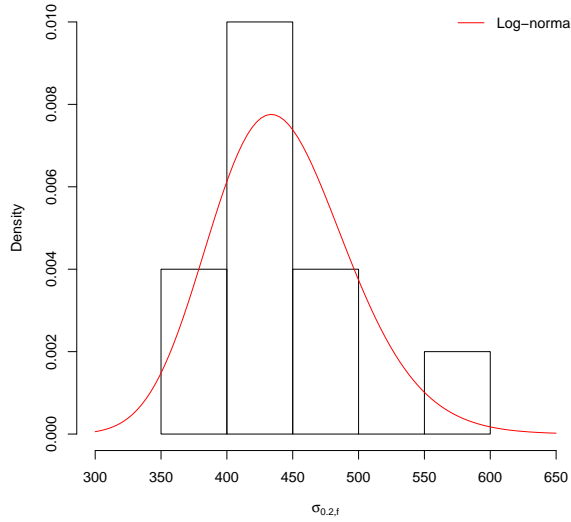
(a) EN 1.4003 (Ferritic).
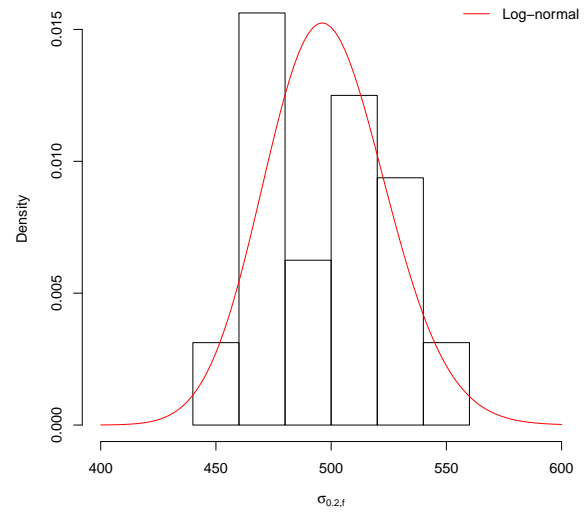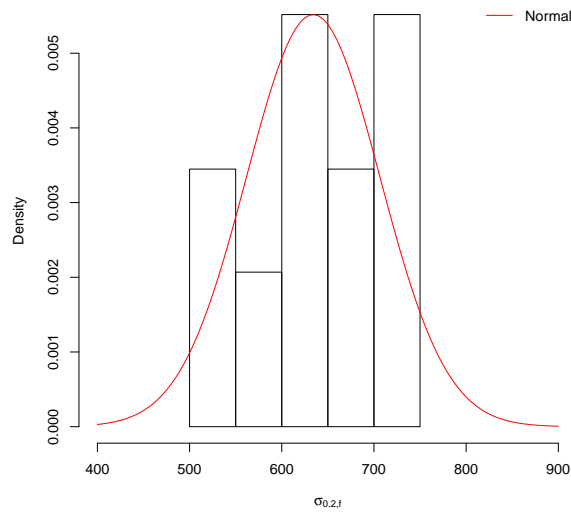
(b) EN 1.4509 (Ferritic).

(c) EN 1.4162 (Duplex).

Figure B.6: Histograms and theoretical densities of yield stress $\sigma_{0.2,f}$ in the flat parts for ferritic and duplex grades.
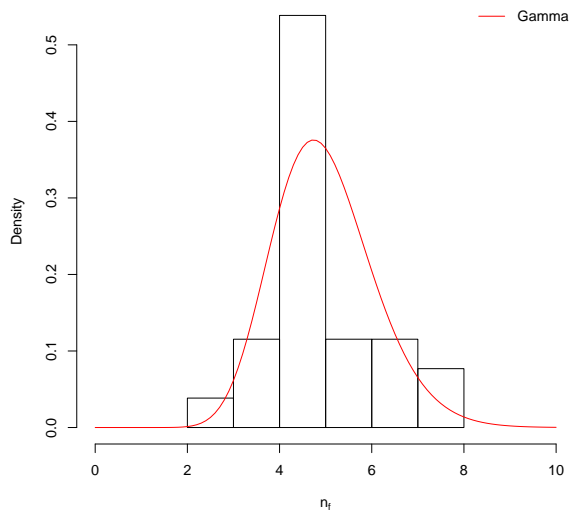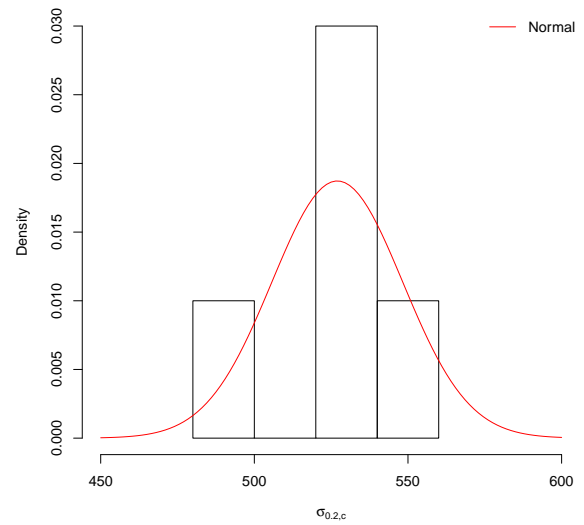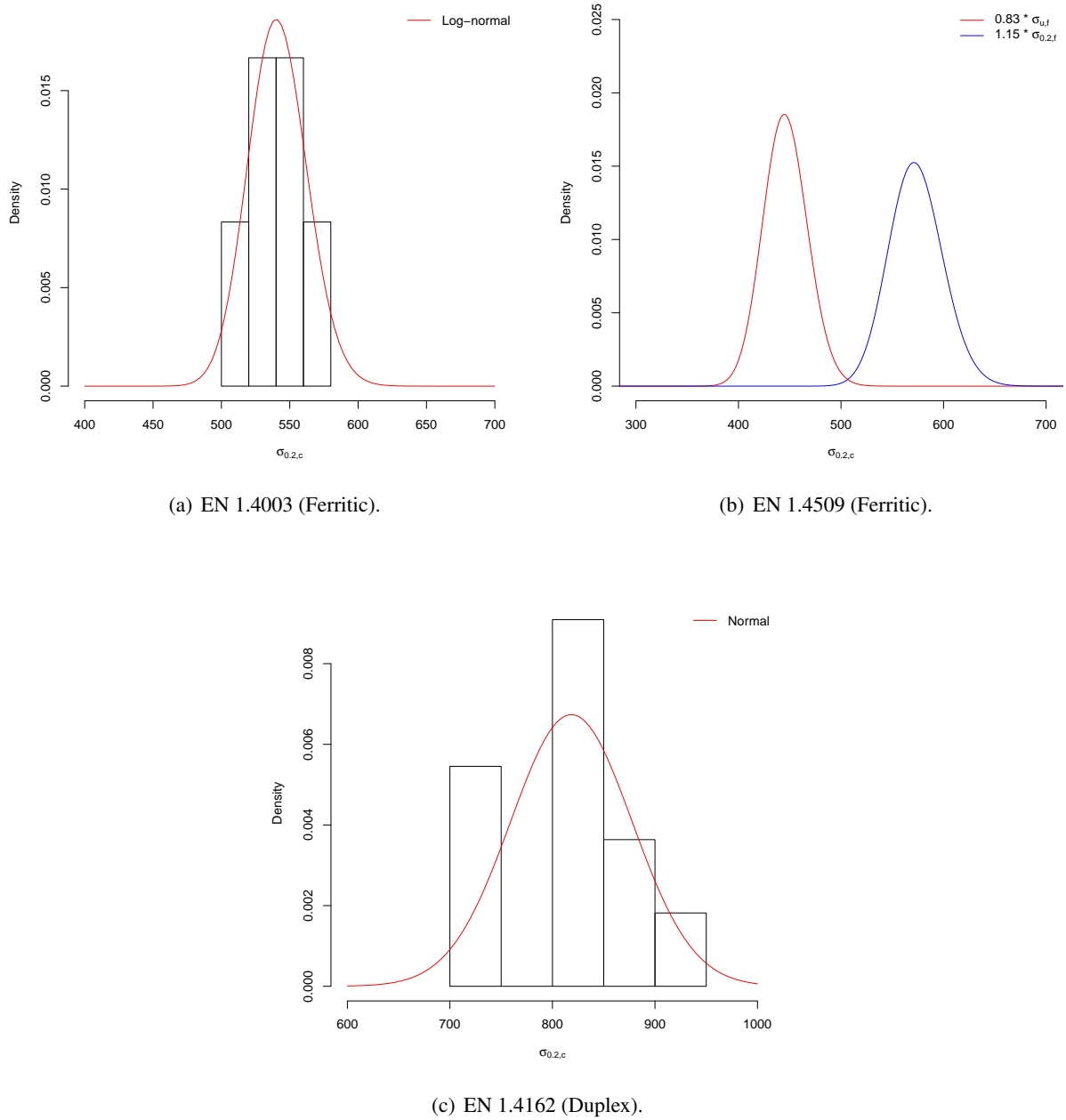
(a) EN 1.4301 (Austenitic).
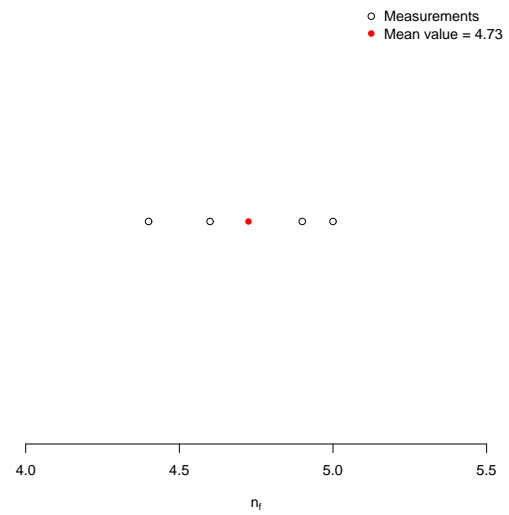
(b) EN 1.4318 (Austenitic).
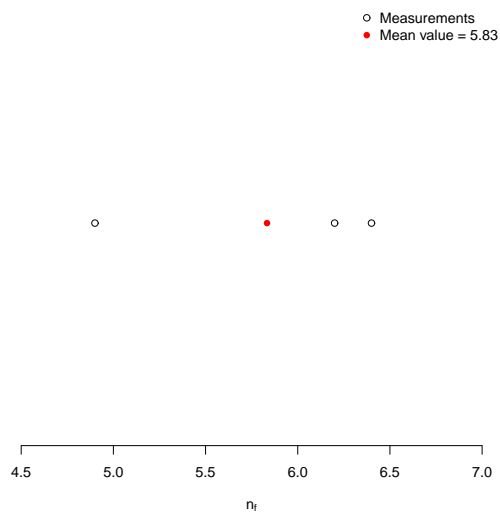
(c) EN 1.4307 (Austenitic).
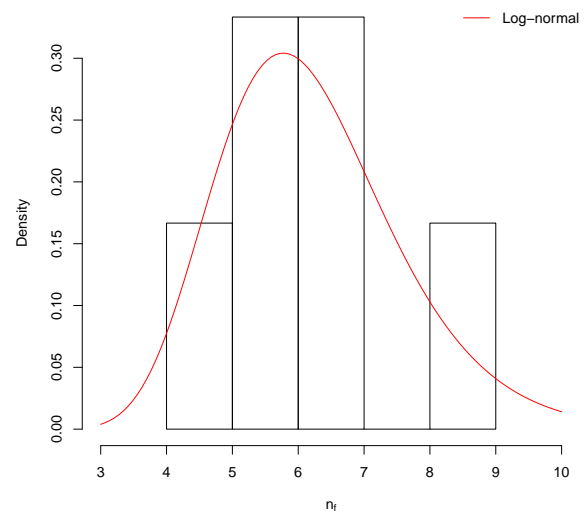
(d) EN 1.4571 (Austenitic).

Figure B.7: Histograms and theoretical densities of strain-hardening exponent n_f in the flat parts for austenitic grades.
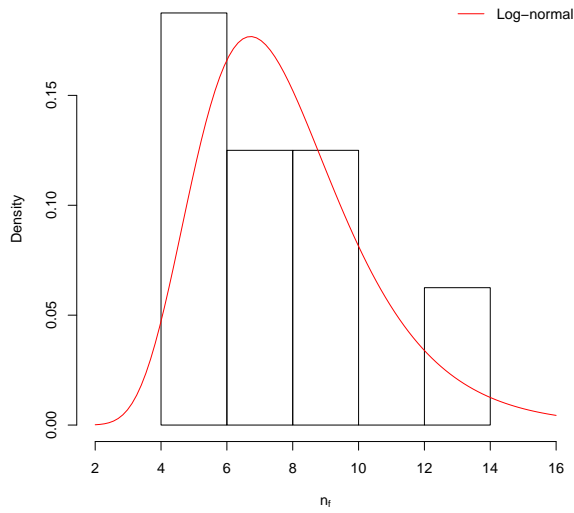
(a) EN 1.4003 (Ferritic).
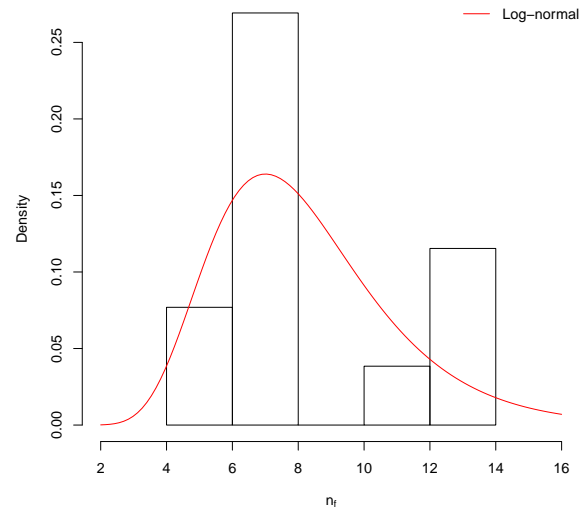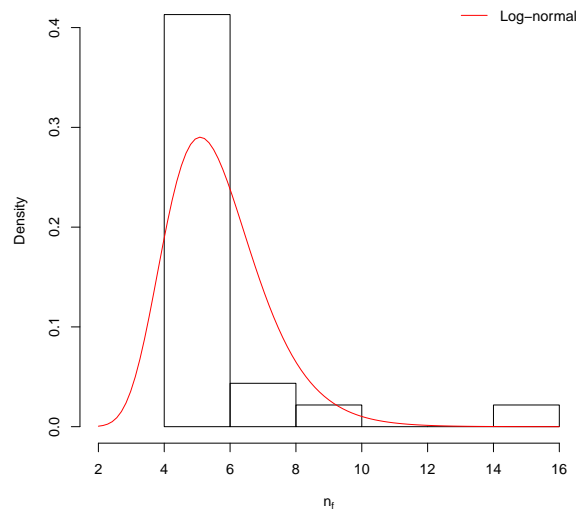
(b) EN 1.4509 (Ferritic).

(c) EN 1.4162 (Duplex).

Figure B.8: Histograms and theoretical densities of strain-hardening exponent n_f in the flat parts for ferritic and duplex grades.
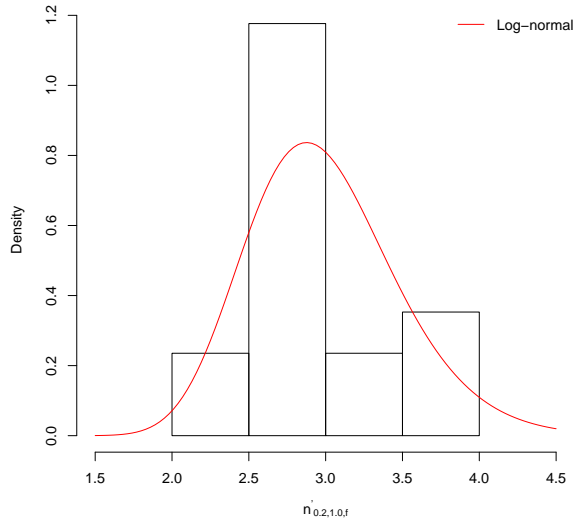
(a) EN 1.4301 (Austenitic).
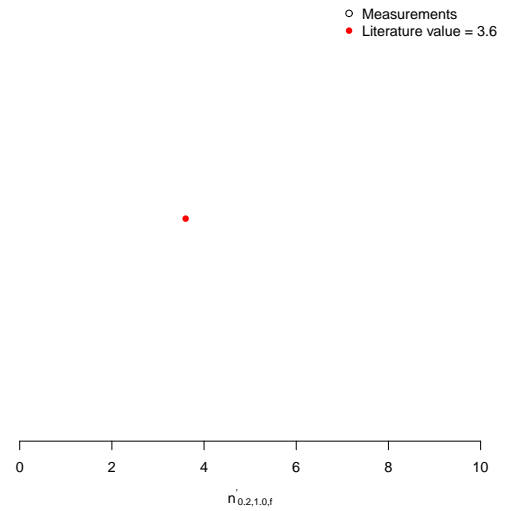
(b) EN 1.4318 (Austenitic).
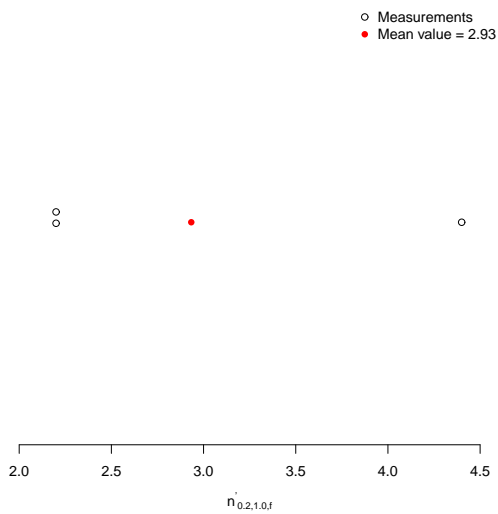
(c) EN 1.4307 (Austenitic).

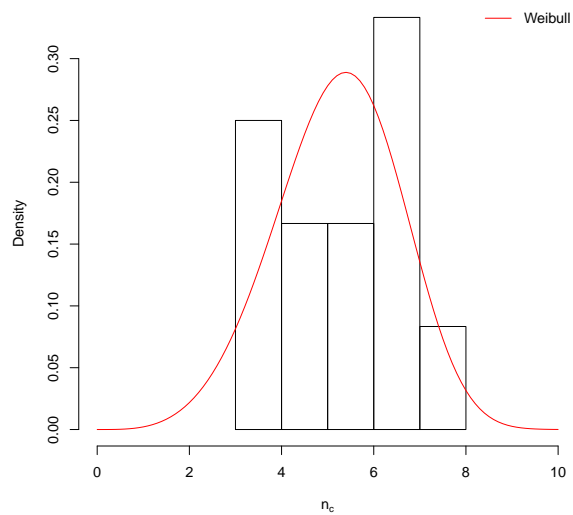(d) EN 1.4571 (Austenitic).

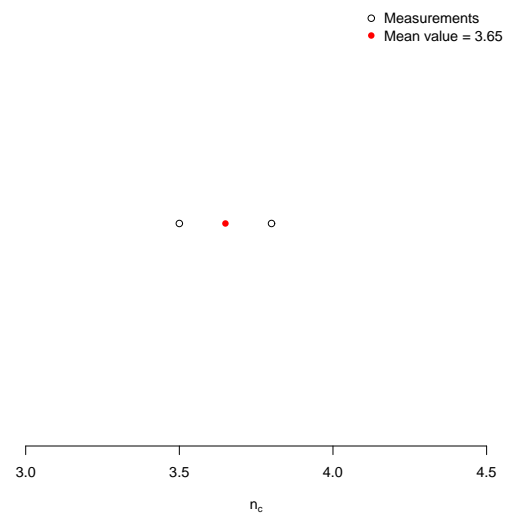**Figure B.9:** Histograms and theoretical densities of second strain-hardening exponent $n'_{0.2,1.0,f}$ in the flat parts for austenitic grades.
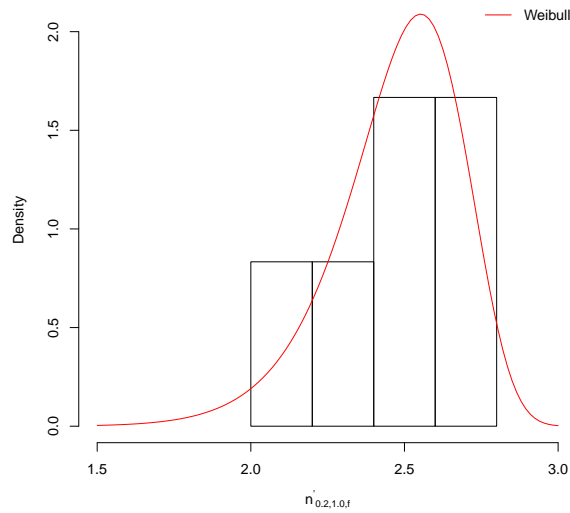
(a) EN 1.4003 (Ferritic).
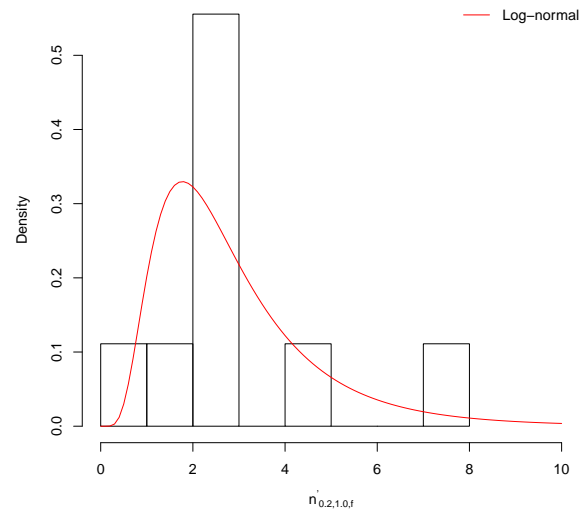
(b) EN 1.4509 (Ferritic).

(c) EN 1.4162 (Duplex).

Figure B.10: Histograms and theoretical densities of second strain-hardening exponent $n'_{0.2,1.0,f}$ in the flat parts for ferritic and duplex grades.
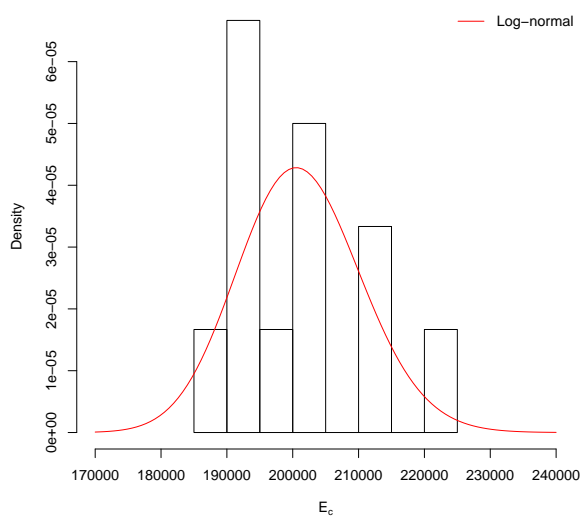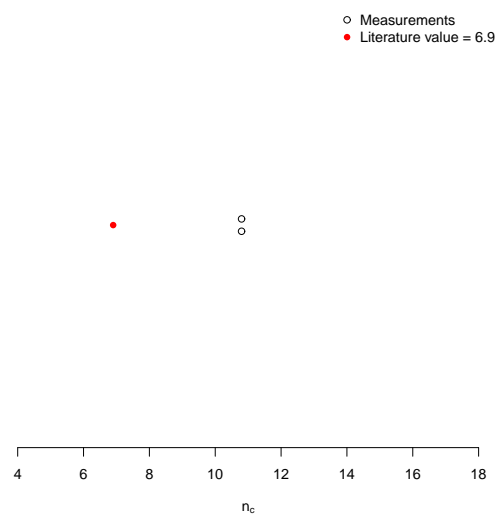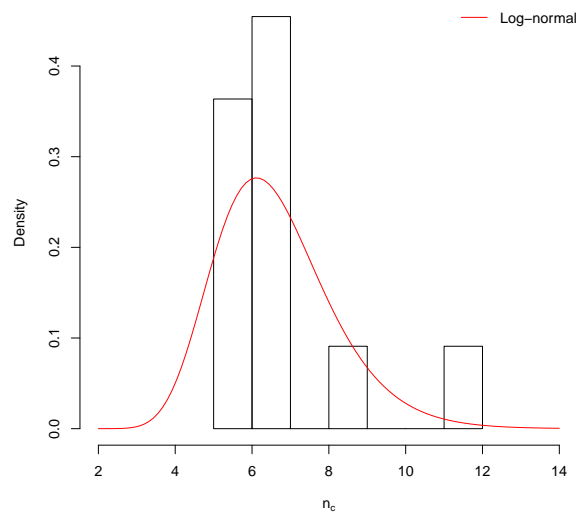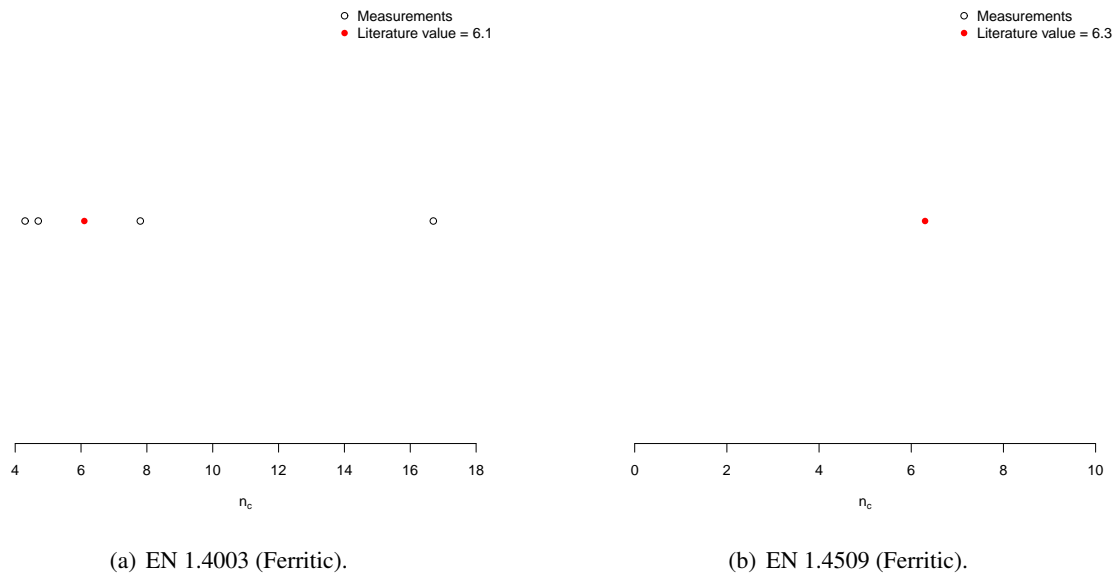
(a) EN 1.4301 (Austenitic).
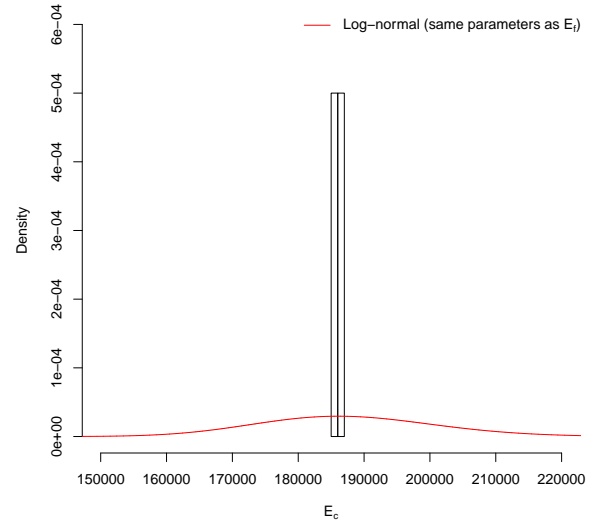
(b) EN 1.4318 (Austenitic).
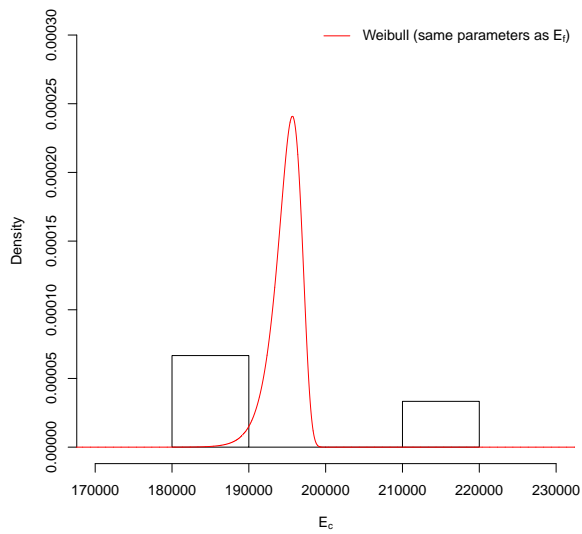
(c) EN 1.4307 (Austenitic).

(d) EN 1.4571 (Austenitic).

Figure B.11: Histograms and theoretical densities of modulus of elasticity E_c in the corner parts for austenitic grades.
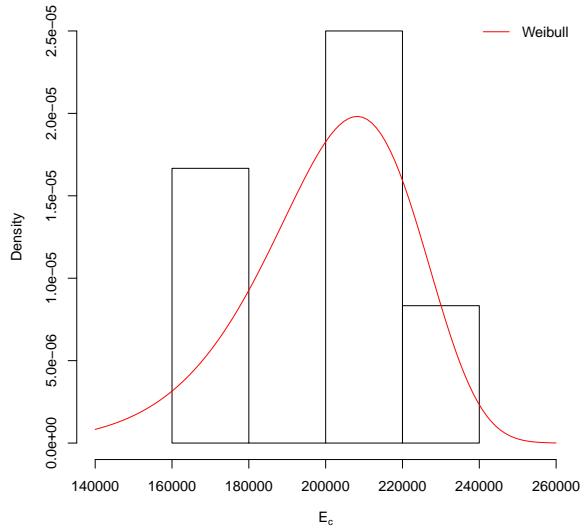
(a) EN 1.4003 (Ferritic).
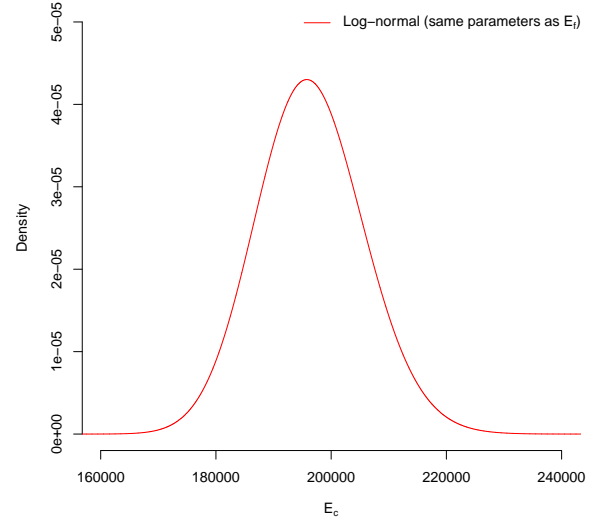
(b) EN 1.4509 (Ferritic).

(c) EN 1.4162 (Duplex).

Figure B.12: Histograms and theoretical densities of modulus of elasticity E_c in the corner parts for ferritic and duplex grades.

(a) EN 1.4318 (Austenitic).

(b) EN 1.4509 (Ferritic).
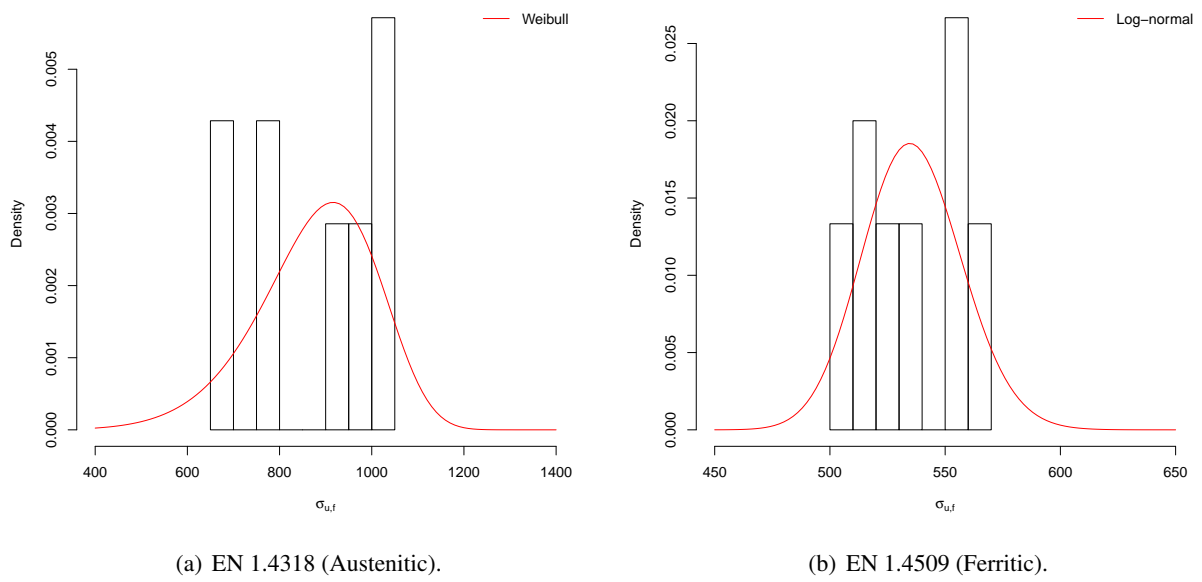
Figure B.13: Histograms and theoretical densities of the ultimate stress $\sigma_{u,f}$ in the flat parts for grades EN 1.4318 and grade 1.4509.
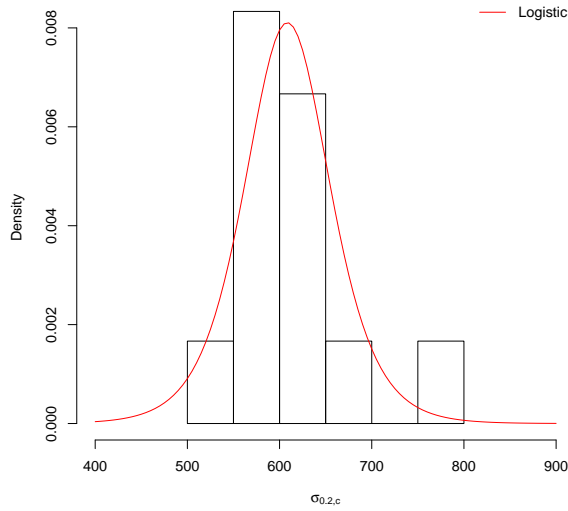
(a) EN 1.4301 (Austenitic).
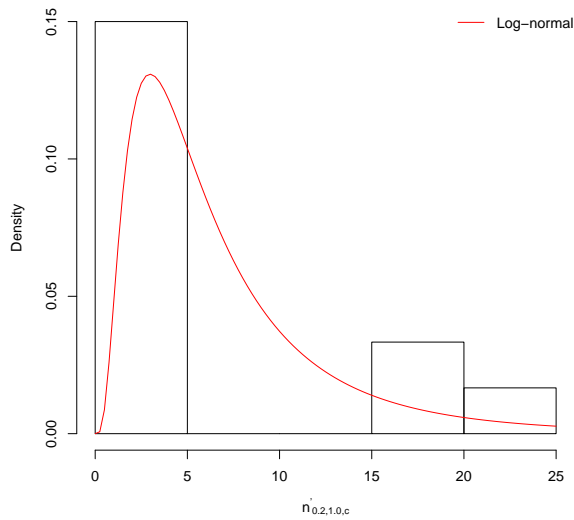
(b) EN 1.4318 (Austenitic).

(c) EN 1.4307 (Austenitic).

(d) EN 1.4571 (Austenitic).

Figure B.14: Histograms and theoretical densities of yield stress $\sigma_{0.2,c}$ in the corner parts for austenitic grades.
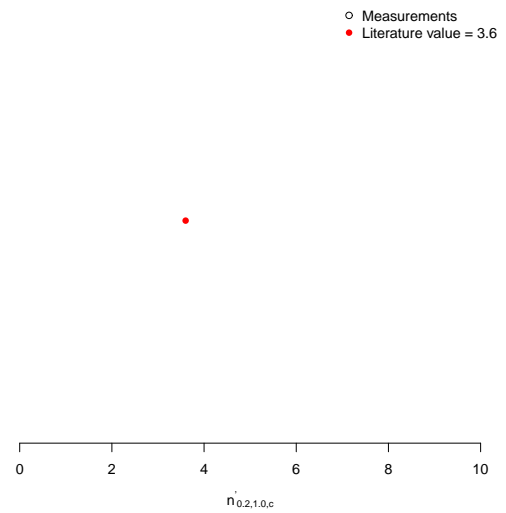
(a) EN 1.4003 (Ferritic).

(b) EN 1.4509 (Ferritic).

(c) EN 1.4162 (Duplex).

Figure B.15: Histograms and theoretical densities of yield stress $\sigma_{0.2,c}$ in the corner parts for ferritic and duplex grades.

(a) EN 1.4301 (Austenitic).

(b) EN 1.4318 (Austenitic).
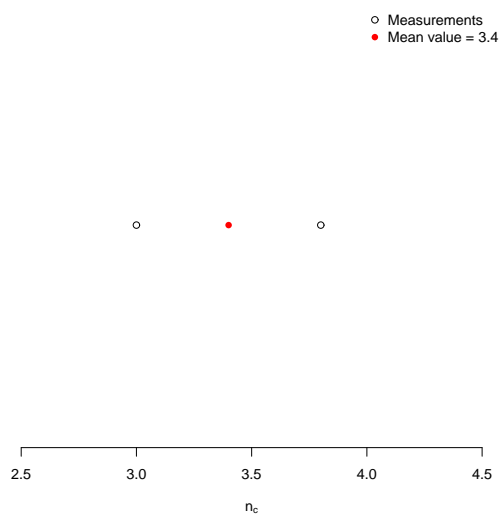
(c) EN 1.4307 (Austenitic).

(d) EN 1.4571 (Austenitic).

Figure B.16: Histograms and theoretical densities of strain-hardening exponent n_c in the corner parts for austenitic grades.
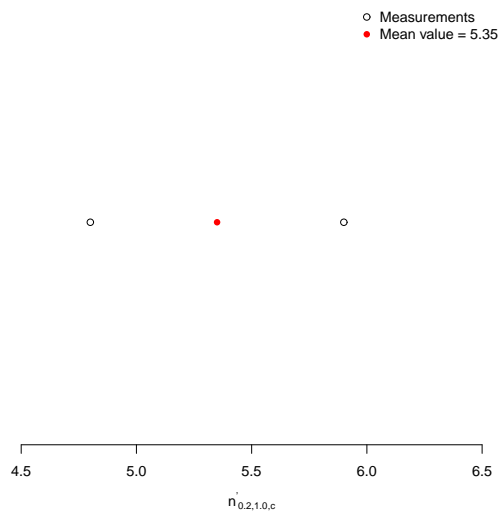
(a) EN 1.4003 (Ferritic).

(b) EN 1.4509 (Ferritic).

(c) EN 1.4162 (Duplex).

Figure B.17: Histograms and theoretical densities of strain-hardening exponent n_c in the corner parts for ferritic and duplex grades.
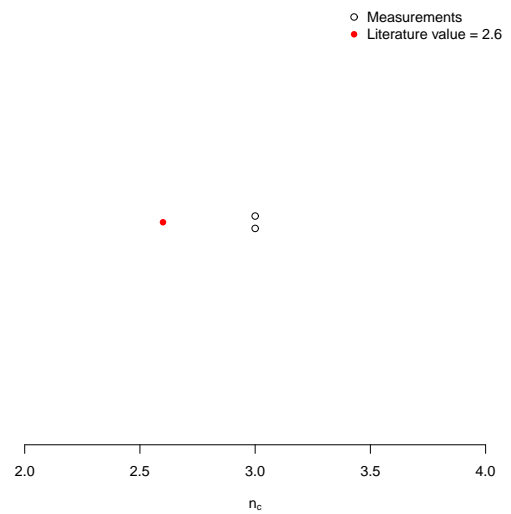
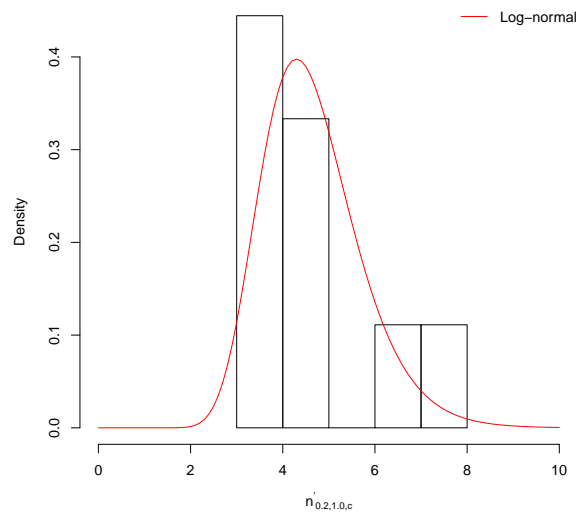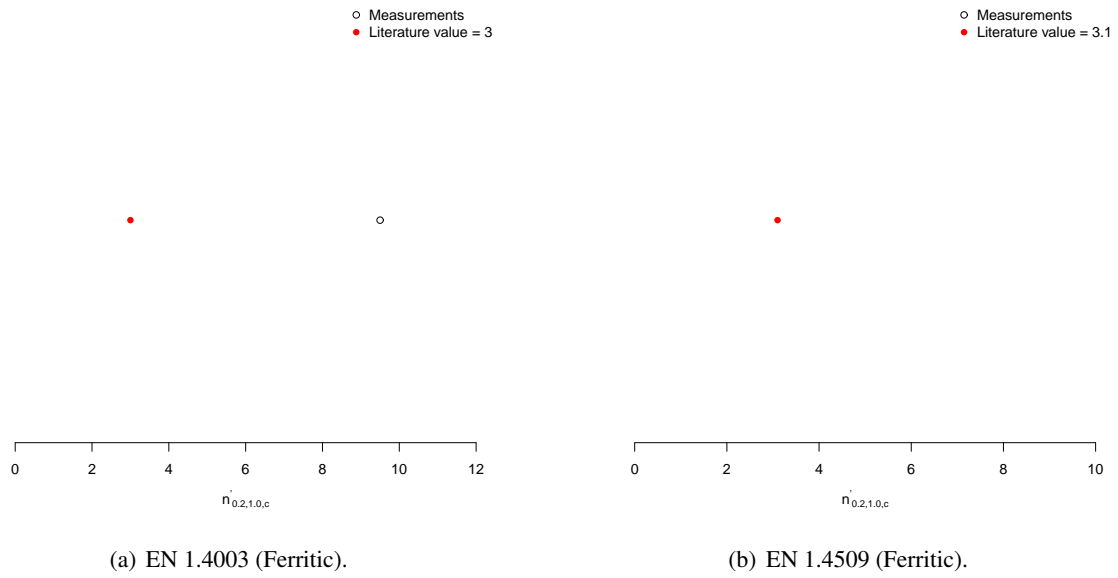(a) EN 1.4301 (Austenitic).

(b) EN 1.4318 (Austenitic).

(c) EN 1.4307 (Austenitic).

(d) EN 1.4571 (Austenitic).

Figure B.18: Histograms and theoretical densities of second strain-hardening exponent $n'_{0.2,1.0,c}$ in the corner parts for austenitic grades.

(a) EN 1.4003 (Ferritic).

(b) EN 1.4509 (Ferritic).

(c) EN 1.4162 (Duplex).

Figure B.19: Histograms and theoretical densities of second strain-hardening exponent $n'_{0.2,1.0,c}$ in the corner parts for ferritic and duplex grades.